Aniket Kum Sharma

Thesis for Plag 12 oct

Literature Survey

Document Details

Submission ID
trn:oid:::27535:154438427

Submission Date
Oct 12, 2026, 3:39 PM GMT+5:30

Download Date
Oct 12, 2026, 3:44 PM GMT+5:30

File Name
Thesis for Plag 12 oct.pdf

File Size
4.4 MB

132 Pages

27,005 Words

150,213 Characters

9% Overall Similarity

The combined total of all matches, including overlapping sources, for each database.

Filtered from the Report

- Bibliography
- Quoted Text
- Small Matches (less than 10 words)

Exclusions

- 3 Excluded Sources

Match Groups

68 Not Cited or Quoted 6%
Matches with neither in-text citation nor quotation marks

38 Missing Quotations 3%
Matches that are still very similar to source material

0 Missing Citation 0%
Matches that have quotation marks, but no in-text citation

0 Cited and Quoted 0%
Matches with in-text citation present, but no quotation marks

Top Sources

6% Internet sources
7% Publications
3% Submitted works (Student Papers)

Integrity Flags

0 Integrity Flags for Review

Our system's algorithms look deeply at a document for any inconsistencies that would set it apart from a normal submission. If we notice something strange, we flag it for you to review.

A Flag is not necessarily an indicator of a problem. However, we'd recommend you focus your attention there for further review.

Match Groups

- **68** Not Cited or Quoted 6%
  Matches with neither in-text citation nor quotation marks
- **38** Missing Quotations 3%
  Matches that are still very similar to source material
- **0** Missing Citation 0%
  Matches that have quotation marks, but no in-text citation
- **0** Cited and Quoted 0%
  Matches with in-text citation present, but no quotation marks

Top Sources

6% Internet sources
7% Publications
3% Submitted works (Student Papers)

Top Sources

The sources with the highest number of matches within the submission. Overlapping sources will not be displayed.

1	Publication	Mohammed A Almajeed A Alabas, Udai A. Jahad, Riyadh Al-Ameri, Ali Chabuk, Mu... <1%
2	Internet	coek.info <1%
3	Internet	espace.library.uq.edu.au <1%
4	Internet	www.researchgate.net <1%
5	Internet	ascelibrary.org <1%
6	Internet	linknovate.com <1%
7	Internet	cronfa.swan.ac.uk <1%
8	Publication	"Hydraulics and Fluid Mechanics, Volume 2", Springer Science and Business Medi... <1%
9	Publication	Dominic E. Reeve, Ali Adel Zuhaira, Harshinie Karunarathna. "Computational inve... <1%
10	Internet	www.extrica.com <1%

11 Internet
scholar.archive.org <1%

12 Publication
Arman Dah-Mardeh, Gholamreza Azizyan, Mahmood Shafai Bejestan, Abbas Pars... <1%

13 Publication
Shimal Mero, Steve Mitchell. "Investigation of energy dissipation and flow regime... <1%

14 Publication
H Chanson, L Toombes. "Experimental investigations of air entrainment in transit... <1%

15 Publication
Xiaoni Yang, Lijuan Han, Yongye Li, Yuchuan Bai. "Slope effects on hydraulic char... <1%

16 Publication
Robert M. Boes, Willi H. Hager. "Hydraulic Design of Stepped Spillways", Journal o... <1%

17 Student papers
Liverpool John Moores University on 2012-04-05 <1%

18 Internet
link.springer.com <1%

19 Internet
assets.researchsquare.com <1%

20 Internet
mdpi-res.com <1%

21 Student papers
Tikrit University on 2025-02-05 <1%

22 Publication
Hubert Chanson. "Energy Dissipation in Hydraulic Structures", CRC Press, 2019 <1%

23 Internet
gdr-isis.org <1%

24 Publication
Mohammad Bagherzadeh, Mirali Mohammadi, Rasoul Daneshfaraz, Amir Ghaderi... <1%

25 Internet

covid19-data.nist.gov <1%

26 Student papers

Al-Qasim Green University on 2025-08-17 <1%

27 Publication

Mahmoud Mohammad Rezapour Tabari, Shiva Tavakoli. "Effects of Stepped Spillw... <1%

28 Internet

www.pjoes.com <1%

29 Publication

Abdelwanees Ashoor, Amin Riazi. "Stepped Spillways and Energy Dissipation: A N... <1%

30 Internet

ethesis.nitrkl.ac.in <1%

31 Internet

utq.edu.iq <1%

32 Internet

hdl.handle.net <1%

33 Internet

ijtech.eng.ui.ac.id <1%

34 Internet

iwaponline.com <1%

35 Internet

pmc.ncbi.nlm.nih.gov <1%

36 Internet

www.coursehero.com <1%

37 Student papers

IIT Delhi on 2015-03-14 <1%

38 Internet

arxiv.org <1%

39	Internet	
brahdet.web.app		<1%
40	Internet	
rke.abertay.ac.uk		<1%
41	Internet	
www.science.gov		<1%
42	Internet	
10wvvw.easychair.org		<1%
43	Publication	
Abbas Parsaie, Saleh Jaafer Suleiman Shareef, Amir Hamzeh Haghiabi, Raad Hoob...		<1%
44	Publication	
Ali Shariq, Ajmal Hussain, Zulfequar Ahmad. "Discharge equation for the gabion ...		<1%
45	Publication	
Binaya Raj Pandey, Megh Raj K C, Brian Crookston, Gerald Zenz. "Numerical Inves...		<1%
46	Publication	
Ritusnata Mishra, C. S. P. Ojha. "Chapter 29 Prediction of Energy Dissipation in Ski...		<1%
47	Publication	
Sadirak Tasissa, Kenatu Angassa, Workineh Tesfaye. "Modeling Water Quality Par...		<1%
48	Internet	
academic-accelerator.com		<1%
49	Internet	
files.thapar.edu		<1%
50	Internet	
staff.civil.uq.edu.au		<1%
51	Internet	
www.journalofbabylon.com		<1%
52	Publication	
Ali Shariq, Ajmal Hussain, Zulfequar Ahmad. "Flow over gabion weir under free a...		<1%

53 Publication
H.-E. Minor, W.H. Hager. "Hydraulics of Stepped Spillways - Proceedings of the Int... <1%

54 Publication
Hamidreza Abbaszadeh, Reza Norouzi, Veli Sume, Alban Kuriqi, Rasoul Daneshfar... <1%

55 Publication
Lecture Notes in Computer Science, 2007. <1%

56 Student papers
MIT Academy of Engineering on 2026-08-10 <1%

57 Publication
Mauricio Santillana, D. Wendong Zhang, Benjamin M. Althouse, John W. Ayers. "W... <1%

58 Publication
O. Faruk Dursun, Mualla Ozturk. "Determination of flow characteristics of steppe... <1%

59 Student papers
University of Adelaide on 2026-05-25 <1%

60 Student papers
University of Leeds on 2021-05-12 <1%

61 Student papers
University of Liverpool on 2026-05-11 <1%

62 Internet
cdn.iferp.in <1%

63 Internet
eprints.qut.edu.au <1%

64 Internet
idr.nitk.ac.in <1%

65 Internet
www.grafiati.com <1%

66 Internet
www.mdpi.com <1%

67 Internet

www.springerprofessional.de <1%

Chapter 1: INTRODUCTION

1.1 General

Dams and reservoirs are essential for water management and flood mitigation. Spillways can be defined as hydraulic structures that act as a safety valve and are essential for safely releasing excess water during heavy rainfall, requiring efficient conveyance and energy dissipation to prevent structural damage. Technological advancements have enhanced spillway designs for effective flood management; **Chanson (2015)**. Over the last few decades, there has been a noticeable increase in flooding frequency around the world, about 40% of embankment dams around the world are damaged due to overtopping. It is crucial to reduce the impact of flooding on dam safety by assuring that spillways are designed to efficiently release excess water during the flood season. In hydraulic engineering, spillways are essential components of dam structures that allow controlled release of excess water from a reservoir to prevent overtopping and potential failure. The selection of a spillway type depends on factors such as topography, dam type, hydrological conditions and downstream requirements. Spillways may be broadly classified by purpose, by gate-control, and by structural form (**Khatsuria, 2005; Pereira, 2020**). As an example, Wivenhoe Dam, a rock and earth-fill embankment dam with a concrete spillway for portable water supply and flood protection, is located across the Brisbane River in Southeast Queensland, Australia. **(Figure 1.1)**. The different type of spillways is classified as per their application and suitability, and **Table 1** shows some dams is India with using different spillways.



Figure 1.1 Wivenhoe dam spillway (Australia, 2010); Chanson (2015)

1. Free overfall (Straight Drop) Spillway

Water flows over a crest and drops freely downstream. It is suitable for low heads, not recommended for very high heads because of jet impact and possible vibration.

Uses:

- Commonly used for low to medium head dams, particularly small concrete or masonry dams, where water can drop freely without excessive energy.
- Suitable for narrow valleys and small catchment areas, where the discharge requirement is moderate and the foundation is strong enough to resist impact from the falling jet.

2. Ogee Spillway

The ogee spillway is one of the most common types used in gravity and arch dams. It features a curved profile that matches the underside of the nappe from a sharp-crested weir under design conditions.

Uses:

- Ideal for concrete dams with sufficient height.
- Provides efficient energy dissipation and smooth water flow.
- Commonly used where precise discharge control is required.

3. Chute (Open Channel) Spillway

This spillway consists of an open channel or chute that carries water from the reservoir to the downstream river at a safe velocity.

Uses:

- Suitable for embankment dams where water must be carried around or over the dam.
- Simple to construct and maintain.
- Can accommodate high discharges with proper energy dissipation arrangements such as stilling basins.

4. Shaft Spillway

A vertical or funnel-shaped structure that allows water to enter from all sides and then flows through a vertical shaft connected to a horizontal conduit.

Uses:

- Employed where narrow valleys or limited space prevent the use of other types.
- Useful in dams with steep abutments and deep reservoirs.

5. Side Channel Spillway

Water flows parallel to the crest before being directed into a side channel that carries it downstream.

Uses:

- Suitable for narrow valleys where direct downstream discharge is not possible.
- It is commonly used in conjunction with chute or tunnel spillways.

6. Siphon Spillway

This type operates automatically using siphon action to draw water from the reservoir once the water level exceeds a certain height.

Uses:

- It is appropriate for small and medium-sized dams.
- Allow automatic operation without mechanical devices.
- It helps to maintain reservoir levels efficiently

7. Stepped Spillway

The spillway surface is made of a series of steps that act as energy dissipators by inducing turbulence and aeration.

Uses:

- Suitable for roller-compacted concrete (RCC) dams.
- Reduces the need for large stilling basins.
- Enhances energy dissipation efficiency.

Table 1.1 Some Dams in India using spillways

Sr. No.	Dam Name	State	Type of Dam	Spillway Type	Height of Dam (m)
1	Bhakra Dam	Himachal Pradesh	Concrete Gravity	Ogee	226
2	Tehri Dam	Uttarakhand	Earth & Rock-fill	Shaft and Chute	260.5
3	Sardar Sarovar Dam	Gujarat	Concrete Gravity	Ogee and Chute	163
4	Hirakud Dam	Odisha	Composite Earth-Concrete	Controlled Ogee	60.96
5	Nagarjuna Sagar Dam	Andhra Pradesh	Masonry Gravity	Crest Gate Chute	124

Stepped spillways must be designed with energy dissipation in mind since excessive flow energy can result in a number of issues at the base of the structure, including the creation of scour holes, which can cause the spillway foundations to fail structurally. Furthermore, overtopping damage could happen, which could result in serious issues for people living nearby. Three hydraulic regimes can be used to classify flow over stepped spillways such as nappe flow, transition flow and skimming flow. Nappe flow occurs when the discharge of water is low; skimming flow occurs when the discharge is high and transition flow might be observed when the discharge is between the nappe flow and skimming flow. Spillways have traditionally been impermeable. However, by increasing energy dissipation, the provision of a permeable layer, like gabions, provides a way to improve hydraulic performance. Depending on the intended usage, gabions can be filled with stones, cobbles, gravel, or other materials. China and Egypt have been using gabions since 1879. Additionally, gabions have been employed for several kinds of purposes, including building retaining walls, stabilizing banks, and protecting riverbeds. Baskets, mattresses, and sacks are the three forms of gabions. These may all be filled with cobbles or gravel. The particular kind of gabion chosen is determined by its intended use. For instance, basket gabions are commonly employed to safeguard stream banks and river beds and to provide stability.

Gabion structures are increasingly used in hydraulic engineering applications such as small earth dams, retaining walls, intake structures, and soil conservation works. Their popularity is attributed to several advantages, including ease of construction, durability, flexibility, and their ability to resist hydraulic loads due to their porous structure. The porous composition of gabions facilitates seepage flow, which reduces hydrostatic pressure behind the structure and promotes drainage efficiency. Moreover, permeability significantly influences surface flow behaviour by allowing shear interaction within the permeable bed, thereby modifying the boundary layer and enhancing momentum exchange between surface and subsurface flows. This interaction leads to increased flow resistance and higher energy dissipation **(Zhang & Chanson, 2016; Wüthrich & Chanson, 2014)**.

Gabion stepped spillways are increasingly utilized in dam engineering, river improvement and erosion-control projects. Compared with conventional impermeable stepped spillways, gabion stepped designs offer greater flexibility, structural stability, and cost efficiency, particularly in stilling basin construction, because they dissipate energy through both overflow and throughflow. Energy loss occurs via jet impingement, friction within the rock-fill voids, and cascading between steps. Gabion mattresses are also widely used for scour protection in riverine and coastal environments, as their porosity reduces the formation of secondary flow structures such as horseshoe and lee-wake vortices, which are responsible for local scour around hydraulic structures.

Gabion spillways are generally constructed in two configurations. In high-chute applications, gabion boxes are placed over the dam surface or channel bed to serve primarily as erosion protection without significant throughflow. Alternatively, the entire dam body may be constructed of gabions, making the spillway an integral part of the main structure. This configuration is common in short diversion dams, soil conservation projects, and river-training works, especially in regions with seasonal flow and flooding. Because of their high porosity, gabion spillways permit partial throughflow, resulting in hydraulic behaviour distinct from that of rigid stepped spillways. These low-head diversion structures, typically featuring fewer steps, effectively dissipate energy and control erosion in flood-prone channels (**Zhang & Chanson, 2016; Gamal M. Abdel Aal et al., 2019)**. **Figure 1.2** shows the different gabion sample pictures.



Figure 1.2 Different gabion samples pictures (Source: YKM Groups of wire mesh specialist (https://ykmgroup.com)

1.2 Flow condition over gabion stepped spillway

When the flow passes entirely through the porous body of the spillway, it results no overflow at the outer edge of the steps. Water seeps into the vertical face of the upstream side and exits only through the vertical face of the lowest step. In the nappe flow regime, the flow occurs over the entire body of the spillway, with water flowing as free-falling nappes and impacting from one step to the next. There is no cavity below the nappe as water seeps out from the vertical faces of the steps. In the transition regime, the flow shifts from nappe to skimming on the lower steps, while the upper steps remain in the nappe flow regime. Essentially, the upper steps exhibit nappe flow, and the lower steps exhibit skimming flow. Water flows down the steps in a sequential manner, with recirculating vortices confined between the steps acting as a cushion, eliminating air pockets under the jets. Consequently, water skims over the pseudo-bottom formed by the outer edges of the steps as in **Figure 1.3, (Rajaei et al. 2020).**

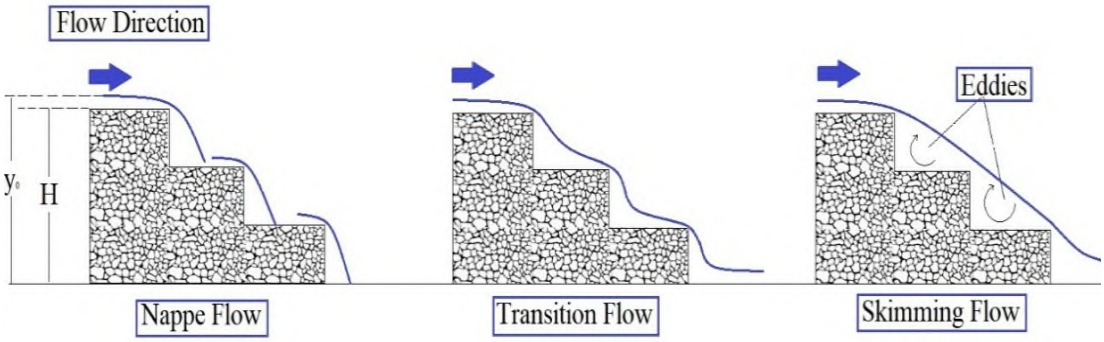

Figure 1.3 Different flow regimes

1.3 Hydraulic sketch of gabion stepped spillway

As per **Figure 1.4**, the energy equation at the upstream and downstream sections of the spillway can be notified by the relation given below in equation (1) and (2):

$$E_0 = y_0 + \frac{\alpha V_0^2}{2g} \quad (1)$$

$$E_1 = y_1 + \frac{\alpha V_1^2}{2g} \quad (2)$$

The relative energy loss can be expressed as per equation (3):

$$\frac{\Delta E}{E_0}\% = \frac{(E_0 - E_1)}{E_0}\% = E_L \quad (3)$$

where H_s is the entire gabion spillway height as determined by a point gauge subsequent to the spillway's installation at the flume, l is step length, h is step height.

E_o = energy at upstream section (m),

E_1 = energy at downstream section (m),

V_o = velocity at upstream section (m/sec),

V_1= velocity at downstream section at toe of spillway (m/sec),

α = kinetic energy correction coefficient,

g = gravitational acceleration (m/sec^2),

$\Delta E/E_o$ % = Relative energy loss between upstream and downstream of stepped spillway

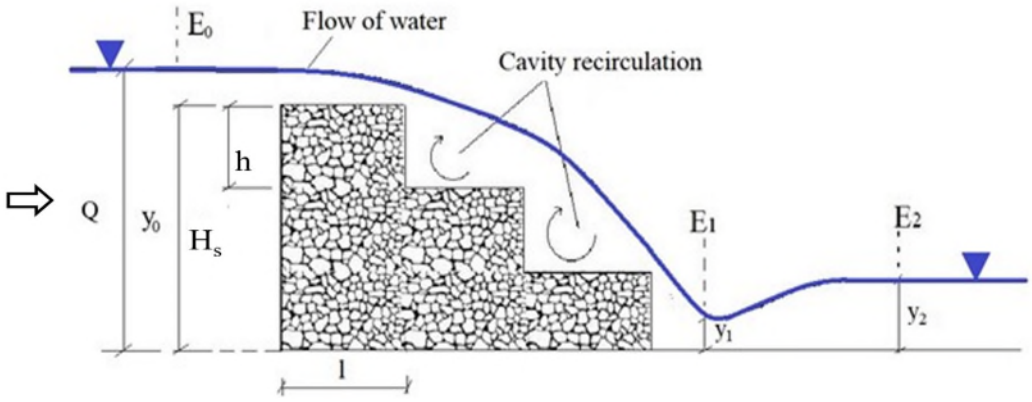

Figure 1.4 Hydraulic dimensions sketch of gabion stepped spillway

1.4 Soft computing techniques

Soft computing models such as Artificial Neural Network (ANN), Adaptive Neuro-Fuzzy Inference System (ANFIS) and Extreme Learning Machine (ELM) are used to predict energy dissipation.

Artificial neural network (ANN)

ANNs are powerful tools in machine learning and artificial intelligence, capable of handling complex, non-linear relationships in diverse scientific fields. It mimics how neurons work in the human brain. ANNs use self-adjusting learning algorithms which are fully linked, multilayer neural networks consisting of an input layer, a few hidden layers, and an output layer make up an ANN **(Basheer and Hajmeer 2000)**. Every node in a layer is linked to every other layer's node. Data collection, data preprocessing, network building, training, and model testing are the systematic steps followed in neural networking **(Dongare et al. 2012)**.

Adaptive neuro-fuzzy inference system (ANFIS)

ANFIS or Adaptive Neuro-Fuzzy Inference System is a hybrid intelligent system **(Walia et al. 2015)** that combines the benefits of neural networks and fuzzy logic. It relates input and output parameters which convert data inputs into fuzzy values using membership functions. ANFIS effectively manages uncertainty and imprecision in data, making it suitable for real-world applications. It can adapt its parameters based on training data, allowing it to improve performance. With properly configured and trained data, ANFIS can achieve high accuracy, particularly in handling nonlinear relationships and uncertain datasets.

Extreme learning machine (ELM)

Extreme Learning Machines (ELM) belong to the family of feed-forward neural networks (FFNN). They are classified as generalized single hidden layer feed-forward neural networks (SLFFNN). ELMs distinguish themselves by their unique training approach, where the hidden layer's weights are randomly assigned and remain fixed, while only the output layer weights are optimized. This allows for faster training and effective performance in various tasks, making ELMs a notable advancement in the field of neural networks. ELM suggests that introducing randomness in the selection of input weights can enhance a learning model **(Huang et al. 2004, 2006)**. This approach allows for effective training and improved performance while maintaining the integrity of the model's overall structure.

1.5 Need of the study

Energy dissipation in open channels downstream of hydraulic structures is a matter of global significance, typically achieved through a variety of structural elements. Among these, gabion stepped spillways represent a practical, easily constructible and cost-effective solution. However, in recent years, their application has been largely overlooked in favour of more complex and artificial structures. Given their inherent advantages, there is a need to re-evaluate and optimize gabion stepped spillways to enhance their energy dissipation performance.

By introducing various arrangements and modifications over the steps, the hydraulic efficiency of gabion stepped spillways can be significantly improved, offering a sustainable and economical alternative to conventional rigid spillways. Furthermore, with the integration of modern optimization approaches such as soft computing techniques, the design of gabion spillways can be refined to achieve optimal structural and hydraulic performance.

In view of above, the following arrangement needs to be explored:

- The effect of variations in gabion stone gradation and the combination of different stone porosity on energy dissipation including key hydraulic parameters.
- The impact of triangular gabion sills placed over the steps under varying downstream slopes and discharge conditions.
- The influence of obstructions placed over the steps across a wide range of discharges.
- A comparative evaluation of the suitability and effectiveness of optimized design of gabion stepped spillways in relation to standard gabion stepped spillways, for which limited studies currently exist.
- Experimental studies need to be explored using modern techniques.

These investigations aim to provide new insights into improving the hydraulic efficiency of gabion stepped spillways while maintaining cost-effectiveness and

structural simplicity, thereby reinforcing their relevance in modern hydraulic engineering practice.

1.6 Objective of the study

- To investigate the energy dissipation in a gabion stepped spillway under different flow regimes while evaluating the effects of porosity, slope and discharge.
- To investigate the effect of vertical obstructions and its various arrangements on energy dissipation in gabion stepped spillways.
- To investigate the influence of a triangular gabion sill placed on the steps of a gabion spillway on energy dissipation under various downstream slopes and discharge conditions.
- To evaluate and compare the hydraulic performance and energy dissipation efficiency of various gabion stepped spillway configurations with rigid stepped spillways under different slope conditions.

1.7 Outline of thesis

The current research work is explained in five chapters in this thesis.

1) **CHAPTER 1** gives a brief introduction to hydraulic structures, theoretical concept of energy dissipation through gabion stepped spillway, need of study, objective and scope of the present study.
2) **CHAPTER 2** presents the literature review and background studies related to experimental and soft computing techniques on gabion stepped spillway for energy dissipation.
3) **CHAPTER 3** elaborate on the methodology and approach utilized for the current study including soft computing validation.
4) **CHAPTER 4** present the results and discussions of energy dissipation through gabion stepped spillway.
5) **CHAPTER 5** conclusion drawn from the present study and scope of future research work.

Chapter 2: LITERATURE REVIEW

2.1 General

Dams and reservoirs represent one of the most effective engineering solutions for providing long-term water storage and mitigating flood risk in communities (e.g., for water supply, irrigation, hydropower generation and flood control). In many cases, multi-purpose reservoirs are constructed not only for water supply or hydropower, but also to provide flood attenuation by absorbing large water inflows during extreme rainfall events and then releasing them in a controlled manner. In order to collect water in a reservoir upstream of the structure, a dam is basically an man-made hydraulic barrier constructed across a valley or stream. During major rainfall or snowmelt events the inflow to the reservoir may increase rapidly, thereby raising the reservoir water level. If such inflows cannot be safely passed downstream or stored, the risk of overtopping the dam crest arises a condition that may lead to progressive erosion, structural instability and catastrophic failure, **Chanson (2015)**.

Therefore, dams need a spillway that allows extra water to flow out of the reservoir safely. The spillway carries excess water over, though or around the dam so that the dam itself and the areas below it does not damage during heavy rains or floods. A spillway act as a safety component of a dam. It is an hydraulic structure which may be gated or ungated that connects the reservoir to downstream channels, allowing the passage of flood waters in a controlled way. The spillway helps to ensure that reservoir levels remain within safe bounds, preventing overtopping of the dam crest and associated risks of structural failure, **Pereira (2020)**. Larger dams and reservoirs can now be built because of developments in materials, design analysis, hydrologic modelling and dam construction technologies. These developments have also increased the demand for more advanced hydraulic systems and spillway designs that can release significant flood waters without causing catastrophic damage or causing hazardous hydraulic conditions downstream.

2.2 Stepped spillway

In past, wide range of literatures are available on hydraulics of spillways which are based on theoretical, physical and mathematical investigations. This chapter tried to explore the current state of knowledge.

Sorensen (1985) done primary research for spillway by conducting a model study on a stepped ogee spillway for Monksville Dam in New Jersey to evaluate flow transition, energy dissipation and step performance. Using 1:10 and 1:25 scale physical models, the study showed that the stepped design achieved smooth flow transition and reduced toe velocities by up to 84% compared to a standard ogee spillway. The steps enhanced energy dissipation through vortex formation and air entrainment, eliminating the need for a stilling basin. Sorensen concluded that stepped spillways offer efficient and economical energy dissipation, though further research is needed to optimize step geometry and flow conditions.

Further, **Rajaratnam (1990)** analyzed the hydraulics of skimming flow over stepped spillways and proposed a method to estimate shear stress and energy loss. He identified two flow regimes, nappe flow and skimming flow and developed a theoretical method to predict shear stress and energy dissipation in the skimming regime. Using **Sorensen's (1985)** experimental data, the study estimated the fluid friction coefficient to average around 0.18, indicating high energy loss due to enhanced turbulence and momentum transfer between the skimming stream and recirculating vortices. The analysis showed that stepped spillways could dissipate up to 89% of the flow energy compared to smooth spillways. Additionally, Rajaratnam suggested a criterion for the start of skimming flow, which happens when the critical depth to step height ratio is greater than 0.8.

Chanson (1993) examined that steps enhance turbulence and air entrainment, which help reduce flow velocity and minimize cavitation damage in spillways. Two main flow regimes are identified as nappe flow and skimming flow. In nappe flow, water cascades step by step with local energy dissipation, suitable for flatter slopes and lower discharges. In skimming flow, water flows as a continuous stream over recirculating vortices between steps, common on steeper slopes and high discharges. Air entrainment plays a significant role in modifying flow characteristics. It increases

flow depth, reduces friction, and decreases the risk of surface damage. The aeration process also influences energy dissipation, particularly for steep slopes where excessive aeration may reduce overall efficiency. Despite high turbulence levels, stepped spillways remain highly effective for dissipating up to nearly all of the potential energy, reducing the need for large downstream stilling basins.

Christodoulou (1993) evaluated energy dissipation on stepped spillways under skimming flow conditions by identifying the ratio of critical depth to step height (Y_c/h) and the number of steps (N) as primary parameters governing energy loss. The results show that energy dissipation is highest for lower values of (Y_c/h) and decreases as flow depth increases, while for a given flow condition, dissipation improves with an increase in the number of steps. The study also demonstrates that stepped spillways with fewer steps exhibit lower energy dissipation compared to large, stepped configurations reported in earlier research, highlighting the importance of geometric scale**.**

Chanson (1996) predicted transition between nappe flow and skimming flow in stepped channels, which is critical for the hydraulic design of stepped spillways. The study identified that the transition is generally governed by the ratio of critical depth to step height and the chute slope and proposed empirical relationships to define skimming flow. Chanson demonstrated that nappe flow occurs at lower discharges with free-falling jets between steps, while skimming flow develops at higher discharges when the flow forms a coherent stream over step cavities. Overall, the study significantly contributed to understanding flow regime transitions and offered a reliable framework for the design and analysis of stepped spillways.

Boes et al. (2000) done experimental on skimming flow over stepped spillways, focusing on flow structure, air entrainment, velocity distribution and energy dissipation. Skimming flow is observed by a coherent stream flowing over recirculating vortices trapped within the step cavities, forming a pseudo-bottom that governs the overall flow behaviour. Significant air entrainment was observed, which increases flow depth and influences velocity profiles and turbulence characteristics. The authors highlighted that velocity distribution follows a power-law trend similar to

smooth chute flows, while the presence of steps enhances energy dissipation through turbulence and vortex interaction. Overall, their findings confirmed that stepped spillways operating under skimming flow conditions are highly efficient energy dissipators, reducing the need for downstream energy dissipation structures.

Chanson and Toombes (2002) done experiment and investigated air entrainment in transition and skimming flows on a stepped chute. It reveals that air entrainment occurs primarily at the step edges and that the flow becomes highly aerated downstream. They found that energy dissipation is closely linked to aeration, with skimming flows exhibiting lower air entrainment near the inception point compared to transition flows. The results provided essential data for understanding two-phase flow behaviour and design of stepped spillways.

Emiroglu and Baylar (2003) investigated the impact of adding an end sill at the downstream toe and aeration performance of stepped chutes. The study measured oxygen transfer efficiency under varying flow conditions and step geometries. The results showed that dimensionless parameters such as step length to step height (l/h) and end sill height to step height (s/h) significantly influence aeration efficiency. An empirical correlation was developed to predict oxygen transfer performance. The authors concluded that stepped chutes equipped with an end sill enhance air entrainment and improve dissolved oxygen levels.

Boes and Hager (2003) investigate two-phase air–water flow characteristics on stepped spillways under skimming flow conditions. The gradual development of aerated flow regions identified on the downstream and proposed empirical relationships to predict key hydraulic parameters. A power-law velocity profile was also introduced to describe the vertical distribution of velocity in aerated flows. The study emphasizes the significant role of air–water interactions in enhancing turbulence and energy dissipation, and its findings have been widely used for validating numerical models and experimental investigations in stepped spillway hydraulics.

Boes and Hager (2003) also done experimental study on the hydraulic design of stepped spillways using a large-scale model to analyze two-phase skimming flow behaviour. The research established that the onset of skimming flow depends on the

16 ratio of critical depth to step height and chute angle, while flow resistance is significantly higher than in smooth spillways due to step-induced macroroughness. Empirical relationships were developed for predicting uniform flow depths, friction factors, and the length required to achieve uniform flow. The study also quantified energy dissipation efficiency, showing that stepped spillways effectively reduce residual energy, thus minimizing stilling basin requirements. Additionally, design guidelines were proposed for determining training wall heights considering aeration and flow bulking. Overall, the paper provides a comprehensive framework for the hydraulic design of stepped spillways, reducing the need for individual physical modelling.

Yasuda et al. (2004) experimentally investigated the flow characteristics of skimming flow in a stepped channel. The study focused on velocity distributions, energy dissipation and flow resistance under skimming flow conditions. Results showed that the main flow region remains relatively uniform, while significant turbulence and energy loss occur in the recirculating cavity regions behind each step. The authors found out the relation between step geometry, Froude number, and energy dissipation efficiency, demonstrating that skimming flow on stepped chutes achieves substantial energy reduction compared to smooth chutes.

Chinnarasri and Wongwises (2006) investigates flow regime and energy dissipation over stepped chutes with varying geometrical configurations and observed that energy dissipation is strongly influenced by step geometry and flow conditions, with skimming flow exhibiting higher dissipation efficiency due to the formation of recirculating vortices within the step cavities. The study also highlights the transition between flow regimes as a critical factor affecting hydraulic performance. It helps to contribute to a better understanding of flow behaviour and optimizing step design to enhance energy dissipation and overall spillway efficiency

Emiroglu and Baylar (2006) compared self-aeration characteristics in smooth and stepped chutes with effects of chute slope, step geometry, and flow discharge on air entrainment inception point and downstream aeration efficiency. Results indicated that stepped chutes initiate air entrainment at lower flow velocities and achieve higher

aeration efficiency compared to smooth chutes due to enhanced turbulence and flow disruption at step edges. The authors proposed empirical relationships linking aeration efficiency to step dimensions and Froude number, demonstrating that stepped chutes are more effective for oxygen transfer applications in hydraulic engineering.

Gonzalez et al. (2008) experimentally examined the effects of step roughness on skimming flows over stepped chutes. By adding roughness elements to step surfaces, they compared flow properties including velocity profiles, air entrainment and energy dissipation with smooth steps. Results showed that increased step roughness enhances near boundary mixing and turbulence, leading to higher energy dissipation rates and earlier air entrainment inception compared to smooth steps. The study demonstrated that step roughness can be a practical design consideration for improving energy dissipation performance in stepped spillways under skimming flow conditions.

Chafi et al. (2010) investigated the flow configurations and energy dissipation rates on a reduced scale physical model of a stepped spillway. The results confirm that, compared to smooth chutes, stepped spillways significantly enhance energy dissipation due to step-induced macro-roughness, which is particularly effective for steep slopes and high-flow conditions.

Felder and Chanson (2011) studied about the air–water flow characteristics within step cavities of stepped spillways, which play a crucial role in energy dissipation. The authors found that intense air entrainment and recirculating vortices within the step cavities significantly enhance energy dissipation and flow aeration. The study also highlights the complex interaction between the air and water phases, showing that cavity flow properties vary with discharge and step geometry. These observations are consistent with later research, such as **Hubert Chanson (2022),** which emphasizes that stepped spillway flows are characterized by highly turbulent, self-aerated multiphase conditions and complex flow regimes, making their hydraulic design challenging. This gives fundamental basis for understanding multiphase flow mechanisms in stepped spillways and supports improved design for effective energy dissipation and cavitation control.

Felder and Chanson (2013) conducted a laboratory study on pooled stepped spillways for embankment dams, comparing their performance to conventional flat-step designs on 8.9° and 26.6° slopes. Under both transition and skimming flows, the research analyzed flow patterns, air-water flow properties (velocity, bubble count, turbulence), and energy dissipation. While the pooled steps enhanced flow aeration, they also introduced significant low-frequency flow instabilities and, particularly on the steeper slope, resulted in higher residual energy compared to the flat-step configuration. The study concluded that for the embankment dam slopes tested, the conventional flat-step design is more efficient and provides more stable and reliable hydraulic performance than the alternative pooled design.

Guenther et al. (2013) experimentally compared flat and pooled stepped spillways for embankment dams, focusing on air entrainment, cavity flow processes, and energy dissipation. The study used a large-scale physical model with a slope of 8.9° and step height of 0.10 m, testing both flat steps and pooled steps (with transverse end sills). Results showed that pooled steps significantly increased air entrainment and flow instabilities, including low-frequency fluctuations (0.5–2 Hz), which could compromise structural safety. While pooled steps enhanced energy dissipation at low flows, flat steps provided more stable hydraulic performance and higher energy dissipation at higher flow rates. The authors concluded that flat stepped spillways remain the preferred design for embankment dams due to their reliability and consistent dissipation efficiency.

Felder and Chanson (2014) also assessed the impact of introducing wall porosity into pooled stepped spillways, using a 26.6° slope and comparing designs with three levels of step porosity to a conventional flat-step configuration. Their results indicated that while porous walls reduced flow instabilities, they also diminished form drag, leading to residual energy levels that were approximately 1.5 to 2 times higher than on the flat-step design. Further, study concluded that the flat step configuration remains the most advantageous for achieving optimal energy dissipation performance and flow stability.

Mero and Mitchell (2017) done experiment investigated the hydraulic performance of stepped spillways with a moderate slope of 26.6° for discharges up to 0.0121 m^3/s. Several new step layouts, including inclined and horizontal curved steps with and without reflector blocks, were tested. While ensuring strong agreement with earlier results for horizontal steps, the inclined and curved step designs dissipated almost twice as much energy as standard horizontal steps.

Zhang and Chanson (2018) found out the effects of step and cavity geometry on the aeration and energy dissipation performance of stepped chutes. Testing a 45° chute with uniform triangular steps, partially blocked cavities, and chamfers, they found that sharp edges enhance aeration, while chamfers reduce friction factor but also lower flow stability. The study reveals aeration and energy dissipation, suggesting that sparsely spaced sharp edges on 30–45° slopes offer the best overall performance.

Torabi et al. (2018) experimentally investigated the effect of step surface roughness on the energy dissipation performance of stepped spillways. The stair surfaces were roughened in two distinct manners: uniformly (using sand with a predetermined grain size) and discretely (using small blocks with predetermined dimensions). The results demonstrated that, under nappe flow conditions, roughening the steps increased energy dissipation by approximately 15–20% compared to smooth stepped spillways. Furthermore, uniform roughness was found to be more efficient than discrete roughness in enhancing energy dissipation.

Parsaie et al. (2019) did a hydraulic investigation of the circular crested stepped spillway (CCSS) including stage-discharge relation, discharge coefficient (C_d), and their energy dissipate capacity. The laboratory models of the circular crested stepped spillway have a height of 0.3 meters and the crest's radius was 0.06 m. The chute's slope (V: H) was 1:1.25, 1:1, and 1:0.75. There were three, five and seven steps. The models were made of concrete. The analysis of the results showed that the C_d of CCSS ranged between 0.9 and 1.4, taking into account the range of the upstream head between 0.3 and 2.1. The ratio of the flow head to the crest radius was the most effective parameter on the C_d. Based on the theory of supercritical flow and the analyzed results, the geometric properties had no significant effect on C_d. An analysis

of the CCSS's energy dissipation capability revealed that it could dissipate between 90 and 40% of the flow's energy, while a typical spillway (smooth chute) could dissipate between 60 and 5% of the flow's energy in the same discharge range. Increasing the number of steps at a given slope (decreasing the size of steps) would reduce the performance of the CCSS concerning energy dissipation. Increasing the slope of the stepped chute at a given number of steps can reduce the hydraulic efficiency of CCSS in terms of energy loss.

Ashoor and Riazi (2019) investigated the performance of stepped spillways for energy dissipation, highlighting their advantage over conventional smooth spillways in reducing downstream erosion through enhanced turbulence, air entrainment and flow recirculation. Earlier studies have mainly focused on uniform stepped configurations, showing that parameters such as step height, length, slope, and discharge significantly influence flow regimes and energy loss. Experimental research indicated that energy dissipation increases with the number of steps and depends on the ratio of critical depth to step height. However, limited investigations on non-uniform stepped spillways have reported inconsistent findings regarding their effectiveness compared to uniform designs. Using computational fluid dynamics (CFD), methods such as the Volume of Fluid (VOF) technique combined with k–ε turbulence models have been widely used to simulate complex air–water flows with good accuracy. Despite these developments, the optimization of non-uniform and hybrid step configurations for maximizing energy dissipation remains an important area for further research.

Ali and Yousif (2019) investigates the hydraulic behaviour of flow over stepped spillways with transversely sloped steps and observed that transverse step configurations modify the flow structure by enhancing lateral mixing and turbulence, which contributes to increased energy dissipation compared to conventional horizontal steps. The study also highlights changes in flow regimes and air entrainment characteristics due to the altered geometry. These findings provide useful insights for improving stepped spillway design by incorporating transverse slopes to achieve better hydraulic performance and dissipation efficiency.

Almeland et al. (2021) studied air entrainment modelling in stepped spillways and pointed out problems with current CFD based methods, mainly the inability to handle grid sensitivity and make accurate predictions of when aeration will start. The study built on earlier work by Lopes et al. (2017) and Hirt and Nichols (1981) by looking at better ways to find interfaces and predict where they will start. The findings showed that boundary-layer-based criteria make more accurate and reliable predictions than standard energy-based approaches.

Chanson (2022) investigates air entrainment mechanisms in stepped spillway prototype operation, with a focus on skimming flow conditions. The study highlights that air entrainment is primarily driven by strong turbulence and shear instabilities at the free surface, leading to continuous air ingestion into the flow. It also emphasizes the role of step geometry and flow conditions in controlling the onset and development of self-aeration. The findings improve the understanding of aerated flow behaviour in prototype-scale spillways and contribute to more accurate prediction of air concentration, energy dissipation, and cavitation resistance in hydraulic design.

21 **Salmasi and Abraham (2022)** investigated the effect of spillway slope on energy dissipation in stepped spillways. The research employs experimental analysis to evaluate how varying chute slopes affect flow behaviour and hydraulic performance. The results indicate that steeper slopes generally enhance energy dissipation due to increased turbulence, flow aeration, and step cavities under skimming flow conditions. The authors conclude that optimizing slope is essential for improving spillway performance, as inappropriate slopes may reduce dissipation efficiency or lead to unfavourable flow regimes. This work contributes to a better understanding of geometric influences on stepped spillway hydraulics and supports the development of more efficient and economical spillway designs.

Dah-Mardeh et al. (2023) conducted study to investigate local scour downstream of a stepped spillway. To assess the impact of hydraulic and sediment 12 factors on the resulting scour hole, laboratory tests were conducted under five flow discharges, three tail-water depths, and two sediment sizes. The results indicated that 12 scour dimensions decrease with increasing sediment size and tail-water depth and with

decreasing particle Froude number and critical depth. Specifically, reducing Froude number led to a 68.6% reduction in relative scour depth, a 75.6% reduction in the relative distance of maximum scour depth and a 73.4% reduction in relative scour length. Based on experimental data, regression-based empirical equations were also developed to estimate scour parameters by offering practical predictive tools for stepped-spillway design.

Salmasi and Abraham (2023) conducted a case study on the hydraulic characteristics of flow over stepped and chute spillways at Zirdan Dam, Iran. Using physical model experiments, they compared energy dissipation, flow velocity and pressure distributions between the two spillway types under various discharge ranges. Results showed that the stepped spillway significantly outperformed the conventional chute spillway in means of energy dissipation, reducing downstream velocity and minimizing scour potential. The step geometry and Froude number also provide the practical design recommendations for dam on hydraulic performance.

Daneshfaraz et al. (2024) investigated hydraulic jump characteristics and energy dissipation downstream of stepped spillways with rough steps, showing that increased step roughness enhances turbulence, improves energy dissipation, and significantly influences flow structure and air entrainment behaviour in the downstream region.

Chanson (2026) provides important insights into high-velocity free-surface flows by examining self-aeration and surface turbulence characteristics in a huge dam spillway with a smooth converging chute. According to the study, self-aeration starts when turbulence adjacent to the free surface gets powerful enough to overcome gravity and surface tension, resulting in considerable air–water mixing. It also demonstrates that surface turbulence plays a critical role in governing aeration rates, flow bulking, and energy dissipation. This work contributes to a deeper understanding of air–water flow mechanisms in spillways and supports improved hydraulic design by emphasizing the importance of turbulence-driven aeration in high-speed chute flows.

Table 2.1 Key Development of research and innovation in stepped spillways (1985-2026)

Author(s)	Innovation	Main Findings	Development Impact
Sorensen (1985)	Hydraulic model study on stepped spillways	Demonstrated that stepped chutes dissipate substantially more energy than smooth spillways, provided base experimental data	Re-established research interest in stepped spillways after decades gives foundation for modern studies
Rajaratnam (1990)	Identification of flow regimes	Distinguished nappe, transition and skimming regimes and showed dependency on geometry and slope	Provided the conceptual basis for flow-regime used in later designs
Chanson (2002)	Comprehensive monograph	Summarized governing parameters: step geometry, slope, aeration, cavitation	Bridged theory and engineering practice
Hager (2003)	Practical design equations	Proposed relationships for friction factor and residual head losses; validated for different slopes	Enabled safe, economical designs; adopted in many dam-design manuals
Chanson & Felder (2011)	Large-scale pooled stepped spillway experiments	Quantified turbulence, aeration, and residual energy; confirmed high dissipation efficiency	Provided design data for high-discharge RCC and embankment dams

Ashoor & Riazi (2019)	Non-uniform (variable) step lengths	Semi-uniform (1:3) step length ratio improved dissipation by 20 % over uniform steps	Demonstrated geometry optimization beyond uniform designs
Chanson (2026)	Large dam spillway with smooth converging chute	Self-aeration is initiated when turbulence near the free surface becomes strong	Air–water flow mechanisms in spillways supports improved hydraulic design

2.3 Gabion stepped spillway

A gabion stepped spillway is a type of spillway which is composed of wire mesh baskets containing rocks situated in steps ascending along the slope of the spillway. This design is rather efficient in energy dissipation as it creates turbulence when the water mass flows over the steps and through the matrix of the gabion. They are effective where the construction of the concrete structure is costly or impossible and the site is more natural.

Sharp (1987) presents a practical field evaluation of gabion drop structures constructed by Alberta Environment. Based on site inspections using a dedicated appraisal form, the paper highlights key design considerations and operational issues. It concludes with recommendations that led to improvements in the design and construction of such permeable hydraulic structures, underscoring the value of systematic performance assessments

Peyras et al. (1992) examined hydraulic and energy dissipation characteristics of stepped gabion weirs which were deployed in locations such as in the African Sahel. The authors analyzed flow regimes, energy dissipation and gabion deformation using one-fifth-scale physical models (Froude similitude) representing prototypes up to 5 m high and discharges up to 3 $m^3/s/m$. The study provides empirical design equations for stilling basins showing that stepped gabion spillways can safely handle flows up to 3

53

$m^3/s/m$ and reduce basin length by 10-30% compared to conventional slope weirs or vertical drops.

Pagliara and Chiavaccini (2006) done experiment to investigate energy dissipation on gabion stepped spillways, focusing on the effects of step geometry, flow rate, and gabion porosity. Unlike solid stepped spillways, gabion steps allow flow percolation through the rockfill, which alters the energy dissipation mechanism. Results showed that gabion stepped spillways achieve significantly higher energy dissipation than solid steps, particularly under low specific flow rates, due to additional internal flow resistance and enhanced turbulence. The study also proposed empirical relationships linking energy dissipation to critical depth, step height, and gabion characteristics, providing design guidance for this environmentally friendly spillway type.

Chinnarasri et al. (2008) carried out research on the hydraulic properties of gabion stepped weirs for energy dissipation using steep slopes. The author experimentally studied flow through and over gabion-stepped weirs with slopes of 30°, 45°, and 60°. They identified two flow components: base flow through stone voids and surface overflow. Compared to horizontal stepped weirs, gabion-stepped weirs showed 7-14% higher energy dissipation (increasing with slope) and 29% lower maximum mean pressure on step faces due to the cushioning effect of the stones. Stone size and shape had minor effects on energy loss, while void ratio influenced pressure and dissipation. The study provides empirical equations for energy loss, outlet velocity, and pressure distribution in skimming flow.

Mohamed (2010) investigated the hydraulic performance of gabion weirs and focused on flow characteristics and discharge coefficients. The study tested gabion weirs with different porosities and step configurations under various flow conditions. Results showed that gabion weirs exhibit higher energy dissipation and lower downstream velocities compared to solid weirs due to flow permeability through the rockfill. The discharge coefficient was found to increase with weir height and porosity, while the nappe flow regime dominated at low heads. The study provided empirical

relationships for estimating discharge coefficients, demonstrating the effectiveness of gabion weirs as energy dissipating structures in hydraulic engineering applications.

Salmasi et al. (2012) experimentally investigated energy dissipation in low-height stepped gabion spillways having three steps, 0.10 m each with slopes of 1:1 and 1:2, porosities of 38-42% and four configurations as fully pervious, horizontal impervious plates, vertical impervious plates and fully impervious. The results showed that at high discharges, pervious configurations dissipated more energy than impervious ones, while the opposite occurred at low discharges. Vertical impervious plates enhanced dissipation more than horizontal plates due to flow impingement. Increasing porosity slightly increased energy dissipation, and milder slopes (1:2) yielded greater dissipation than steeper slopes (1:1). Findings agreed well with Peyras et al. (1992) and Kells (1994) but showed lower dissipation than Chinnarasri et al. (2008) due to differences in spillway height and gabion placement.

Ramli et al. (2013) investigated the stability of gabion walls used as scour-arresting devices for earth retaining structures in flood-prone areas. Physical model tests compared conventional rectangular (stack-and-pair) gabion walls with an interlocking hexagonal gabion design under incremental soil-hydrostatic loading. The hexagonal configuration exhibited significantly lower lateral deformation, more controlled displacement, and reduced shear failure susceptibility, particularly in the critical zone between 0.35 and 0.55 times of wall height. The interlocking design overall shows better structural integrity than conventional box gabions, suggesting as an improved scour protection system for bridge abutments and piers.

Wüthrich and Chanson (2014) done experiment using a laboratory setup with a 26.6° slope (1V:2H) and 0.10 m step height gabion stepped weirs, focusing on flow patterns, air-water flow properties, and energy dissipation and compared gabion steps against smooth impervious steps. Visual observations revealed that seepage flow through the gabions modified cavity flow dynamics, particularly under skimming flow conditions. In comparison to the impermeable stepped chute, the gabion arrangement in skimming flows led to lower friction factors, lower energy dissipation rates, and higher downstream velocities.

Al-Mohammed and Mohammed (2015) experimentally investigated the hydraulic behavior of gravel-filled gabion weirs, focusing on the combined flow passing over the crest and through the porous rockfill. They used six physical models with varying downstream slopes and rockfill materials, examined water surface profiles, overflow velocity distributions, and the ratio of through-flow to total flow. The findings indicated that milder downstream slopes produce higher water levels and velocities, while increased porosity from 0.38 to 0.42 resulted in approximately a 27% increase in through-flow. The research also developed four novel empirical relationships for estimating through-flow and overflow ratios, highlighting the complex flow dynamics in gabion structures which offer both energy dissipation and enhanced discharge capacity compared to conventional solid weirs.

Zhang and Chanson (2016a) focused on the complex interactions among free-surface flow, cavity recirculation and seepage flow through the porous rockfill. The study showed that seepage flow significantly modifies the main flow characteristics by reducing cavity turbulence and altering pressure distributions, leading to lower energy dissipation compared to solid stepped spillways. The authors identified distinct flow regimes providing insights into the hydraulic performance of gabion steps for river restoration applications.

Zhang and Chanson (2016b) examined the developing flow region of stepped spillways under skimming flow conditions through physical modelling. The study quantified boundary layer development, velocity profiles, and turbulence intensity from the inception point to the fully developed region. Results showed that step-induced macroroughness accelerates boundary layer growth, with the apparent origin of the turbulent boundary layer located upstream of the step edge. Empirical relationships were proposed for predicting boundary layer thickness and energy dissipation in the developing region, contributing to improved hydraulic design of stepped spillway.

Rajaei, Khodashenas, and Esmaili (2017) conducted a laboratory analysis of energy losses in gabion stepped spillways, specifically examining the influence of upstream sedimentation on hydraulic performance. The study found that the presence

of sediment upstream significantly reduced energy dissipation efficiency by altering flow patterns and causing partial blockage of the porous gabion steps. Under clear-water conditions, the gabion stepped spillway achieved substantial energy losses due to increased flow resistance and turbulence generated by the step geometry. However, sedimentation led to a notable decrease in energy dissipation, with the most pronounced effects observed at lower flow rates where sediment accumulation was more extensive. This research highlighted the vulnerability of gabion stepped spillways to upstream sedimentation and underscored the need for regular maintenance to preserve their energy dissipation capacity in practical applications.

Salmasi and Sattari (2017) developed an M5 model tree to predict the discharge coefficient of rectangular broad-crested gabion weirs based on experimental tests on eight physical models with different porosities. They found that the average Cd was 0.66 in free flow and 0.53 in submerged flow, with porosity having a more pronounced effect at low discharges. The M5 tree model yielded 12 piecewise linear equations, achieving a correlation coefficient of 0.95 and an RMSE of 0.036, demonstrating that data-mining techniques can provide an accurate and interpretable representation of gabion weir hydraulics.

Aal et al. (2019) investigated the hydraulic performance of two permeable gabion structures having conventional stepped gabion spillway and a newly proposed buttress gabion spillway. The buttress design incorporates support walls to increase the maximum allowable head. The study found that both energy dissipation and the discharge coefficient increase with larger rockfill particle sizes. However, increasing the number of buttress walls was shown to reduce both the energy dissipation and the discharge coefficient. Furthermore, as the Froude number increases, the relative energy loss reduces for a constant particle size. These findings provide insights for optimizing gabion spillway design.

51

Jalil et al. (2019) experimentally investigated the influence of gravel size and weir height on the flow properties of gabions in an open laboratory flume, focusing on the upstream flow depth across different flow regimes. Testing four gabion heights and four aggregate sizes, they found that increasing material coarseness and discharge

reduced the relative flow depth by 17-38% under through-flow conditions. In the transition regime, these factors led to average decreases of 7.6% and 4.4% for 15 cm and 30 cm gabion heights, respectively. The gabion began functioning as an overflow weir when the average water depth reached 1.19 times its height, yielding a 15% average discharge increase compared to a solid weir.

Rajaei et al. (2020) experimentally compared energy dissipation in short stepped gabion spillways having three steps and 1:1 (V:H) side slope, with equivalent rigid spillways under nappe flow. Models were built at 1:5 scale (step height 20 cm, stone diameter 4-8 cm). Increasing the number of steps improved dissipation, with the second step providing a greater increase than the third. Energy dissipation decreased with increasing discharge (or drop number) for both gabion (overflow) and rigid models but increased for throughflow-only conditions.

Shariq et al. (2020) derived an improved discharge equation for gabion weirs operating under through-flow (non-overflow) conditions. Through a series of laboratory experiments, they found that Ergun's equation predicted the hydraulic gradient in the highly porous boulder-filled material more accurately than other existing relationships. By extending Ergun's equation, they developed a new discharge equation validated with their experimental data, achieving a correlation coefficient of 0.956, an RMSE of 0.002, and a MAPE of 16.9%, with almost all discharge predictions falling within a ±10% error. A sensitivity analysis revealed that discharge is more sensitive to boulder diameter and upstream depth than to downstream depth, providing a practical and environmentally friendly design alternative for flash flood mitigation.

Zuhaira et al. (2021) performed a numerical investigation to examine skimming flow characteristics over non-uniform gabion-stepped spillways (GSS). Using the Reynolds-averaged Navier-Stokes (RANS) approach with the software NEWFLUME, the study focused specifically on the inception point location where aerated flow becomes fully developed. The numerical predictions were compared with existing empirical formulas, leading to the development of two new equations via nonlinear multiple regression (NMR) and evolutionary polynomial regression (EPR).

The EPR model achieved R^2 values of 0.93 (training) and 0.83 (testing), outperforming the NMR approach ($R^2 = 0.91$).

Salmasi et al. (2021) determines the discharge coefficients for rectangular broad-crested gabion weirs in a free-flow condition. The study examined the effects of weir height, porosity and flow rate on discharge behaviour, showing that the discharge coefficient increases with weir height and porosity but decreases with increasing upstream head.

Shariq et al. (2022) investigated the effects of weir height, porosity, and downstream submergence on discharge coefficients and flow behaviour in an experiment conducted across gabion weirs under both free and submerged flow conditions. The result shows that the discharge coefficient decreases with increasing submergence and is significantly influenced by weir porosity and height. Under submerged conditions, energy dissipation remains substantial due to percolation through the rockfill. Empirical relationships were developed for predicting discharge coefficients under free and submerged regimes, providing gabion weir applications in flood control and river engineering.

Hasanian Shirvan et al. (2023) experimentally examined the hydraulic performance of gabion broad-crested weirs (GBCWs) under upstream partial blockage caused by sedimentation. Using 147 free-flow tests with five blockage levels (0%, 25%, 50%, 75% and 100% of weir height), they found that increasing blockage reduces the discharge coefficient (C_d). Changes in C_d are minor for blockages below 25% but decrease significantly when blockage exceeds 50%. As blockage increases, the influence of the filling-material size on C_d diminishes. Finally, a non-linear regression equation was developed to estimate the discharge coefficient under partial-blockage conditions.

Alabas et al. (2023) experimentally studied gabion stepped weirs with different slopes (1:1, 1:2 and 1:3) and rockfill porosities (0.38, 0.42). Milder slopes (1:3) increased water surface and overflow velocity compared to steeper slopes. Higher porosity (0.42) raised through-flow ratio by 27%. Four regression equations were

developed to estimate throughflow and overflow ratios with high accuracy (R^2 up to 0.98), providing novel predictive tools for gabion stepped weir design.

Shirvan et al. (2025) addressed a key operational challenge for porous gabion weirs—upstream partial blockage from sediment by evaluating multiple methods to predict the discharge coefficient. Using 140 experimental data points, they compared the machine learning model CatBoost against gene-expression programming (GEP) and standard nonlinear regression (SNR). CatBoost achieved the highest accuracy (training $RMSE = 0.002$, $R^2 = 0.999$; testing $RMSE = 0.003$, $R^2 = 0.996$) with prediction errors below 3%, followed by GEP and SNR. The study demonstrates that advanced machine learning can reliably estimate the discharge coefficient of partially blocked porous weirs, offering a practical tool for assessing hydraulic performance under sediment-prone conditions.

2.4 Soft computing techniques

There is much more use of physical modelling in practical aspects of hydraulic engineering. However, soft computing and machine learning methods have been actively used to model complex processes of hydraulics. Moreover, the literature combines high level data-driven and modelling techniques, such as artificial neural networks (ANN), adaptive neuro-fuzzy inference systems (ANFIS) and extreme learning machines (ELM) to compare and forecast energy dissipation, which improves the outcomes. The findings provide practical design considerations for optimizing stepped spillway design configurations to achieve improved energy dissipation and overall hydraulic efficiency. **Kecman (2001), Wang and Fu (2005)** present a systematic integration of computational intelligence techniques into the data mining process.

Basheer and Hajmeer (2000) provided fundamental concepts, computational principles, network design considerations, and practical applications on artificial neural networks (ANN). It includes neuron models, activation functions, feedforward and recurrent architectures and supervised learning algorithms such as backpropagation. It also consists key data preprocessing, selection of hidden layers and neurons, initialization and overfitting prevention. The authors also surveyed

diverse applications of ANNs in classification, regression, and pattern recognition across various fields.

Kisi (2004) demonstrated the application of artificial neural networks (ANNs) for river flow modelling, specifically predicting daily flow rates. Using a feedforward backpropagation network with different input combinations (previous flow and rainfall data), the study compared ANN performance against conventional multiple linear regression and autoregressive moving average models. Results showed that ANNs significantly outperformed traditional methods in capturing the nonlinear hydrological relationships, achieving higher prediction accuracy and lower error metrics. This work reinforced the potential of soft computing techniques for time-series forecasting in water resources engineering.

Yuhong and Wenxin (2009) used an artificial neural network (ANN) to forecast the open channel flow friction factor, which is a crucial parameter for estimating hydraulic resistance. Using experimental data, they developed a three-layer feedforward ANN with the Levenberg Marquardt training algorithm, taking Reynolds number and relative roughness as inputs. The ANN model demonstrated high accuracy in predicting friction factors across a wide range of flow conditions, outperforming traditional empirical formulas such as the Moody chart and Colebrook equation. This study highlighted the capability of neural networks to capture complex nonlinear relationships in hydraulic resistance, offering an efficient alternative for friction factor estimation in open channel design and analysis.

Dongare et al. (2012) provided introduction to artificial neural networks (ANNs), covering their biological inspiration, basic architecture and learning mechanisms. It explained the structure of artificial neurons, activation functions, network topologies (feedforward and recurrent) and training algorithms including supervised, unsupervised, and reinforcement learning. The authors also propose diverse applications of ANNs in pattern recognition, function approximation, control systems and prediction tasks. This work serves as a useful primer for researchers new to neural network methodologies in engineering disciplines.

Khatibi et al. (2014) utilized gene expression programming (GEP), artificial neural networks (ANN) and multiple regression analysis. in modelling the dissipation of energy through the gabion stepped weir using experimental data and indicated that the ANN models delivered better results with relatively high prediction.

Parsaie et al. (2018) compared four soft computing techniques as artificial neural network (ANN), support vector machine (SVM), multivariate adaptive regression splines (MARS) and group method of data handling (GMDH) to simulate and forecast energy dissipation through stepped spillways. Input parameters included Froude number, drop number, step geometry and critical depth ratio. MARS performed best (R^2 = 0.999, RMSE = 0.65 in testing), followed by SVM (R^2 = 0.98, RMSE = 2.61). GMDH and ANN also showed acceptable accuracy. The study identified Froude number and drop number as the most influential parameters. MARS and SVM are recommended for reliable energy dissipation modelling.

Parsaie and Haghiabi (2019) employed evolutionary computing to predict energy dissipation in stepped spillways, comparing an M5 model tree algorithm with a multilayer perceptron neural network (MLPNN). Using data from reliable sources, the M5 algorithm achieved excellent predictive accuracy in both training ($R^2 = 0.99$, RMSE = 2.48) and testing ($R^2 = 0.99$, RMSE = 2.23), slightly outperforming the MLPNN model. The analysis identified the Drop number and Froude number as the most influential parameters for modelling energy dissipation. The study demonstrates that evolutionary computing techniques provide reliable and precise tools for estimating energy dissipation in stepped spillway design

Takagi & Sugeno (1985) introduced the Takagi-Sugeno fuzzy model, where each rule's consequent is a linear function rather than a fuzzy set. This allows efficient modelling of nonlinear systems by interpolating local linear models. This model is widely used in control and hydraulic engineering.

Jang (1993 & 1996) proposed an easy and fast approach toward input selection in neuro-fuzzy modelling based on ANFIS (Adaptive Neuro-Fuzzy Inference System). Hence, the two main learning models that ANFIS consists of, the fuzzy logic and the

neural network. In the past decades, ANFIS has been used for modelling and identification of systems, and the results have been found satisfactory.

Wang and Fu (2005) focused on data mining with computational intelligence, that examines the application of fuzzy neural networks (FNNs) to bioinformatics. This chapter specifically addresses the inherent challenges of biological data such as noise, high dimensionality, and non-linearity and argues that the synergy of fuzzy logic and neural networks offers a superior approach for analysis. The authors detail architecture and learning algorithms for FNNs, demonstrating, likely through case studies, their effectiveness in tasks like gene expression analysis and protein structure prediction. This work is significant for establishing a framework that not only provides predictive accuracy but also maintains the interpretability of fuzzy rules within a robust learning system.

Baylar et al. (2007) used adaptive neuro-fuzzy inference system (ANFIS) to model aeration efficiency of stepped cascades from a laboratory model, they considered dimensionless parameters such as the Froude number, step height to critical depth ratio, and number of steps as inputs. The ANFIS model accurately predicted aeration efficiency, outperforming traditional regression methods with higher correlation coefficients and lower error metrics.

Vasant and Bhattacharya (2007) introduced a modified flexible S-curve membership function to capture the degree of fuzziness in multi-criteria decision-making (MCDM) models. This allows decision-makers to adjust the shape of the membership function based on sensitivity and uncertainty levels in real-world industrial problems, such as production planning. By varying the fuzziness parameters, the model provides more flexible and realistic solutions compared to conventional linear or fixed membership functions.

Hanbay et al. (2009) studied intermediate flow conditions in stepped chutes where the case was analysed with the help of the Adaptive Network Based Fuzzy Inference System (ANFIS). The cross-validation of the model was done using three-fold cross-validation in order to achieve an accuracy of 99.01%. The results further

demonstrated the applicability of the suggested ANFIS model for precise hydraulic process control.

Salmasi and Ozger (2014) examined the hydraulics of stepped spillways using mathematical models and laboratory tests involving the application of neuro-fuzzy models. They concluded that the neuro-fuzzy approach provides more accurate predictions for energy dissipation compared to traditional regression methods.

Walia et al. (2015) studied the adaptive neuro-fuzzy inference systems (ANFIS), a hybrid intelligence mechanism that combines fuzzy logic's capacity for processing with neural networks' capacity for learning. It includes fundamental architecture of ANFIS, its learning algorithms (hybrid learning combining backpropagation and least squares estimation) and various membership functions. The authors highlighted ANFIS's advantages including faster convergence, better interpretability and adaptive rule extraction from data. This approach serves as a useful reference for researchers seeking to apply ANFIS in various hydraulic and environmental modelling.

Roushangar et al. (2017) employed neural networks and adaptive neuro-fuzzy inference systems (ANFIS) to identify the most effective parameters affecting energy dissipation over stepped spillways under the nappe flow regime. Using experimental data, they analysed input variables including the Froude number, step height to critical depth ratio, number of steps, and spillway slope. The models successfully ranked the relative importance of each parameter, revealing that the Froude number and step geometry exert the strongest influence on energy dissipation efficiency.

Gerger et al. (2017) applied five data-driven models—feed-forward neural networks (FFNN), radial basis neural networks (RBNN), generalized regression neural networks (GRNN), and two adaptive neuro-fuzzy inference system (ANFIS) variants (with subtractive clustering and fuzzy c-means)—to predict the aeration efficiency of baffled chutes equipped with stepped (S), wedge (W), trapezoidal (T), and T-shaped (TS) baffle blocks. All tested soft computing methods successfully captured the oxygen transfer performance, with the FFNN model yielding the highest accuracy

overall, outperforming both the other machine-learning models and conventional regression equations.

Azimi et al. (2018) proposed a hybrid adaptive neuro-fuzzy inference system - firefly algorithm (ANFIS-FA) model to estimate the roller length of hydraulic jumps. The study considered three dimensionless input parameters as Froude number, sequent depth ratio and relative roughness. Experimental data from previous research was used for model training and testing. The findings shows that the ANFIS-FA model outperformed the standard ANFIS model, achieving a MAPE of 7.606%, RMSE of 1.771, and correlation coefficient of 0.970. All three input parameters were included, highlighting the importance of sequent depth and relative roughness for roller length prediction.

Parsaie and Haghiabi (2019c) analysed the comparisons of the proposed M5 algorithm with a multilayer perceptron neural network (MLPNN) for the estimation of energy dissipation (ED) on stepped spillways and concluded that the M5 algorithm had better prediction accuracy than the MLPNN.

Karaboga and Kaya (2019) presented a comprehensive survey of Adaptive Network-Based Fuzzy Inference System (ANFIS) training approaches, reviewing various optimization techniques and highlighting their effectiveness in improving prediction accuracy, convergence speed and applicability across complex engineering and modelling problems.

Mojtahedi et al. (2020) combined physical and numerical modelling with a fuzzy inference system (FIS) to predict energy dissipation over stepped spillways. The FIS model, using number of steps, adverse slope and critical depth to step height ratio as inputs, achieved a mean absolute percentage error (MAPE) of 7.8% and demonstrated that energy dissipation increases with more steps and steeper adverse slopes.

Yildiz et al. (2020) compared experimental, numerical (CFD) and ANFIS models for flow over an ogee spillway. Experiments were conducted for 16 total heads for that relative head (H_e/H_0) ranged 0.28 to 1.43. The CFD model solved RANS equations with RNG turbulence, while the ANFIS model used head as input and

discharge as output. Results showed good agreement among all three approaches, with ANFIS achieving RMSE = 0.23×10^{-4} and $R^2 = 0.99$. The study concluded that both CFD and ANFIS are cost-effective and reliable tools for ogee spillway design, noting that USBR theoretical values underestimate discharge at $H_e/H_0 > 1$ due to neglected approach velocity.

Nou et al. (2021) developed a hybrid ANFIS–PSO (adaptive neuro-fuzzy inference system with particle swarm optimization) model to predict the dimensions of scour holes downstream of ski-jump spillways. Using experimental data, they considered key parameters such as discharge, jet impact velocity, tailwater depth, and sediment characteristics. The ANFIS–PSO model significantly outperformed standalone ANFIS and traditional regression equations, achieving high accuracy ($R^2 > 0.96$) and low error metrics for predicting scour depth, length, and width.

Baharvand et al. (2022) analysed a stepped vertical overfall (SVO) spillway and evaluated its energy dissipation performance through physical modelling and soft computing techniques. The number of steps, dimensionless step shape, Froude number, and relative critical depth were found to be the key factors affecting energy dissipation. Laboratory experiments showed that energy dissipation of the spillway ranged from 88.53% to 98.06%, increasing gradually with relative water depth. Validation using support vector regression (SVR) and random forest regression (RFR) is done to evaluate energy dissipation, with input selection by the Gamma test. The RFR model outperformed SVR, achieving RMSE values of 0.128 and 0.115 and R^2 values of 0.99 in both training and testing stages, while SVR yielded RMSE of 0.67 and 0.61 with R^2 of 0.88 and 0.90, respectively.

Srinivas and Tiwari (2022) used soft computing models to predict the oxygen aeration efficiency (OAE_{20}) of gabion spillways, identifying porosity as the most critical parameter. After gathering data from a laboratory model, the performance of adaptive neuro-fuzzy inference system (ANFIS), backpropagation neural network (BPNN) and deep neural network (DNN) were evaluated. Among the three, the DNN model performed the best in predicting OAE_{20}, with the lowest error values (RMSE = 0.03465; MSE = 0.00121; MAE = 0.02721) and the highest correlation coefficient (CC

= 0.9757). While ANFIS and BPNN also produced comparable results, the overall findings demonstrate that deep neural networks can be a highly accurate tool for estimating the aeration performance of these permeable hydraulic structures.

Rahmanshahi et al. (2023) proposed a novel hybrid AI framework that couples an Adaptive Neuro-Fuzzy Inference System (ANFIS) with an Improved African Vultures Optimization Algorithm (IAVOA) to accurately predict energy dissipation on environmentally friendly block ramp structures. Using a dataset of 451 laboratory measurements, the hybrid ANFIS-IAVOA model (RMSE = 0.018–0.020, R^2 = 0.98) consistently outperformed standalone ANFIS and other hybrid models (e.g., with standard AVOA, HBA, GWO), demonstrating superior predictive efficiency and generalization for this challenging hydraulic application.

Sangar et al. (2024) proposed an improved ANFIS-based model predictive current control for PMSM-driven electric vehicles, demonstrating significant reduction in torque and current ripples compared to conventional methods. Experimental results demonstrated that the improved ANFIS-MPCC approach achieves smoother torque response, lower current harmonics, and better steady-state performance compared to traditional MPCC and PI-based controllers.

Huang (2003) theoretically examined the learning and storage capacities of two hidden layer feedforward networks (TLFNs). The study proved that TLFNs can learn any arbitrary set of N distinct samples with zero error, provided the number of hidden neurons is sufficiently large, and established that a two-hidden-layer architecture can achieve the same learning capability as a single-hidden-layer network while potentially using fewer total neurons. These theoretical findings provided a foundation for understanding the advantages of deeper architectures in feedforward neural networks and guided the design of network structures for practical applications.

Huang, Zhu and Siew (2006) extended their previous work on extreme learning machine (ELM) by providing a comprehensive theoretical framework and demonstrating its broad applicability. The paper rigorously proved that ELM can universally approximate any continuous target function given sufficiently many hidden neurons, and that the randomly assigned input weights and biases need not be

tuned during training. By analytically computing output weights via a Moore-Penrose generalized inverse, ELM achieves dramatically faster learning speeds (often hundreds to thousands of times faster than backpropagation) while maintaining superior generalization performance. The authors validated ELM on benchmark regression and classification problems, showing its effectiveness across diverse domains. This work established ELM as a robust and efficient alternative to traditional iterative neural network training algorithms, particularly suitable for real-time or large-scale applications.

33 **Liang et al. (2006)** developed an online sequential extreme learning machine (OS-ELM) that learns data sequentially, one-by-one, or in chunks. It updates output weights recursively without retraining, achieving fast, accurate learning comparable to batch ELM, making it suitable for real-time and large-scale applications.

67 **Huang and Chen (2008)** proposed an enhanced random search based incremental extreme learning machine (EI-ELM) to improve the original incremental ELM (I-ELM). EI-ELM includes a random search method that generates various hidden nodes at each stage and chooses the one that minimizes the residual error, whereas I-ELM randomly adds hidden nodes one at a time and freezes previously supplied parameters. This enhanced strategy leads to a more compact network architecture with fewer hidden neurons while maintaining or improving generalization performance. The authors theoretically proved that EI-ELM can still universally approximate any continuous target function and demonstrated through experiments that it outperforms I-ELM and other incremental learning algorithms in terms of convergence rate and network complexity.

18 **Rong et al. (2008)** implemented a fast pruned-extreme learning machine (P-ELM) for classification problems to address the issue of network redundancy in standard ELM, which often uses more hidden neurons than necessary. The P-ELM algorithm trains a single-hidden-layer feedforward network using the conventional ELM approach, then prunes hidden neurons with low output relevance to the target classes based on a statistical measure. This pruning process reduces network complexity, improves generalization performance, and accelerates testing speed

without retraining. Experimental results on benchmark classification datasets demonstrated that P-ELM achieves comparable or better accuracy than standard ELM and support vector machines while using significantly fewer hidden neurons, making it suitable for real-time or resource-constrained applications.

Huang, Ding, and Zhou (2010) proposed an optimization method based extreme learning machine (OM-ELM) for classification tasks to address the sensitivity of standard ELM to randomly assigned hidden node parameters. While conventional ELM randomly generates input weights and biases, OM-ELM employs an optimization procedure such as particle swarm optimization or differential evolution to determine optimal hidden node parameters before analytically computing output weights. This approach enhances classification accuracy and generalization performance, particularly for complex or imbalanced datasets.

Wang et al. (2011) found out a novel image deblurring approach using extreme learning machine (ELM) to learn optimal filters for blind deconvolution. Unlike conventional methods that require iterative optimization of the point spread function, their ELM-based framework directly learns a mapping from blurred image patches to sharp ones using a single-hidden-layer feedforward network with randomly assigned input weights and determined output weights. The learned filters effectively capture local blur patterns and restore image details. Experimental results demonstrated that the ELM-based method outperforms traditional deblurring techniques in both restoration quality and processing speed, highlighting ELM's potential for low-level vision tasks.

Lim, Lee, and Pang (2013) proposed a low-complexity adaptive forgetting factor to improve the nonstationary system estimate performance of the online sequential extreme learning machine (OS-ELM). Standard OS-ELM lacks a mechanism to discard outdated information, causing degraded accuracy when system dynamics change over time. The authors introduced an adaptive forgetting factor that selectively weights recent data more heavily, allowing the model to track time-varying characteristics without significant computational overhead. The method was validated on both synthetic and real-world nonstationary datasets, demonstrating enhanced

tracking capability and estimation accuracy compared to conventional OS-ELM and other recursive algorithms, while maintaining low computational complexity suitable for real-time applications.

Ding, Xu and Nie (2014) provided a comprehensive review of the extreme learning machine (ELM), a single-hidden-layer feedforward neural network training algorithm known for its extremely fast learning speed with better generalization performance. Unlike traditional gradient-based methods that needed iterative tuning of all network parameters, ELM uses a straightforward matrix inversion or least-squares solution to analytically calculate the output weights after randomly assigning the input weights.. The authors summarized ELM's key advantages, including minimal human intervention, avoidance of local minima, and scalability for large datasets.

Gharib et al. (2020) used modern adaptive extreme learning machine (SAELM) to model the side weir's discharge coefficient in convergent canals. Using experimental data, they considered input parameters including upstream and downstream Froude numbers, weir length to channel width ratio, and weir height to upstream depth ratio. The SAELM model demonstrated high predictive accuracy (RMSE = 0.027, R^2 = 0.976), outperforming conventional ELM and artificial neural network models. Sensitivity analysis identified the downstream Froude number as the most influential parameter. This study demonstrates that self-adaptive ELM is an efficient and robust tool for modelling complex hydraulic phenomena in non-prismatic channels.

Narwal et al. (2024) applied three machine learning models as extreme learning machine (ELM), online sequential extreme learning machine (OS-ELM), and incremental extreme learning machine (I-ELM) to predict the aeration performance of three Piano Key Weir (PKW) types (A, B, C) based on discharge, crest length, and total head. Among the models evaluated using MSE, RMSE, MAE, correlation coefficient, and Nash–Sutcliffe efficiency, the I-ELM emerged as the most accurate predictor, particularly for time-invariant datasets.

Shen, Cao, and Parsaie (2024) applied machine learning methods to predict the discharge coefficient (C_d) of triangular broad-crested weirs. Comparing

generalized regression neural networks (GRNN), genetic programming (GP), and extreme learning machines (ELM), they found that the ELM model exhibited the highest stability and predictive ability. The model achieved near-perfect accuracy in the testing phase, with an R^2 of 0.99982, an NSE of 0.99977, an RMSE of 4.17E-05, and a MAPE of 0.000261. The weir's apex angle (θ) was shown to be the most significant parameter in a sensitivity analysis, accounting for 52.45% of the model's predictions.

2.4 Motivation for present work

Gabion stepped spillways are widely used across India and other parts of world as cost-effective, flexible and locally adaptable hydraulic structures, particularly in regions such as Uttarakhand, Himachal Pradesh and Maharashtra, as well as countries like Nepal and Bangladesh. They are commonly implemented in check dams, watershed projects, irrigation systems and urban drainage channels to manage high-velocity flows, reduce erosion and dissipate energy during peak discharges. However, despite their practical advantages, most existing designs rely on empirical approaches with limited scientific optimization of key parameters such as porosity, step slope, obstruction configuration, and sill placement. This often leads to inconsistent hydraulic performance, inadequate energy dissipation, downstream scouring, and reduced efficiency due to sediment clogging

Despite the established advantages of gabion stepped spillways such as cost-effectiveness, ease of construction and enhanced energy dissipation through combined overflow and throughflow, their hydraulic performance remains underexplored compared to conventional rigid stepped spillways. Early studies by **Sorensen (1985) and Rajaratnam (1990)** demonstrated the energy dissipation potential of stepped chutes, while **Chanson (1993)** highlighted the role of step-induced turbulence and air entrainment. However, most research has focused on solid impervious steps, with limited attention to the porous nature of gabion structures. Pagliara and **Chiavaccini (2006) and Chinnarasri et al. (2008)** showed that gabion steps can achieve higher energy dissipation than solid steps, yet systematic

optimization of key geometric and hydraulic parameters such as porosity, step slope, obstruction arrangements and sill placement remains incomplete.

Furthermore, existing studies on gabion stepped spillways (**Salmasi et al. (2012); Zhang and Chanson (2016a, b)** have largely examined uniform configurations under limited flow ranges, leaving gaps in understanding the combined effects of vertical obstructions and triangular sills on energy loss across varying slopes and discharges. **Rajaei et al. (2017)** noted that sedimentation can significantly impair dissipation efficiency, emphasizing the need for robust designs. Meanwhile, soft computing techniques such as ANFIS and ELM have proven highly effective in predicting complex hydraulic phenomena **(Azimi et al., 2018; Shen et al., 2024)**, yet their application to gabion stepped spillways with modified step geometries is scarce.

Therefore, the present work is motivated to experimentally investigate and optimize the energy dissipation of gabion stepped spillways under various porosities, slopes, vertical obstruction patterns, and triangular sill placements, and to develop reliable predictive models using ANN, ANFIS and ELM. The findings aim to provide practical design guidelines for sustainable, high-efficiency spillway alternatives.

2.5 Summary of the chapter

The literature review confirms that stepped spillways significantly enhance energy dissipation through step-induced turbulence, air entrainment, and flow recirculation. Gabion stepped spillways offer additional advantages due to throughflow, increasing energy loss compared to rigid counterparts. Key influencing parameters include step geometry, slope, porosity, and discharge. Soft computing techniques such as ANFIS and ELM have proven effective in predicting hydraulic performance with high accuracy. However, research gaps remain regarding the systematic optimization of vertical obstructions, triangular sills, and their combined effects under varying slopes. This chapter establishes the foundation for the present experimental and soft computing modelling work.

Chapter 3: METHODOLOGY

3.1 General

This chapter presents the detailed methodology adopted to investigate the hydraulic performance and energy dissipation characteristics of gabion stepped spillways under varying geometric and hydraulic conditions. The study was conducted through controlled laboratory experimentation combined with dimensional analysis and soft computing modelling techniques such as Adaptive Neuro-Fuzzy Inference System (ANFIS), Extreme Learning Machine (ELM) and Artificial Neural Network (ANN).

The detailed study examined the influence of gabion porosity, spillway slope and discharge on energy dissipation behaviour. It also explored the role of vertical obstructions, considering both their height and arrangement, in modifying flow structure and turbulence characteristics. In addition, the hydraulic response of triangular gabion sills installed on spillway steps was analysed to determine their effectiveness in enhancing energy dissipation. A comparative evaluation between gabion stepped spillways and conventional rigid stepped spillways was conducted to highlight differences in hydraulic efficiency and flow performance. This chapter presents a comprehensive description of the experimental facility, model fabrication process, testing procedures, measurement techniques, dimensional analysis and the soft computing modelling framework adopted to support and interpret the experimental findings.

3.2 Experimental facility

All experiments were conducted in the Hydraulic Engineering Laboratory at Delhi Technological University, Delhi, India. The side view (actual flume) and plan view (line diagram) of the laboratory flume are shown in **Figure 3.1**. The experimental setup consisted of a horizontal rectangular recirculating flume of 10 m length, 0.516 m width, and 0.60 m depth. The flume sidewalls were constructed of transparent acrylic sheets to allow clear visualization of flow regimes. Water was supplied from a storage tank with a capacity of 3096 L using a pipe of 0.10 m supply coupled to a 20.0 horsepower (HP) centrifugal pump, ability to discharge up to 50 L/s. An orifice meter

is used to calibrate the flume's supply line, with a 0.25% margin of error. The discharge was regulated using a reflux valve installed in the supply line. A sluice gate was provided at the upstream end to control inflow conditions, while a tailgate was installed at the downstream end to regulate tailwater depth and maintain desired hydraulic conditions. The system allowed continuous recirculation of water throughout the experimental runs. **Table 3.1** represents the objective wise summary of the parameters analysed in experimental work.



(a)

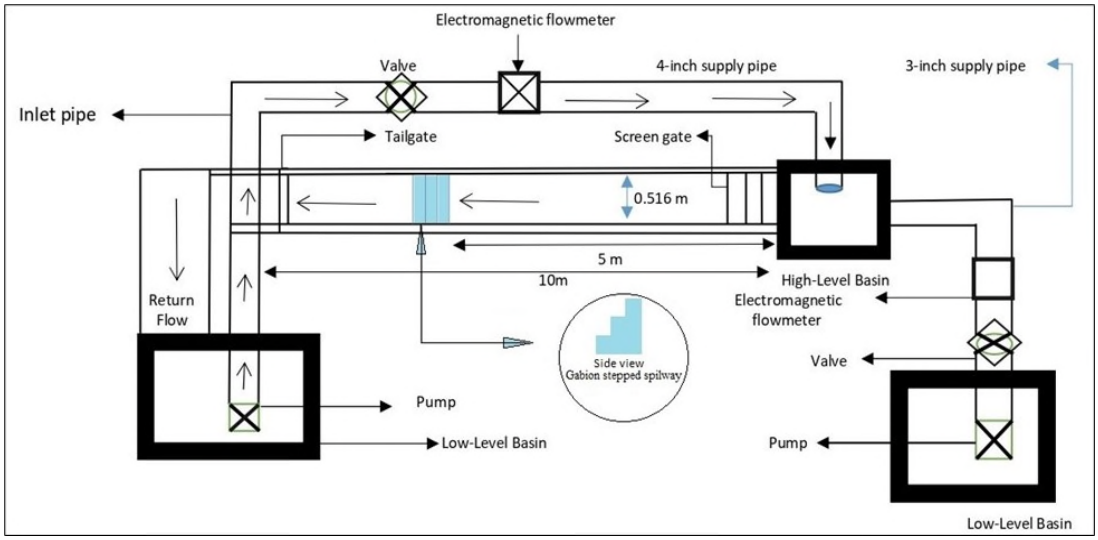

(b)

Figure 3.1 Representation of experimental flume (a) side view (actual flume); (b) plan view (line diagram)

Table 3.1 Objective wise summary of the parameters analyzed in experimental work

Objective	Description	Parametric variations	Dimensionless parameter	Model fabricated
1	To investigate the energy dissipation in a gabion stepped spillway under different flow regimes while evaluating the effects of porosity, slope and discharge	➢ Three stepped gabion spillways ➢ Crushed stone ➢ Three Distinct porosity ➢ Three spillway downstream slopes ➢ Varying discharge	S D_N Y_c/h Fr n	GS-1 GS-2 GS-3
2	To investigate the effect of vertical obstructions and its various arrangements on energy dissipation in gabion stepped spillways	➢ Three stepped gabion spillways ➢ Crushed stone ➢ Vertical obstruction-Uniform, staggered-1 and staggered-2 ➢ Three spillway downstream slopes ➢ Varying discharge	D_N Y_c/h Fr hv/h	Model with uniform, staggered and staggred-2 obstructions

Objective	Description	Parametric variations	Dimensionless parameter	Model fabricated
3	To investigate the influence of a triangular gabion sill placed on the steps of a gabion spillway on energy dissipation under various downstream slopes and discharge conditions	➢ Three stepped gabion spillways ➢ Crushed stone ➢ Triangular gabion sill ➢ Different sill height ➢ Three spillway downstream slopes ➢ Varying discharge	D_N Y_c/h Fr t/l	GT-1 GT-2 GT-3 GT-4 GT-5 GT-6 GT-7 GT-8 GT-9
4	To evaluate and compare the hydraulic performance and energy dissipation efficiency of various gabion stepped spillway configurations with rigid stepped spillways under different slope conditions	➢ Three stepped rigid spillways ➢ Three spillway downstream slopes ➢ Varying discharge	D_N Y_c/h Fr	R-1 R-2 R-3

3.3 Physical model fabrication

3.3.1 Standard gabion stepped spillway models for objective-1

The gabion stepped spillway models were fabricated using steel frames covered with 5 mm thick galvanized iron mesh having diamond-shaped openings of 1.75 × 1.75 cm. The mesh was coated with anti-rust paint to ensure durability during repeated experimental runs. Uniform crushed stones ranging in size from 20-40 mm ($D_{50} \approx 28$ mm) were used as rockfill material. The porosity of the gabion media was determined through sieve analysis and direct volumetric measurement and was varied systematically as 34%, 38% and 42% to examine its influence on hydraulic performance.

Each standard model had a total height (H_s) of 0.33 m, consisting of three equal steps. The step heights were 0.09 m and 0.11 m respectively, depending on the model configuration. A significant geometric scale was adopted for fabrication to maintain hydraulic similarity. Three downstream slopes 1:1.5 (33.69°), 1:1 (45°) and 1:0.5 (63.43°) (*V:H*) were considered. The variation in slope allowed investigation of its effect on flow regime transition and energy dissipation characteristics. **Figure 3.2** illustrates the model setup for standard gabion stepped spillway without stones and filled with stones.

In gabion structures, the flow passes through the body of the structure with low discharges, it is known as the nappe flow regime. Jet collisions occur as the nappe free-falls and moves from one step to another. There is no cavity formation below the nappe. The flow regime changes from nappe to skimming at the stage of the transition flow regime. On higher steps, nappe flow happens, but on lower steps, skimming flow occurs. Water skims down from the steps during the skimming flow regime and recirculating vortices form between them, acting as a pseudo bottom for flow originating from the steps' outer edges. In throughflow conditions, entire discharge passed through the porous gabion structure without overtopping and the free surface remained below the step crest. Although, in overflow conditions the upstream water level exceeded the crest elevation and water flowed over the stepped profile. For

61 each test run, the flow was allowed to stabilize for approximately 2-3 minutes before measurements were recorded. **Table 3.2** shows the criteria for the flow regime.

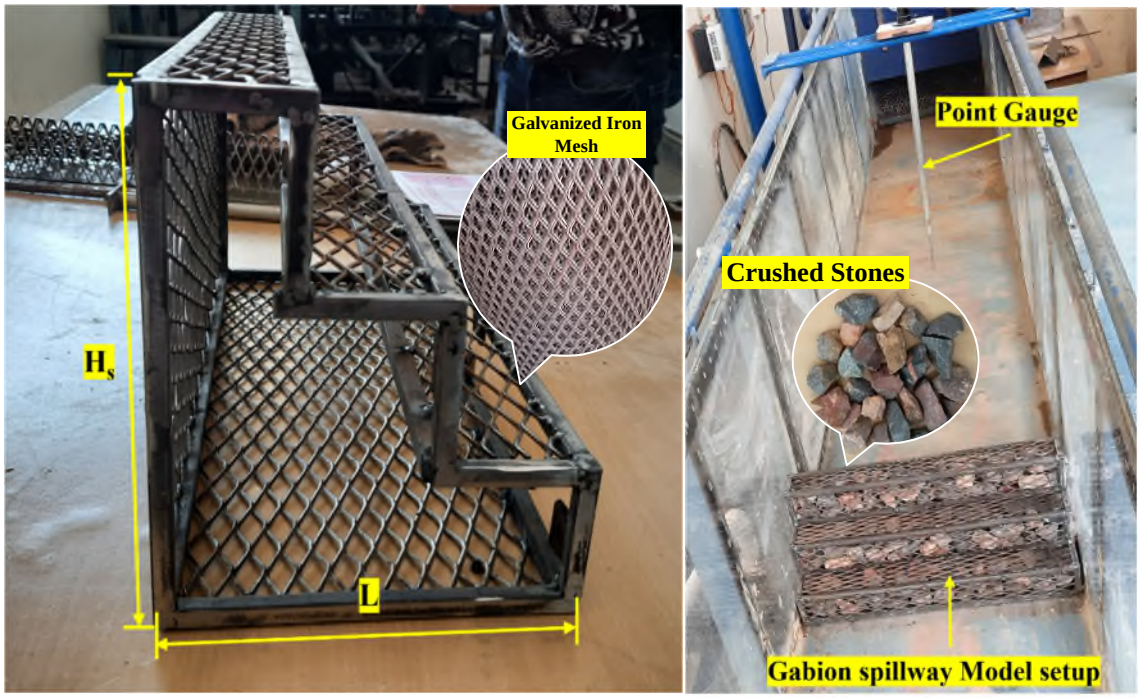

(a) (b)

Figure 3.2 Model setup for standard gabion stepped spillway (a) without stones; (b) filled with stones

Further, **Table 3.3** represents the details of experimental runs under various spillway slope and porosity conditions. A total of 540 runs were performed for objective-1 with 180 runs each for subsequent models, ensuring sufficient data for statistical reliability and modelling purposes.

Table 3.2 Criteria for flow regime

Flow Regime	Description
Through flow	No overflow at the outer edge of the steps
Nappe flow	Jet impact and free-falling nappes from one step to the next
Transition flow	Nappe on the upper steps while skimming on the lower steps
Skimming flow	Water skimming over the steps outside edge, which creates a pseudo-bottom

Table 3.3 Details of experimental runs under various spillway slope and porosity conditions

Model height (H_s) in m	Spillway slope (S)	Porosity (n)	Number of experimental run	Stepped spillway model classification
0.33	33.69^0	34%	60	Standard Gabion type (3 models each)
	45^0		60	
	63.43^0		60	
	33.69^0	38%	60	Standard Gabion type (3 models each)
	45^0		60	
	63.43^0		60	
	33.69^0	42%	60	Standard Gabion type (3 models each)
	45^0		60	
	63.43^0		60	

3.3.1.1 Role of Gabion Material Porosity

Porosity refers to the void spaces within the gabion material. It is a measure of the ratio of void volume to the total gabion stones volume. High porosity allows for more water infiltration and greater turbulence within the gabion matrix, whereas low porosity limits flow penetration, leading to surface-dominated flow.

3.3.1.2 Property of filling material

Uniform crushed-type stones ($D_{50} \approx 28$ mm) had three different porosities of 34%, 38% and 42%, calculated from the direct method in laboratory. The value of permeability was nearly 10^{-1} m/s for these stones. **Figure 3.3** shows the fabrication of standard gabion stepped spillway models.



Figure 3.3 Standard gabion stepped spillway models fabrication

3.3.2 Gabion stepped spillway model with vertical obstruction configurations for objective-2

To examine the effect of surface roughness modification, cylindrical vertical obstructions were installed on the step surfaces of gabion model of height (H_s) 0.27 m with slope of 45^0. Uniform crushed stones of size 20-40 mm were used with average porosity of 0.40. The obstructions had a diameter of 1.6 cm and were fabricated in three different heights of 3 cm, 6 cm and 9 cm respectively. These corresponded to relative obstruction heights (h_v/h_s) of 0.33, 0.67 and 1.0. The obstructions were arranged in three configurations Uniform pattern, Staggered-1 pattern, Staggered-2 pattern. Depending on the arrangement, the number of obstructions were 16, 15, and 12, with a center-to-center spacing of 5.5 cm. The obstruction plates were fixed to the spillway steps using a nut-bolt system to ensure stability during experimentation. The schematic diagram and physical model of hydraulics of flow with different heights of vertical obstructions is shown in **Figure 3.4**. For above used configurations, Figure 3.4 shows the arrangements of vertical obstructions using uniform, satggered-1 and staggered-2 obstructions. **Table 3.4** below shows the detailed information of the tested models of the relative height of vertical obstruction for step height (h_s) = 9 cm.

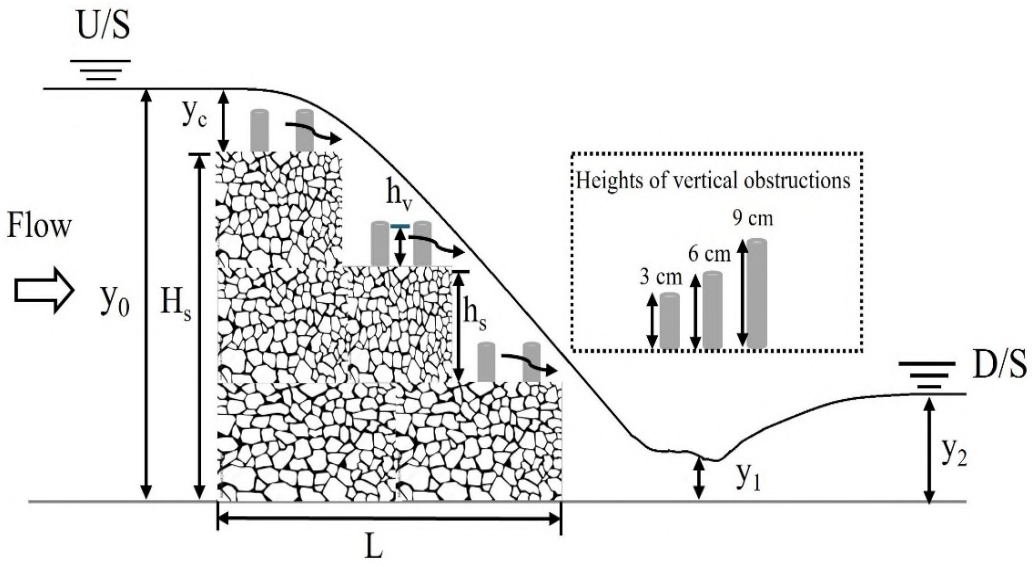

(a)



(b)

Figure 3.4 Schematic diagram and physical model of hydraulics of flow with different heights of vertical obstruction (a) line diagram; (b) model setup filled with stones

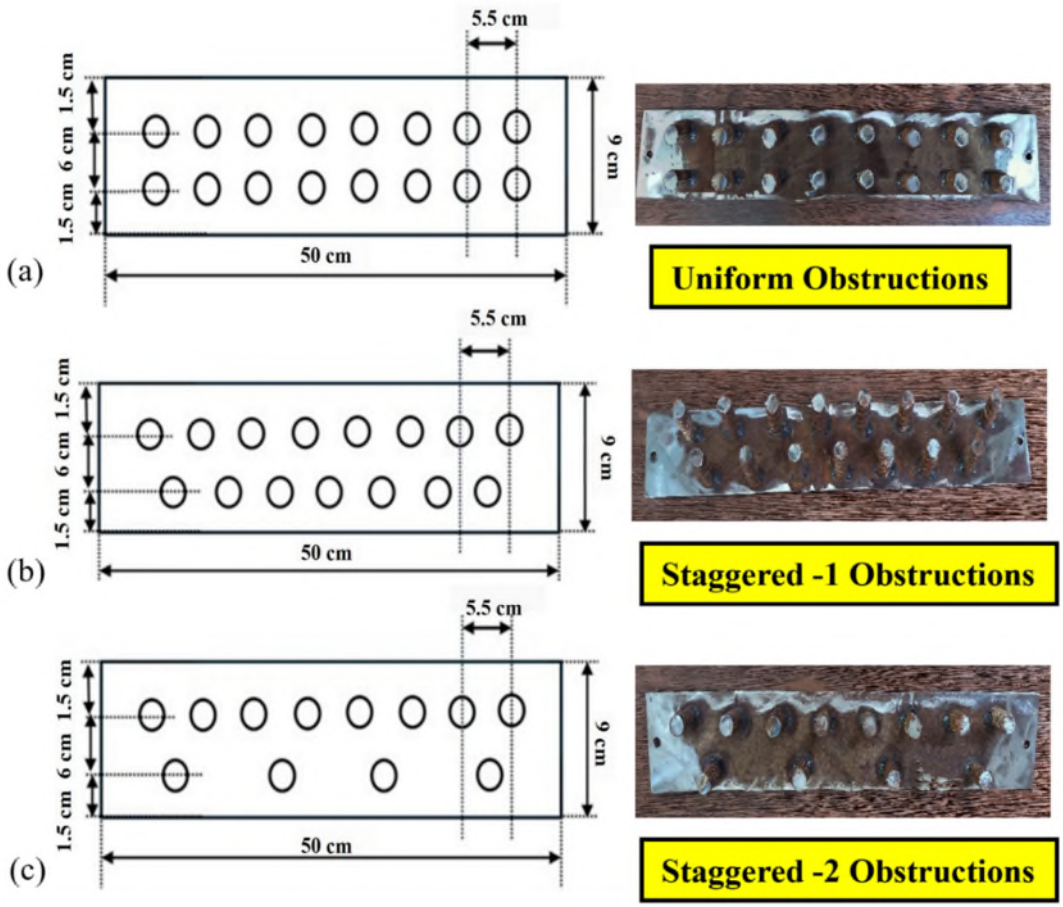

Figure 3.5 Arrangement of vertical obstruction (a) Uniform obstructions; (b) Satggered-1 obstructions; (c) Staggered-2 obstructions

Table 3.4 Details of tested model with the relative height of vertical obstruction for step height 9 cm

Condition	Without obstruction	Uniform pattern			Staggered- 1 pattern			Staggered- 2 pattern		
h_v (cm)	-	9	6	3	9	6	3	9	6	3
$\boldsymbol{h_v/h}$	-	1	0.67	0.33	1	0.67	0.33	1	0.67	0.33

3.3.3 Gabion stepped spillway model with triangular gabion sill over steps for objective -3

For investigating enhanced energy dissipation, triangular gabion sills were introduced on steps of gabion spillway model for a height of 0.33 m. Nine physical models of gabion stepped spillways were made and a triangular gabion sill fabricated using similar galvanized iron mesh filled with uniform crushed stones (20-40 mm size and average porosity of 0.40) was placed over the steps one by one. **Figure 3.6** shows the placing triangular gabion sill placed on the steps of the gabion stepped spillway.

The height (t) of the three different triangular sills used are 15 cm, 11cm and 7 cm, and the width of the steps is 18.70 cm, 11cm and 9.94 cm corresponding to spillway slopes 33.69^0, 45^0 and 63.43^0 respectively. A significant scale of all the models had been taken. A total of 540 test runs were performed (60 runs for each model) for a wide range of discharge ranges between 10 to 50 L/s in overflow and throughflow conditions. The relative sill ratio (t/l) defined as the ratio of sill height to step length, was used as a key dimensionless parameter in the analysis. Models were tested with the sill placed on different steps to evaluate its positional influence on hydraulic performance. **Figure 3.7** illustrates the model setup of the gabion stepped spillway with triangular gabion sill over the steps and variation of the different heights of triangular gabion sill. **Table 3.5** and **Table 3.6** represent the details of different combinations of the tested models and geometrical characteristics of spillways height (H_s = 33cm).

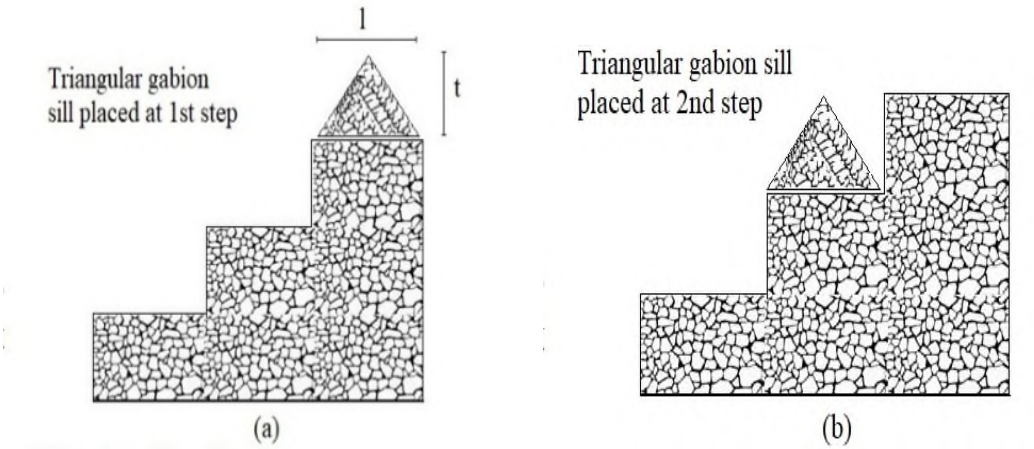

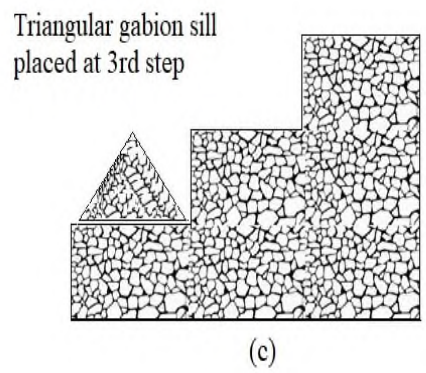

Figure 3.6 Placing of triangular gabion sill over the steps of the gabion stepped spillway (a) on 1st step; (b) on 2nd step; (c) on 3rd step

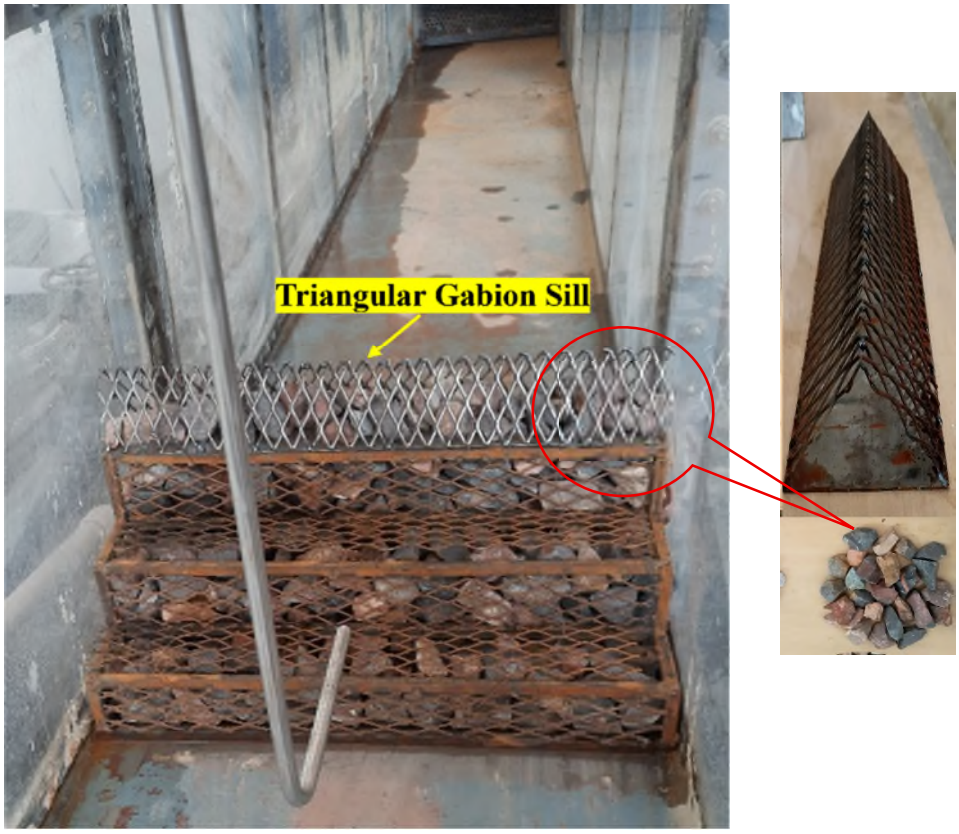

(a)

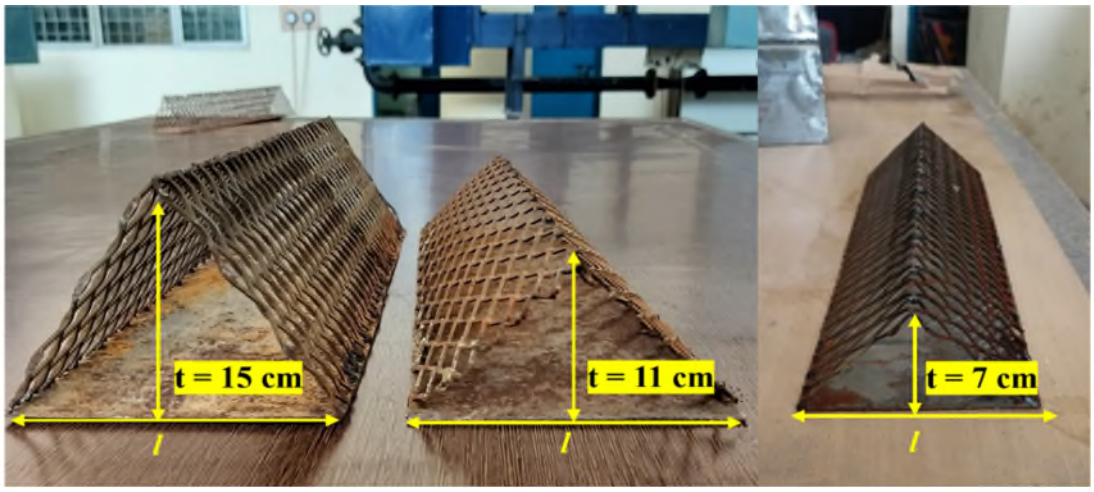

(b)

Figure 3.7 Model setup of the gabion stepped spillway (a) with triangular gabion sill over the steps; (b) pictorial representation of variation of the different heights of triangular gabion sill

Table 3.5 Details of different combinations of the tested models and geometrical characteristics of Spillways height (H_s = 33cm)

Spillway slope (in degree)	Model classification	Step height (h) (cm)	Step length (l) (cm)	Model type	Dataset used/ Total experimental run
33.69	GS-1	11	18.70	Standard Gabion (GS) type	Dataset (540 run)
45	GS-2	11	11		
63.43	GS-3	11	9.94		
33.69	GT-1	11	18.70	Gabion type with triangular gabion sill (GT) placed on step-1	Dataset-1 (180 run)
45	GT-2	11	11		
63.43	GT-3	11	9.94		
33.69	GT-4	11	18.70	Gabion type with triangular gabion sill (GT)placed on step-2	Dataset-2 (180 run)
45	GT-5	11	11		
63.43	GT-6	11	9.94		
33.69	GT-7	11	18.70	Gabion type with triangular gabion sill (GT) placed on step-3	Dataset-3 (180 run)
45	GT-8	11	11		
63.43	GT-9	11	9.94		
33.69	R1	11	18.70	Rigid (R) type	Dataset-3 (180 run)
45	R2	11	11		
63.43	R3	11	9.94		

Table 3.6 Relative sill ratios for gabion model

Model classification	Triangular sill height *t* (cm)	Triangular sill base angle (degree)	Relative sill ratio (*t*/*l*)
GT	15	58.06	0.802
(Nine model)	11	49.48	0.588
	7	36.82	0.374

3.3.4 Rigid stepped spillway models for objective-4

To compare performance, rigid stepped spillway models corresponding to the three slopes were also fabricated. These models had identical geometric dimensions as the gabion models but were constructed as impermeable solid structures. The rigid models served as control generalized cases for evaluating the effectiveness and suitability of gabion stepped spillways. The methodology was designed to ensure geometric, kinematic and dynamic similarity between the prototype and laboratory models. The experiment was done to evaluate the influence of discharge, number of steps, downstream slope on the percentage of energy dissipation. The experimental framework follows the approach presented by **Rajaei et al. (2019)**, with careful control of hydraulic and geometric parameters.

59

Each spillway model was tested under three geometric configurations to evaluate the influence of slope and step arrangement on hydraulic performance. The upstream face of the spillway was maintained vertical in all cases to replicate typical diversion structure geometry and to ensure consistent flow conditions. A spillway height of 0.33 m having each step of vertical height of 0.11 m was used to compare the results while the total model width was taken as same as designed proportionally to maintain geometric similarity and structural stability within the laboratory flume.

To investigate the effect of spillway inclination on energy dissipation, three downstream slopes were examined, 1:1.5 (33.69°), 1:1 (45°) and 1:0.5 (63.43°), expressed as vertical to horizontal *(V:H)* ratios. These slopes were selected to represent mild, moderate and steep spillway geometries commonly encountered in small

54

diversion dams and river training structures. For each rigid spillway configuration, a total of 60 experiments were conducted covering a wide range of discharges to ensure reliable statistical interpretation of the results. In the rigid spillway models, flow occurred exclusively as overflow, and the dominant hydraulic regime observed was nappe flow.

Energy dissipation performance was evaluated by comparing specific energy upstream and downstream of the spillway. To ensure objective comparison among different slopes and configurations, energy dissipation was analyzed for equal discharge values as well as for equivalent drop numbers. The use of the drop number as a governing dimensionless parameter enabled normalization of results across varying total heads and facilitated consistent comparison between configurations. This approach ensured that variations in hydraulic efficiency could be attributed primarily to geometric parameters rather than discharge magnitude alone. **Figure 3.8** shows the visualization of flow over stepped chute.

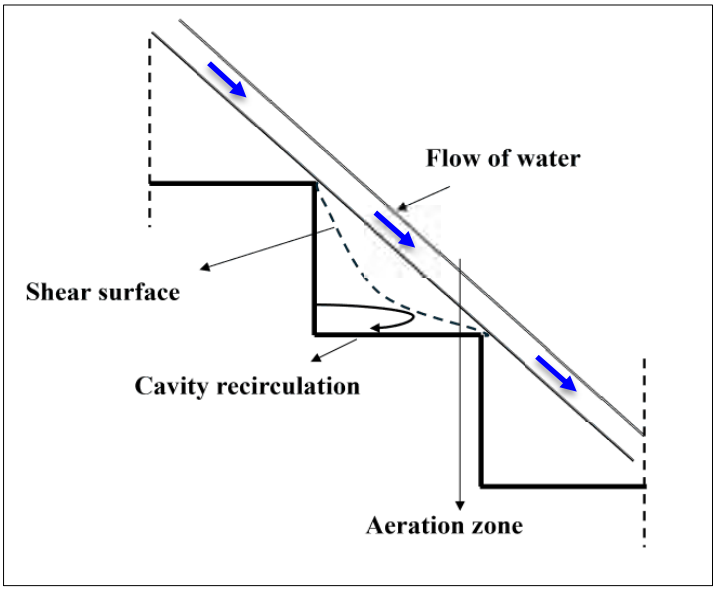

Figure 3.8 Visualization of flow over stepped chute

3.4 Measurement techniques

3.4.1 Water depth and velocity measurement

Water depths were measured using a point gauge mounted on a movable trolley set up at the upstream section, over the crest and downstream of the each spillway model with graduations in centimeters followed by the least count in millimeters with an accuracy of ±0.1mm. To minimize free-surface curvature and aeration effects, upstream depths were measured at a longitudinal distance equal to twice the spillway height (2*H*) from the crest. Downstream depths were recorded at 8H, where steady and uniform conditions were established. All measurements were taken along the centerline of the flume to avoid sidewall effects. Flow velocity was measured using a Pitot tube (1 m length, 4.7 mm diameter) connected to a digital manometer. The Pitot tube was aligned with the flow direction and positioned vertically at 0.4-0.6 times the local flow depth measured from the pseudo-bottom formed by the step edges. This region corresponds to the skimming flow zone, where velocity fluctuations are relatively small and representative of depth-averaged velocity. **Figure 3.9** shows the combined picture for magnetic flow meter, pitot tube and digital manometer used in the laboratory study. **Table 3.7** shows the detailed experimental investigation on Gabion and Rough Impervious stepped weirs.

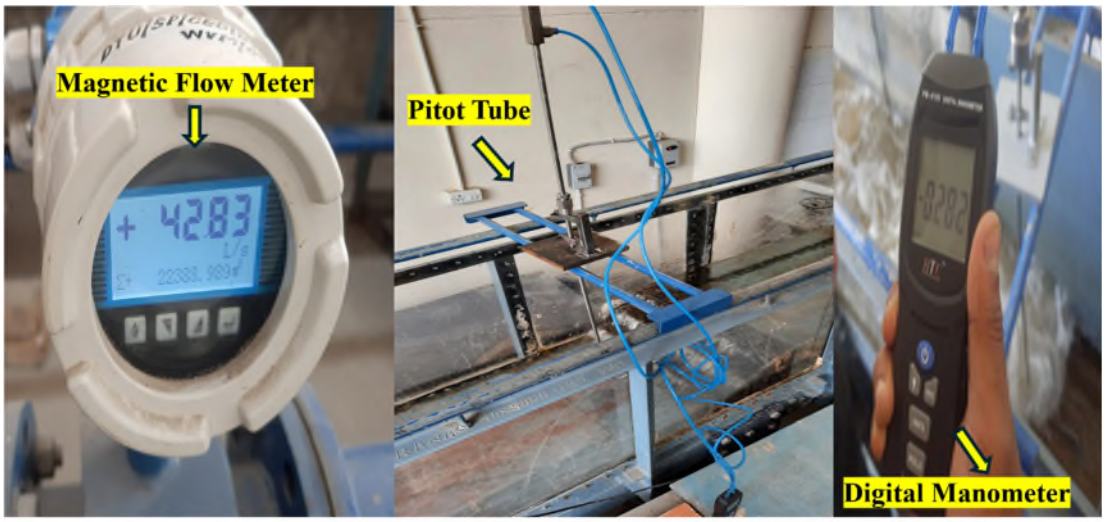

Figure 3.9 Combined picture for magnetic flow meter, pitot tube and digital manometer used in the laboratory study

Table 3.7 Detailed experimental investigation on gabion and rough impervious stepped weirs; Wüthrich and Chanson (2014)

Reference	Spillway slope (in degree)	Geometry Parameters	Types of steps	Flow Parameters	Instrumentation used
Gabion Steps Peyras et al. (1991)	45, 26.6 &18	$h = 0.2$ m, $l = 0.4$ m, $w = 0.8$ m	Gabion steps, plain Capped steps, Layer cake upward steps	$Q = 0.05$-0.2 m^3/s, $R = 2.5\times10^5$ to 1.0×10^6	Pitot tube array, copper pipe with inlet holes every 5 cm
Rough impervious steps Gonzalez et al. (2008)	21.8	$h = 0.1$ m, $l = 0.25$ m, $w = 1$ m	Rough impervious step faces Rough vertical and horizontal faces, smooth steps	$Q = 0.01$-0.22 m^3/s, $R = 5\times10^4$ to 7×10^{5x}	Double tip conductivity probe, $\emptyset = 0.025$ mm
Bung and Schlenkhoff (2010)	26.6	$h = 0.06$ m, $w = 0.30$ m	Rough impervious horizontal faces, in row shifted Smooth steps	$Q = 0.021$,0.027 and 0.33 m^3/s, $R = 2.7\times10^5$ to 3.6×10^5; 4.4×10^{5x}	Double tip conductivity probe, $\emptyset = 0.13$ mm, $\Delta x = 5.1$ mm, $\Delta y = 1$ mm
Wüthrich and Chanson (2014)	26.6	$h = 0.1$ m, $l = 0.2$ m, $w = 0.52$ m	Smooth and impervious step, Gabion and Porous step	$Q = 0.02$-0.11 m3/s, $R = 1.4\times10^5$ to 8.8×10^{5x}	Double tip conductivity probe, $\emptyset = 0.25$ mm, $\Delta x = 6.2$ mm, $\Delta z = 1.35$ mm

Reference	Spillway slope (in degree)	Geometry Parameters	Types of steps	Flow Parameters	Instrumentation used
Present Study	33.69, 45 & 63.43	$h = 0.9$ m & 0.11 m, $w = 0.516$ m	Smooth gabion step, Rough vertical obstruction with gabion porous step, triangular gabion sill on steps	$Q = 0.015$-0.050 m^3/s, $R = 1.5 \times 10^5$ to 6.8×10^{5x}	Double tip conductivity probe, $\emptyset = 0.15$ mm, $\Delta x =$ 6.1 mm, $\Delta y = 1.35$ mm

Remark: h = step height; l = step length; Q = discharge, R = Reynolds number in terms of hydraulic parameter; w = width of channel; Δx = streamwise distance between the probe tips; Δy = vertical distance between the probe tips; Δz = transverse distance between the probe tips; ^{x}Air water flow measurement.

3.5 Dimensional analysis

Dimensional analysis using the Buckingham π-theorem was applied to identify the governing dimensionless parameters influencing energy dissipation. The relative energy dissipation was expressed as a function of upstream Froude number (F_r), drop number (D_N), slope ratio (h/l), critical depth ratio (Y_c/h), porosity (n), relative obstruction height (h_v/h), and relative sill ratio (t/l). This formulation provided the basis for both regression and soft computing modelling.

3.5.1 Generalized functional relationship

The dimensionless form of the energy dissipation equation can be expressed as in equation (4):

$$\frac{\Delta E}{E_0} = f\left(Fr, \frac{h}{l}, \frac{h}{H}, \frac{Y_c}{h}, D_N, n, \frac{h_v}{h}, \frac{t}{l}\right) \quad (4)$$

For stepped spillways of fixed total height (H_s) and constant number of steps, the parameter h/H_s remains constant and may be omitted for simplification. Thus, the governing relationship reduces to as per equation (5):

$$\frac{\Delta E}{E_0} = f\left(Fr, \frac{h}{l}, \frac{Y_c}{h}, D_N, n, \frac{h_v}{h}, \frac{t}{l}\right) \quad (5)$$

Each parameter has following hydraulic significance:

- Froude number (Fr): Represents the ratio of inertial to gravitational forces and governs flow regime transition.
- Spillway slope (h/l): Controls acceleration and vortex formation between steps.
- Relative critical depth (Y_c/h): Reflects flow intensity relative to step geometry.
- Drop number (D_N): $q^2/gH_s{}^3$ term was known as drop number or gabion number.
- Porosity (n): Governs internal flow resistance and seepage-induced momentum loss.
- Relative obstruction height (hv/h): Quantifies macro-roughness enhancement.

- Relative sill ratio (*t/l*): Represents artificial geometric modification for turbulence amplification.

This dimensional structure ensures that the formulation is independent of scale and directly applicable to prototype spillways under Froude similarity. Stepped spillway flows are predominantly governed by gravity-driven free-surface dynamics, Froude number similarity was maintained as the primary criterion for hydraulic similarity. Reynolds numbers during experimentation were sufficiently high to ensure fully turbulent conditions, thereby minimizing viscous scaling distortions. This justifies neglecting viscosity-dependent π-terms in the final reduced formulation.

Based on dimensional reduction and sensitivity analysis, the final predictive expression used for regression and soft computing modelling was formulated as per equation (6):

$$\frac{\Delta E}{E_0} = f(q^2/gH_s{}^3, h/l, t/l, Y_c/h, , Fr_1) \quad (6)$$

Equation (6) can be written as:

$$1/(1-K) = f(q^2/gH_s{}^3, h/l, t/l, Y_c/h, Fr_1) \quad (7)$$

Where $K = (E_0 - E_1)/H$, $q^2/gH_s{}^3$ term was known as drop number or gabion number (D_N), h/l is spillway slope (S), Y_c/h *is* critical depth to step height ratio and *t/l* was introduced as a 'relative sill ratio' which is taken as constant for this study. Froude numbers at upstream is $Fr_1 = V_1/\sqrt{gy_1}$.

3.6 Soft computing modelling

To enhance predictive capability, three soft computing models were developed: Artificial Neural Network (ANN), Adaptive Neuro-Fuzzy Inference System (ANFIS) and Extreme Learning Machine (ELM). The dataset comprised 180 experimental observations for each models, which were normalized to eliminate scale effects using data normalization. The data were randomly divided into training (70%) and testing (30%) subsets.

The ANFIS model combined neural network learning capability with fuzzy logic inference to handle nonlinear relationships. The ELM model, a single

hidden layer feed-forward neural network, randomly assigned hidden layer weights and computed output weights analytically using the Moore–Penrose generalized inverse, resulting in faster training.

3.6.1 Artificial neural network (ANN)

ANN is a powerful tool in machine learning and artificial intelligence, capable of handling complex, non-linear relationships in diverse scientific fields. The ANN model consisted of an input layer, one or more hidden layers and an output layer trained using backpropagation. It shows how neurons work in the human brain. ANNs use self-adjusting learning algorithms which are fully linked, multilayer neural networks consisting of an input layer, a few hidden layers and an output layer make up an ANN. Every node in a layer is linked to every other layer's node. Data collection, data preprocessing, network building, training, and model testing are the systematic steps followed in neural networking. **Figure 3.10** below shows the ANN model architecture.

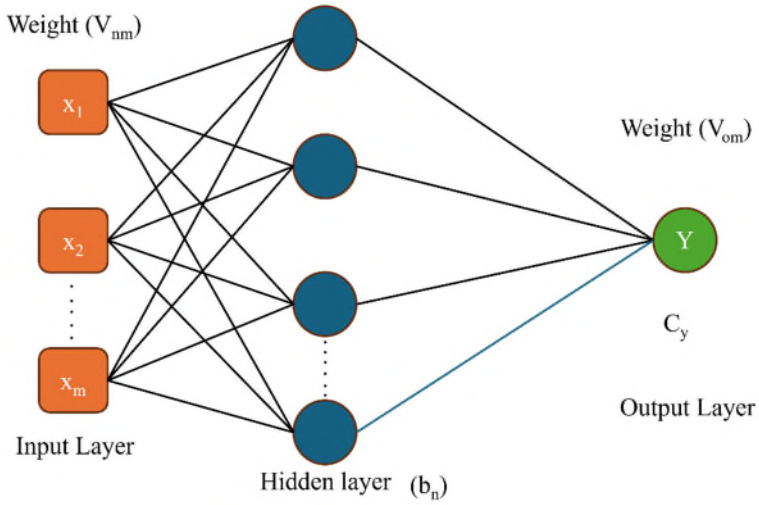

Figure 3.10 ANN model architecture

3.6.1.2 Steps followed in ANN

Step-1: Define ANN architecture

- Input layer: Number of selected inputs.
- Output layer: Number of predicted outputs.

- Hidden layer(s): Start with one hidden layer; set neuron count heuristically from rule base.

Step-2: Set training strategy

- Split data: In training, validation and testing.
- Choose training algorithm
- Use Mean Squared Error (MSE) for regression

Step-3: Training and optimization

- Train on training set while monitoring validation performance

Step-4: Evaluate on test data

- Test the final model on unseen test set.
- Metrics like R^2, RMSE, MAE calculated for accuracy check.

3.6.2 Adaptive neuro-fuzzy inference system (ANFIS)

To get an input-output data mapping, ANFIS is a hybrid artificial intelligence approach that seamlessly combines artificial neural networks with fuzzy logic. It is a multilayer feed-forward network in which each node processes incoming signals according to a specific purpose. Different aspects of adaptive learning are represented by the square and circle node symbols. Adaptive learning parameters are changed using gradient learning algorithms to achieve desired input-output characteristics. The ANFIS model is one of the implementations of a first order Sugeno fuzzy inference system **(Takagi and Sugeno 1985)** shown in **Figure 3.11** shows the ANFIS architecture.

In this system if x_1 is A_1, x_2 is B_1,

then $y = p_1x_1 + q_1x_2 + r_1$

And if x_1 is A_2, x_2 is B_2,

then $y = p_2x_1 + q_2x_2 + r_2$

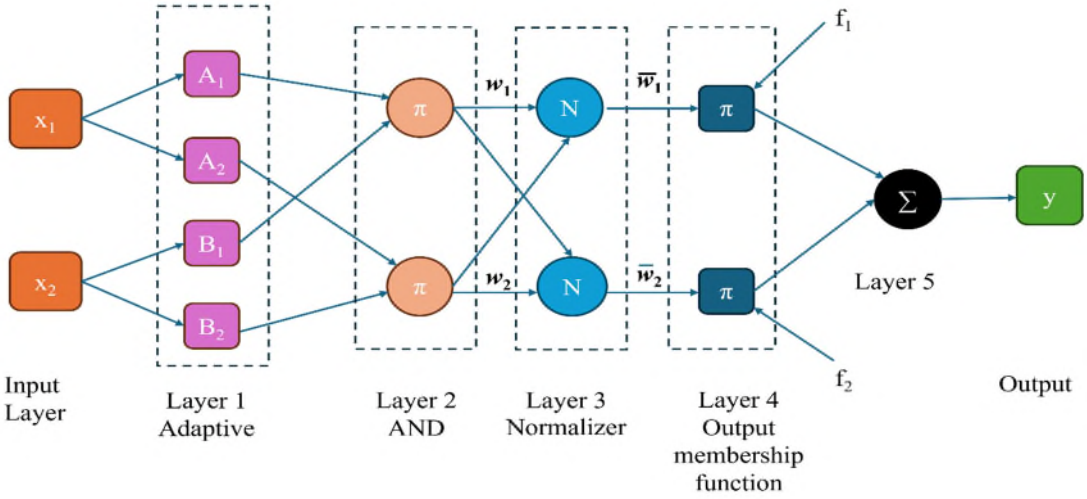

Figure 3.11 ANFIS architecture

Layer 1: This layer assimilates fuzzy clusters from input data through the utilization of membership functions, articulated as per equation (8):

$$O_i^1 = \mu A_i(x) \tag{8}$$

In this equation, μ is the membership function, x represents the input to node *i*, and *Ai* indicates the linguistic label of the node function.

Layer 2: The rule layer determines strengths by multiplying the membership values obtained from the fuzzification layer as per equation (9):

$$O_i^2 = w_i = A_i(x) \times B_i(y) \tag{9}$$

Layer 3: This layer calculates normalized strengths associated with each rule through the following formula as per equation (10):

$$O_i^3 = \overline{w_i} = \frac{w_i}{\sum_i^n w_i} \tag{10}$$

Where $\overline{w_i}$ is the normalized strength and n is the number of nodes.

Layer 4: The defuzzification layer employs first-order polynomials to compute the weighted values of rules, converting fuzzy outputs into a precise decision as per equation (11).

$$O_i^4 = w_i f_i = w_i (p_i x + q_i y + r_i) \tag{11}$$

In these references, f_i constitutes the polynomial incorporating the parameter set $\{p_i,q_i,r_i\}$ identified as consequence parameters.

Layer 5: This layer consolidates all outputs from the defuzzification layer, yielding the ANFIS output as per equation (12):

$$y = O_i^5 = \text{overall output} = \frac{\sum_i w_i f_i}{\sum_i w_i} \quad (12)$$

The ANFIS structured system comprises effective learning of input parameters to output as guided by providing the dataset **(Jang 1993)** as shown in **Figure 3.12**.

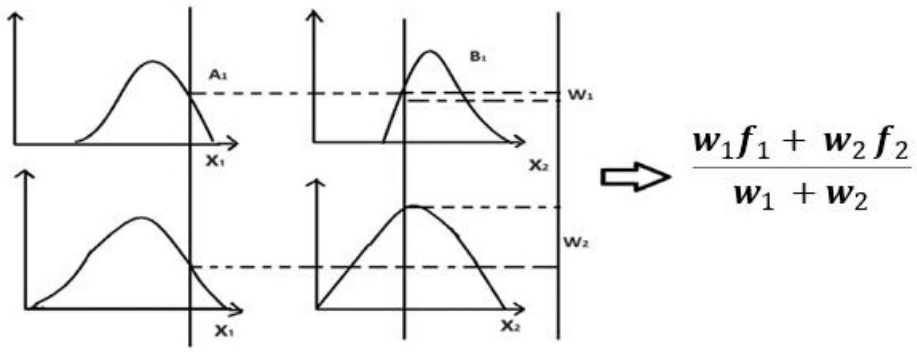

Figure 3.12 First-order sugeno fuzzy model

Here, for objective-1, the fuzzy inference system (FIS) has five inputs i.e. spillway slope (S), critical depth to step height ratio (Y_c/h), drop number (D_N), Froude number (Fr) and porosity (n) called input-1, input-2, input-3, input-4 and input-5 and one output is relative energy dissipation ($\Delta E/E_0$). For objective-2, five inputs are spillway slope (S), critical depth to step height ratio (Y_c/h), drop number (D_N), Froude number (Fr), relative obstruction height (hv/h). Similarly, for objective-3, relative obstruction height (hv/h) *is* replaced by relative sill ratio (t/l) for the analysis.

In this study, ANFIS is used to train the proposed model and fetching the output. ANFIS Editor GUI of MATLAB (Version: R2023a) was used for implementation. 180 runs of each data set were divided into two parts in which 70% are the training data (126 data points) and 30% testing part (54 data points). The testing data is selected randomly, and it is independent of training data. An initial FIS model

structure should be specified prior to FIS training. The FIS model consists of grid partitioning techniques that apply grid partition on the data.

All programs were developed in MATLAB to evaluate energy loss through a gabion-stepped spillway. Three datasets were used in the Neuro-Fuzzy Designer, featuring five input variables and one output variable. The datasets were imported into the MATLAB workspace and entered into the Neuro-Fuzzy Designer for analysis. Membership functions for the inputs were configured in the fuzzy designer, with three adaptive layers assigned to each input variable. Once trained, the FIS was validated using independent testing data not included in the training phase. Training data, testing data and FIS output were plotted in the Neuro-Fuzzy Designer to evaluate energy dissipation, as represented in **Figure 3.13** (a), (b) respectively. This structured approach demonstrated the effectiveness of the ANFIS model in predicting energy loss with high precision. Detailed information of steps followed in Neuro-fuzzy controller is shown in flow chart given in **Figure 3.14**.

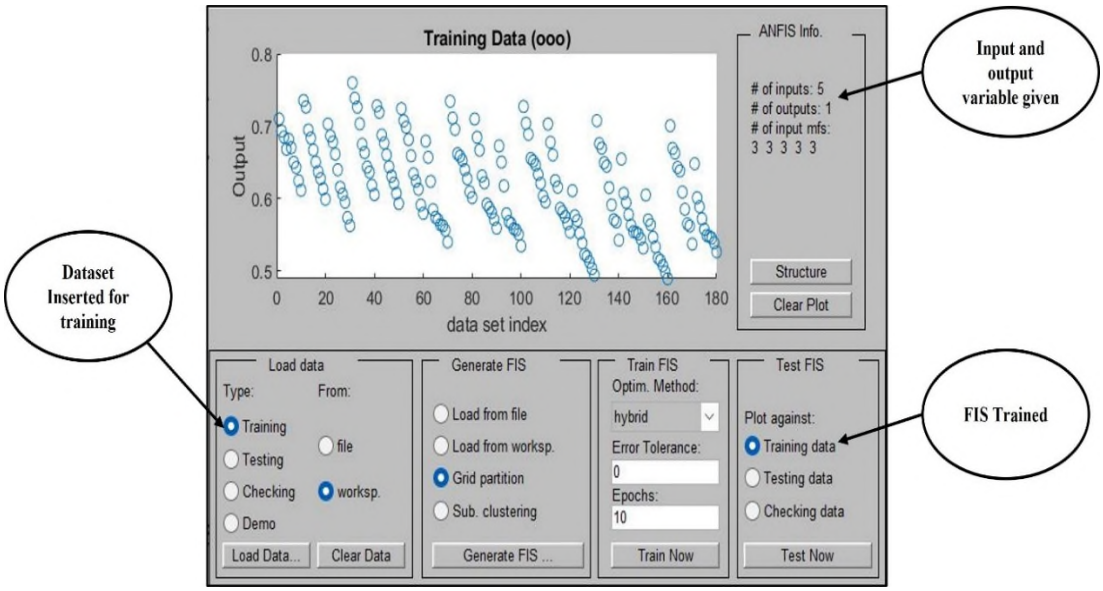

(a)

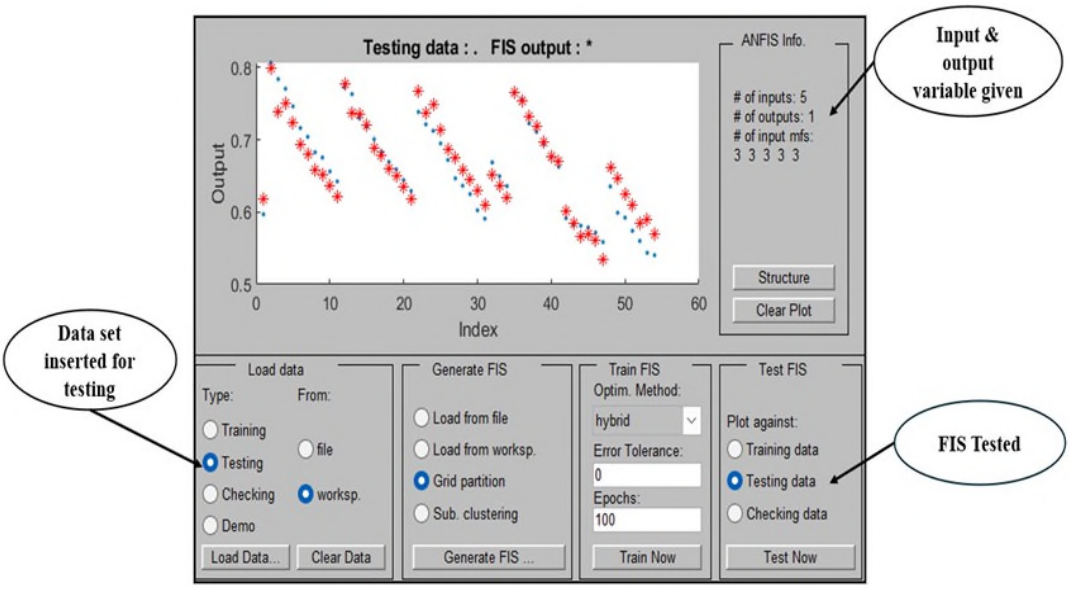

(b)

Figure 3.13 (a) Training data; (b) Testing data and FIS output versus output (rate of energy dissipation)

3.6.2.1 Steps followed in Neuro-Fuzzy Controller

Import Dataset: Load the dataset into MATLAB and create a new array.

Open Controller: Use the command ‘anfisedit’ to open the Neuro-Fuzzy controller in the workspace.

Train Model: Import datasets, set epochs and membership functions, and record RMSE.

Export Model: Import the dataset again and export as a .exe file.

Setup Simulink: Use Demux and Mux blocks to connect input and output parameters.

Run Simulation: Execute the program for 180 seconds per dataset to generate output curves.

Refer Architecture/Output: Output simulink configuration details.

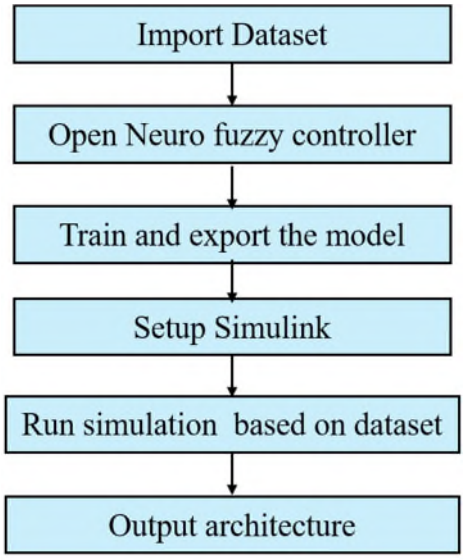

Figure 3.14 Flow chart for steps to be followed in Neuro-Fuzzy Controller

Relative error (RE) between observed data and predicted data can be computed by the following relation shown in equation (13).

$$RE = \frac{Observd\ value - Predicted\ value}{observed\ value} \tag{13}$$

3.6.3 Extreme learning machine (ELM)

In comparison to slow gradient-based learning conventional algorithms, a new fast learning algorithm was introduced as an extreme learning machine (ELM) for training neural networks. ELM is a generalized single hidden layer feed-forward neural network (SLFFNN) given by **(Huang et al. 2004, 2006)**. An ELM consists of hidden neurons with randomly assigned input weights and analytically determines output weight.

For *N* distinct arbitrary dataset (x_i, t_i)

as $x_i = [x_{i1}, x_{i2}, \dots, x_{iU}]^T \in R^U$ and $t_j = [t_{i1}, t_{i2}, \dots, t_{iV}]^T \in R^V$

U and *V* are the number of nodes in the input and output layers and *Y* is an output. A detailed single hidden layer ELM model architecture is shown in **Figure 3.15**.

The standard equation of ELM with *L* hidden nodes with activation function *g(x)* can approximated for the *N* sample with zero error, for that $\sum_{J=1}^{L} \|O_j - t_j\| = 0$, i. e. , $\beta_i, \widetilde{w}_i$ and bi exist given in equation (14):

$$f_L(x) = \sum_{i=1}^{L} \beta_i g_i(x) = \sum_{i=1}^{L} \beta_i g(\tilde{w}_i . x_j + b_i), j = 1,2, \dots N \quad (14)$$

Where x is an input vector, N is the number of training samples, $\beta_i = [\beta_{i1}, \beta_{i2}, \dots, \beta_{in}]^T$ is the weight vector between the ith hidden layer and output, $\tilde{w}_i = [\tilde{w}_{i1}, \tilde{w}_{i2}, \dots, \tilde{w}_{in}]^T$ is the weight vector between the input and the ith hidden layer, is an, b_i is the threshold of the ith hidden layer. $\tilde{w}_i . x_j$ represents the inner product of $\tilde{w}_i$ and x_j.

The above equation (14) can be written as:

$$H\beta = T \quad (15)$$

where,

$$H = \begin{bmatrix} g(\tilde{w}_1 . x_1 + b_1) & \cdots & g(\tilde{w}_L . x_1 + b_L) \\ \vdots & \dots & \vdots \\ g(\tilde{w}_1 . x_N + b_1) & \cdots & g(\tilde{w}_L . x_N + b_L) \end{bmatrix}_{N \times L}, \beta = \begin{Bmatrix} \beta_1^T \\ \vdots \\ \beta_L^T \end{Bmatrix}_{L \times V} \text{ and } T = \begin{Bmatrix} t_1^T \\ \vdots \\ t_N^T \end{Bmatrix}_{N \times V}$$

H is the hidden layer output matrix and T is the training data target matrix of the neural network

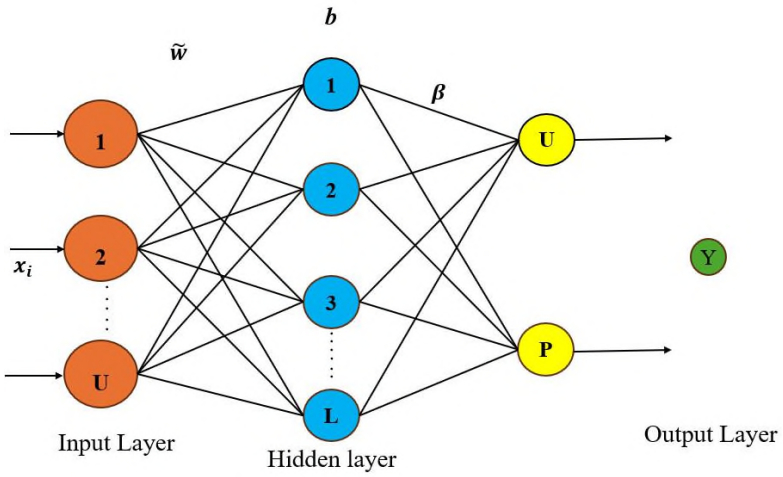

Figure 3.15 Single hidden layer ELM model architecture

3.6.3.1 Algorithm for ELM

The following steps involved in ELM are summarized below:

Input: a training set $(x_i, t_i) \in R^U \times R^V$ $(i = 1,2, \ldots N)$, the activation function $g(x)$ and L hidden nodes.

Output: the output weights β.

1. Randomly assign the parameters of hidden nodes (a_i, b_i) $(i = 1,2, \ldots L)$.

2. Compute the output matrix of the hidden layer H.

3. Calculating the output weight as $\beta = H^{\dagger} T$

Here, $H^{\dagger}$ is the Moore–Penrose generalized inverse of H.

3.7 Data normalization

It is crucial to preprocess the data to prevent the negative impact of varying variable scales on estimation models. The normalization of the data was carried out using the following equation (16):

$$X_{norm} = \frac{X - X_{min}}{X_{max} - X_{min}} \quad (16)$$

where X is the observed value, X_{min} is the minimum value and X_{max} is the maximum value. Modelling data was randomly selected, and a total of 180 data was split into two stages as training dataset (70%) and testing dataset (30%).

3.8 Performance evaluation matrices

The performance of ANFIS and ELM models for a dataset using the goodness of fit test by considering the correlation coefficient (R^2), root mean squared error (RMSE), mean absolute error (MAE) and Nash–Sutcliffe coefficient (NSE) is given in equation (17), (18), (19) and (20) respectively; **(Shen et al. 2024)**.

The correlation coefficient is the degree of correlation between the experimental and modeled outputs.

$$R^2 = [\sum_{i=1}^{N}(y_i - y_o)(t_i - z_a)]^2 / \sum_{i=1}^{N}(y_i - y_o)^2 \sum_{i=1}^{N}(t_i - z_a)^2 \quad (17)$$

Further, RMSE to show a better result in terms of performance calculated as:

$$\text{RMSE} = \sqrt{\frac{1}{n}\sum_{i=1}^{n}(t_i - y_o)^2} \quad (18)$$

The performance of the model was also analyzed using MAE and NSE calculated from:

$$\text{MAE} = \frac{1}{N}\sum_{i=1}^{N}|t_i - y_o| \quad (19)$$

$$\text{NSE} = 1 - \frac{\sum_{i=1}^{N}(t_i - y_o)^2}{\sum_{i=1}^{N}(t_a - z_a)^2} \quad (20)$$

Where N represents the total number of observations; y_i and t_i represents the experimental value and model predicted value from the *i*th element; and y_o and z_a denote average of experimental value and model predicted value respectively.

3.9 Sensitivity analysis

Sobel's method is a variance decomposition based global sensitivity analysis method for the purpose of evaluating the sensitivity of mathematical model outputs to input variables **(Sobol, 1990)**. The Sobol sequence and variance decomposition are employed to quantify the impact of each input variable on the model output, thereby determining the system's sensitivity. It offers a detailed understanding of each input variable in the model. It offers a detailed understanding of every model input variable. This approach efficiently evaluates the relationship between the input variable and the model output and is particularly suitable for complicated multidimensional nonlinear systems **(Nossent et al., 2011).**

3.9.1 Quantitative analysis for input variables

Sobol's method was used to compute the model's first-order and global sensitivity coefficients based on various soft commuting methods. For each objective, sensitivity analysis was carried out to evaluate the relative influence of each input parameter on the predicted relative energy dissipation before finalizing the model inputs. Each variable given in equation (6) was systematically analyzed while keeping the remaining inputs constant and the corresponding variation in model output was monitored. For objective-3, the analysis indicated that spillway slope *(S)*, drop number *(D_N)*, Froude number *(Fr)*, critical depth to step height ratio *(Yc/h)* and relative sill

ratio *(t/l)* exhibited the highest sensitivity with respect to energy dissipation, whereas other tested parameters showed comparatively negligible influence. Therefore, only the most influential variables were retained in the final ANN, ANFIS and ELM models to improve predictive efficiency and avoid redundancy. Similarly, for the objective-2, relative sill ratio (*t/l*) *is* replaced by relative obstruction height (*hv/h*) and for the objective-1, it is replaced by porosity (*n*) for the analysis.

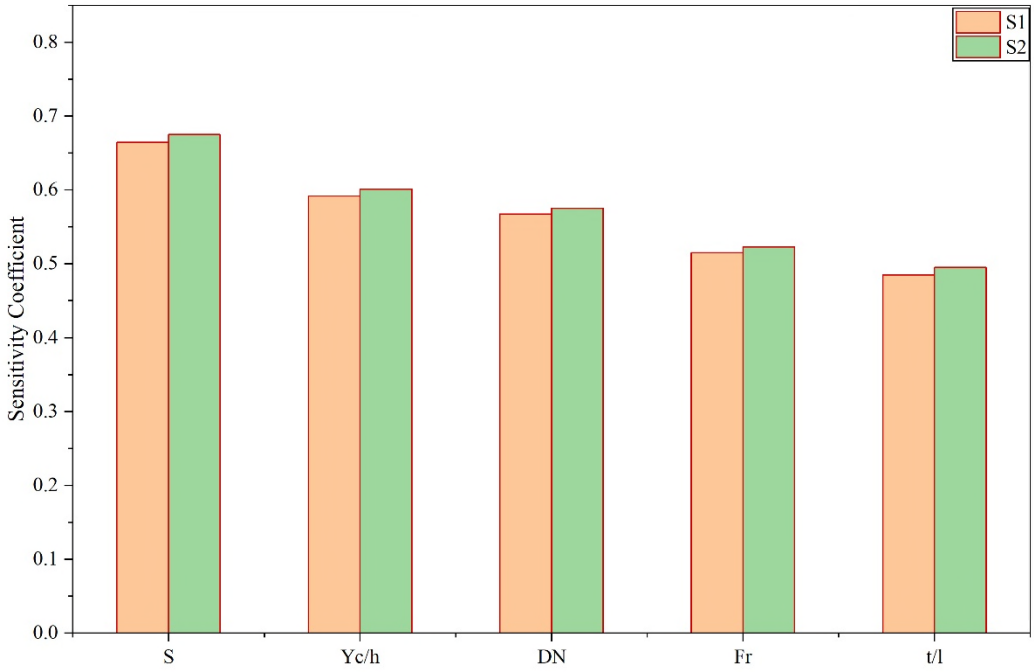

Figure 3.16 Sensitivity coefficients for dimensionless parameters

In **Figure 3.16** the input parameters spillway slope (*S*), critical depth to step height ratio (*Yc/h*), drop number (D_N), Froude number (*Fr*), and relative sill ratio (*t/l*) have first-order sensitivity coefficients ranging from approximately 0.48 to 0.68 for both scenarios (*S1* and *S2)*. The sensitivity coefficients indicate that, under the independent action of each parameter, the influence of *S* on energy dissipation is the most pronounced, with coefficients of about 0.665 and 0.675 for S1 and S2, respectively **(Shen et al. 2024)**. This is followed by *Yc/h (*0.590 and 0.600), D_N (0.565 and 0.572), *Fr* (0.512 and 0.520), and *t/l* (0.483 and 0.492).

3.10 Scale effect in hydraulic analysis

Earlier, it was emphasized that minimum step heights and flow depths are required to ensure realistic reproduction of nappe breakup, splash generation and aeration processes. Further it was reported that for stepped spillways, Reynolds numbers below approximately 1×10^5 to 2×10^5 result in significant scale distortions, affecting velocity profiles, pressure distributions and step cavity recirculation, **Boes and Hager (2003); Chanson and Toombes (2002)**. To reduce scale effects in stepped spillway, it is generally recommended that model step heights varies 0.03-0.05 m, flow depths remain sufficiently large to ensure fully turbulent flow. Dimensionless parameters such as critical depth to step height fall within prototype representative ranges. To mitigate the scale effects in gabion stepped spillway, large-scale physical models are used, ensuring model stone sizes ranges 20-30 mm, flow depths are significantly larger than the characteristic void size and flow regimes correspond to skimming flow, where scale effects are generally less severe.

Chapter 4: RESULT AND DISCUSSION

4.1 General

This chapter presents and discusses the experimental findings obtained to evaluate the hydraulic performance of gabion stepped spillways under varying structural and flow conditions. The results examine the influence of gabion porosity, downstream slope, and discharge variation on energy dissipation characteristics. The effects of vertical obstructions, including their height and arrangement, are analyzed to determine their contribution to turbulence generation and flow resistance. Additionally, the performance of triangular gabion sills installed on the steps is assessed under different slopes and discharge conditions. Finally, a comparative evaluation between gabion and rigid stepped spillways is conducted to determine overall suitability and hydraulic efficiency.

4.2 To investigate the energy dissipation in a gabion stepped spillway under different flow regimes while evaluating the effects of porosity, slope and discharge

The experiments were conducted on nine physical models filled with crushed stone of 20-40 mm size having three different porosities (34%, 38% and 42%) with varying slopes of 33.69°, 45°and 63.43°. Total 540 runs were performed over a wide discharge range (refer **Appendix I)**. The height for each tested model was 0.33 m. The soft computing model Adaptive Neuro-Fuzzy Inference System (ANFIS) was employed to assess the experimental data. The observed nappe, transition and skimming flow regimes are shown in **Figure 4.1 (a-c)**.



(a)



(b)



Figure 4.1 (a-c) Nappe, Transition and Skimming flow regime over a gabion stepped spillway with 33.69°slope with $n = 34\%$

4.2.1 Experimental findings

Threshold discharge refers to the minimum flow rate at which a spillway flow transitions from throughflow to overflow conditions. When the flow rate exceeds this threshold over a gabion stepped spillway, water flows from the crest to the downstream section. Further, it was observed that at step-2, more eddies were generated, leading to higher aeration efficiency. As the flow continues downstream from the steps, the intensity of the recirculating vortices begins to diminish.

The experimental results demonstrated that flow conditions on stepped spillway depend on flow rate, step height and spillway slope. Three distinct flow conditions were identified i.e. nappe, transition, and skimming flow (refer **Figure 4.1**). When the critical depth to step height ratio (Y_c/h) is low, combined with lower unit discharge and a milder spillway slope, the flow shifts toward the nappe flow regime. However, higher unit discharge and steeper spillway slopes, along with higher critical depth to step heights, tend to promote transition and skimming flow regime conditions. Figure **4.1** illustrates the classification of these flow conditions on gabion stepped spillway.

4.2.2 Effect of Y_c/h on energy dissipation performance

Figure 4.2 shows the plot between Y_c/h and E_L for GS-1, GS-2 and GS-3. It is observed that as values of Y_c/h increase, relative energy loss decreases. The values of Y_c/h are in scattered nature in all test runs with the similar finding of **(Salmasi and Özger, 2014)**.

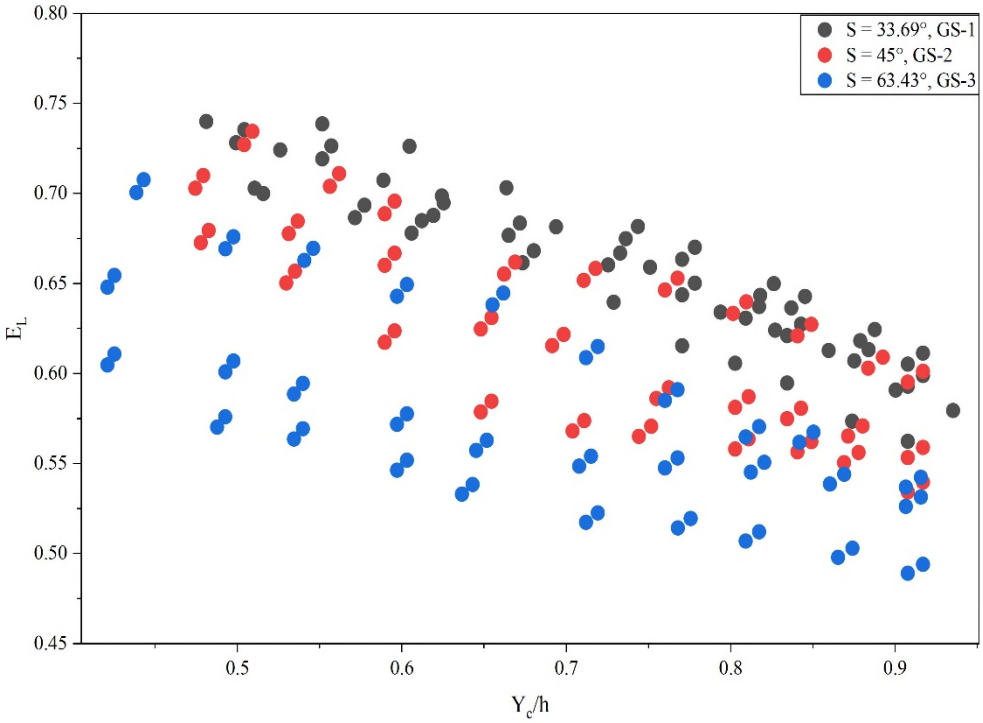

Figure 4.2 Y_c/h vs E_L plot for GS-1, GS-2 and GS-3 models

4.2.3 Effect of discharge and downstream slope on energy dissipation performance

In the context of **Figure 4.3**, the variation of relative energy loss with discharge for standard gabion stepped (GS), is plotted for three downstream slopes of 33.69°, 45°and 63.43°. For all configurations, relative energy loss exhibits a decreasing trend with increasing discharge, indicating a progressive dominance of inertial forces over frictional resistance and form drag at higher flow rates. The threshold discharge for the initiation of overflow conditions in GS models varies between 15 and 21 m^3/s, reflecting the influence of gabion porosity and sill-induced flow obstruction on upstream head development.

Figure 4.3 shows the variation of relative energy loss vs discharge for different spillway slopes at constant porosity ($n = 34\%$). The gabion stepped spillway (GS) models, showed energy dissipation with an average relative energy loss of between 49% and 74%. Higher surface roughness, flow penetration into the porous gabion matrix and higher turbulence formation were the reasons for the flows. The upstream

flow depth increases to a range of 0.33-0.46 m, further contributing to higher dissipation through increased flow structure interaction.

A comparative assessment across downstream slopes reveals that milder slopes consistently dissipate more energy than steeper slopes for a given discharge. The spillway slope of 33.69° configuration exhibits the highest overall energy dissipation, followed by slopes of 45°and 63.43°. This behavior is attributed to reduced flow velocity, increased flow residence time and more pronounced vortex formation within step cavities for milder slopes. Conversely, steeper slopes promote higher velocities and shorter interaction lengths between the flow and step geometry, which suppress turbulence development and reduce dissipation efficiency.

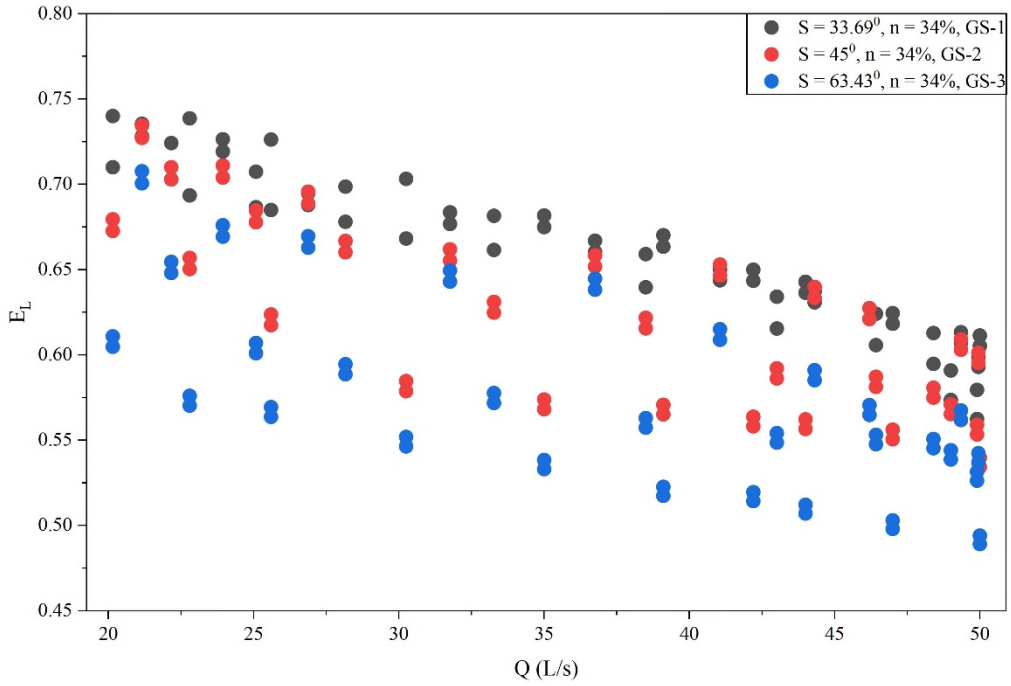

Figure 4.3 Q vs E_L plot for different spillway slopes model at porosity ($n = 34\%$)

4.2.4 Effect of Drop Number and Downstream Slope on Energy Dissipation Characteristics

Relative energy loss (E_L) is expressed as a function of the drop number, a dimensionless parameter defined in equation (7), which incorporates the effects of discharge and spillway geometry. When the downstream slope is considered, the

modified drop number $q^2 tan(\theta)^2 / gH^3$ provides a comprehensive representation of flow intensity over stepped spillways. In the present study, the drop number varies from 0.003 to 0.027, covering a wide range of hydraulic conditions (refer **Figure 4.4**).

The variation of relative energy loss with drop number indicates a consistent decreasing trend for gabion stepped (GS) spillways. This behavior reflects the progressive dominance of inertial forces as flow intensity increases, which reduces the effectiveness of form drag, surface roughness and cavity-scale recirculation. Among the GS models, higher energy dissipation is observed for milder slopes at lower drop numbers, indicating stronger flow structure interaction due to reduced velocities and enhanced turbulence development. A combined comparison across downstream slopes further demonstrates that, for a given drop number, milder slopes dissipate more energy than steeper slopes. The 1:1.5 (*V:H*) configuration consistently exhibits the highest relative energy loss, followed by 1:1 and 1:0.5 (*V:H*). Steeper slopes are associated with higher flow velocities and shorter interaction lengths over the steps, which restrict the formation of vortices and reduce turbulence intensity within the step cavities. In contrast, milder slopes increase flow residence time and promote stronger recirculation zones, resulting in higher dissipation efficiency.

Overall, the results confirm that relative energy loss decreases with increasing drop number for all spillway configurations, while downstream slope and structural modifications play a critical role in controlling dissipation efficiency. The inclusion of a triangular gabion sill particularly when positioned on the second step provides a consistent and substantial enhancement in energy dissipation across all slopes, with the most pronounced benefits observed under milder downstream slope conditions.

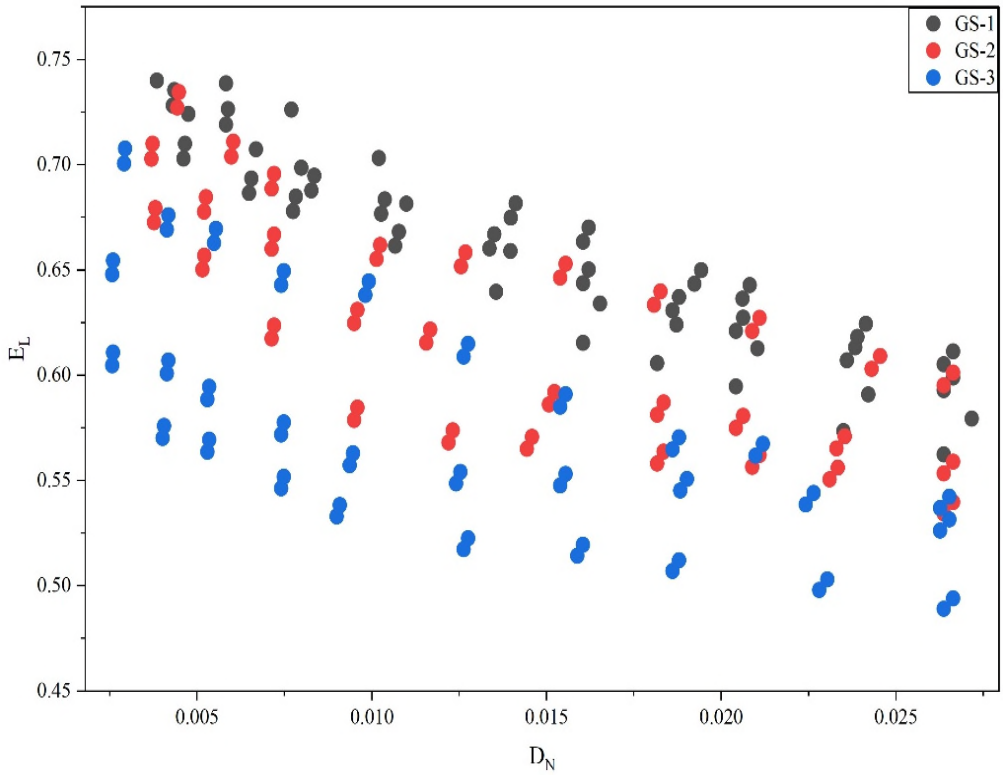

Figure 4.4 D_N vs E_L plot for GS-1, GS-2 and GS-3 models

4.2.5 Effect of porosity on energy loss

Figure 4.5 represents the variation of energy dissipation efficiency with slope angle of 33.69° and for all three porosity for stepped gabion structures. From the experimental findings it was observed that the relative energy dissipation rate decreases as porosity increases from 34% to 42%, with the maximum occurring at 34% porosity**.** This shows an optimal porosity value around 34 % for maximizing the energy dissipation. Additionally, as slope angle increases from 33.69^0 to 63.43^0, performance decreases consistently across all porosity levels, indicating that milder slopes are more effective. However, at 34% porosity, values drop from 74.0% to 48.0% at 33.69^0. The findings highlight the influence of slope and porosity, with a recommended porosity of 34% and milder slopes for better hydraulic performance.

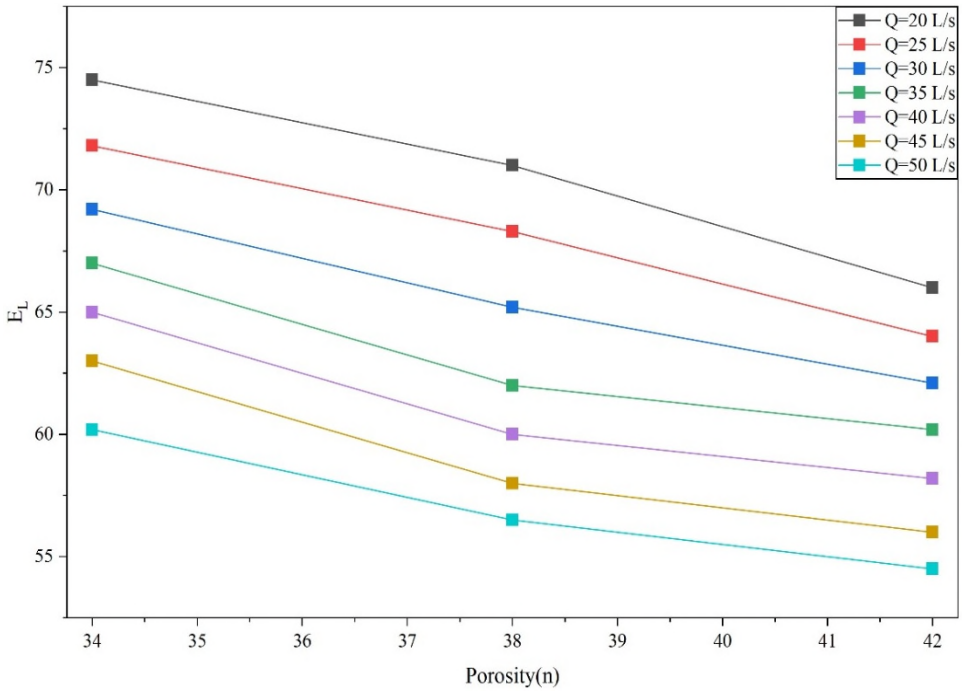

Figure 4.5 *Q* vs *n* plot for energy dissipation for various porosity at slope 33.69^0

4.2.6 Validation of experimental findings

The result obtained from the experimental findings is validated using the ANFIS technique. In ANFIS, the fuzzy inference system (FIS) has five inputs i.e. spillway slope (S), critical depth to step height ratio (Y_c/h), drop number (D_N), Froude number (F_r) and porosity (n) and one output is relative energy dissipation ($\Delta E/E_0$). The structure of proposed fuzzy inference system (FIS) is shown in **Figure 4.6 (a)**.

The datasets were imported into the MATLAB workspace and entered into the Neuro-Fuzzy Designer for analysis. Training was conducted with 100 epochs, a training error tolerance limit of +0.01, and different membership functions. The FIS was generated using grid partitioning, and the hybrid method was adopted for training. **Figure 4.6 (b)** illustrates the simulink architecture which consists of the imported ANFIS model integrated with input-output connections using Mux and Demux blocks, enabling the processing of dataset parameters to generate the corresponding energy dissipation output over the simulation period.

The prediction accuracy for the datasets is summarized in **Table 4.1**, with the gbellmf membership function achieving the highest average prediction accuracy. In dataset-1, the minimal training and testing RMSE was 0.017 and 0.024 for the gbellmf function. This structured approach demonstrated the effectiveness of the ANFIS model in predicting energy loss with high precisions. **Table 4.2** below shows the ANFIS structure for gbellmf.

Table 4.1 Test performance of different membership functions

Membership function	Minimal training RMSE (Dataset-1)	Prediction Accuracy (Dataset-1) (%)	Minimal training RMSE (Dataset-2)	Prediction Accuracy (Dataset-2) (%)	Minimal training RMSE (Dataset-3)	Prediction Accuracy (Dataset-3) (%)	Average Prediction Accuracy (%)
trimf	0.225	99.775	0.792	99.208	0.730	99.270	99.418
trampmf	0.156	99.844	0.325	99.675	0.420	99.580	99.700
gbellmf	0.017	99.983	0.102	99.808	0.130	99.870	99.887
gaussmf	0.112	99.488	0.88	99.12	0.930	99.070	99.226
gauss2mf	1.226	98.774	0.945	99.055	1.330	98.670	98.833
pimf	0.721	99.279	0.965	99.035	0.839	99.161	99.158
dsigmf	1.327	98.673	1.045	98.955	1.191	98.809	98.812
psigmf	1.120	98.880	1.026	98.974	1.930	98.070	98.641

Table 4.2 ANFIS structure for membership function (gbellmf)

Number of nodes	524
Number of linear parameters	243
Number of non-linear parameters	45
Total number of parameters	288
Number of training data pairs	180
Number of checking data pairs	95
Number of fuzzy rules	243

4.2.6.1 Membership functions plot

The membership function can be plotted for input variables in **Figure 4.6 (c)**. MF-1, MF-2 and MF-3 are plotted for different inputs. for selected membership functions the values of input variables are plotted with respect to the output. Prediction of input values can also be done with the help of these plots **Mojtahedi et al. (2020)**.

4.2.6.2 Surface plots

These plots can be seen in the surface viewer of the neuro-fuzzy designer **Mojtahedi et al. (2020)**. Input variables are plotted with respect to the output represented in **Figure 4.6 (d)**. The variation of the range of two input variable values is shown with the range of output function.

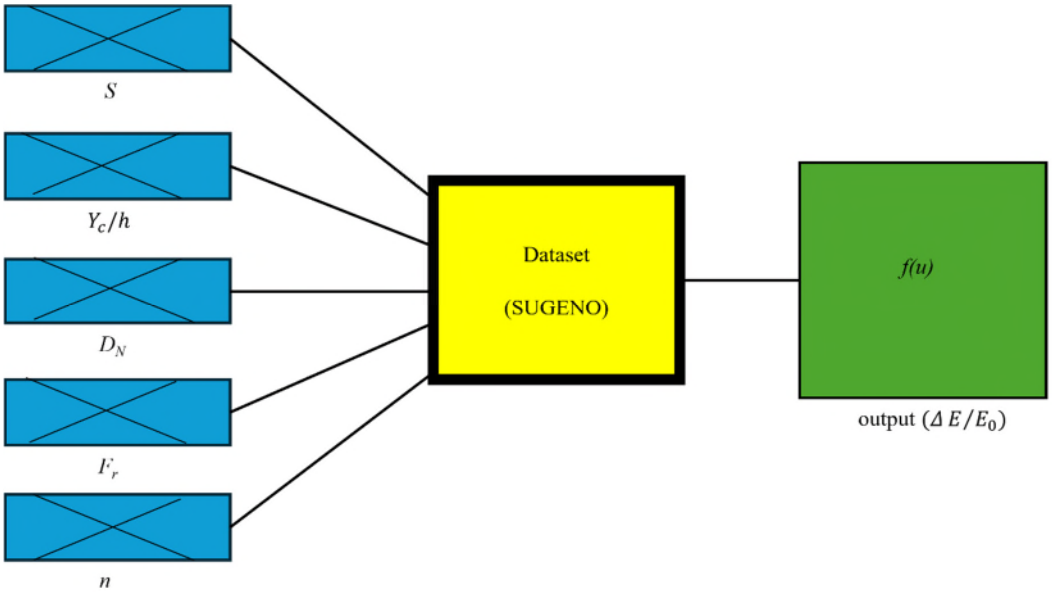

(a)

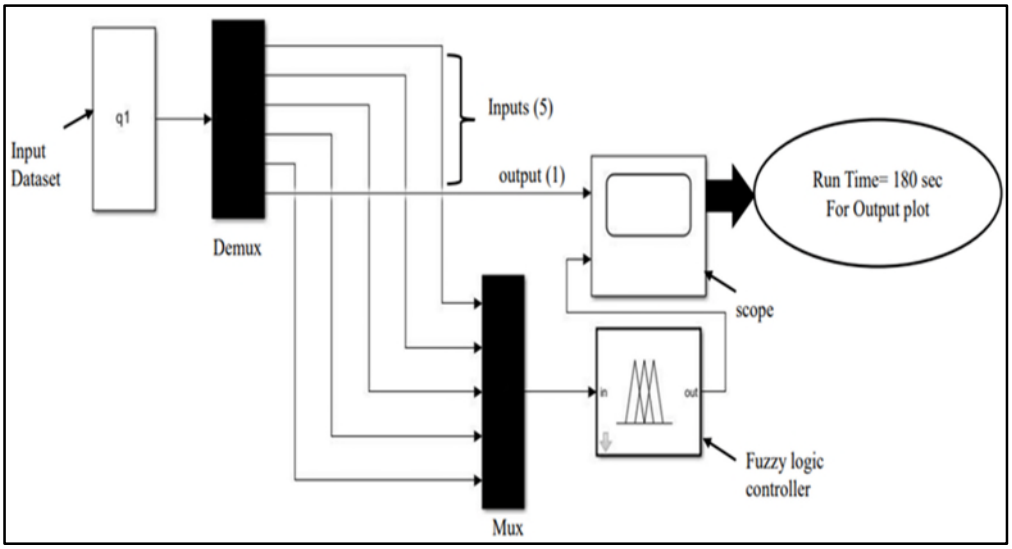
Input
Dataset
q1
Demux
Inputs (5)
output (1)
Run Time= 180 sec
For Output plot
scope
in
out
Fuzzy logic
controller
Mux

(b)

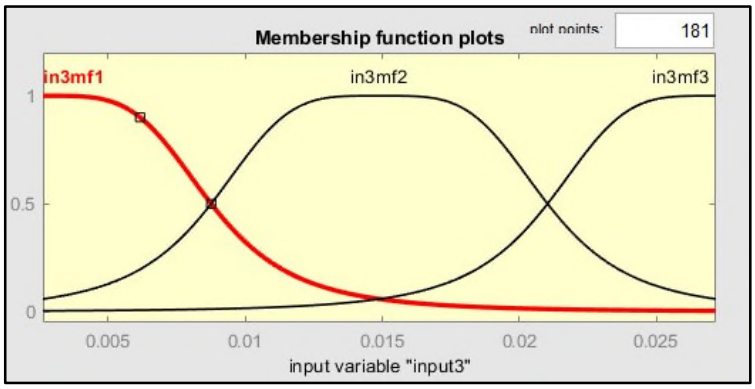
Membership function plots
plot points:
181
in3mf1
in3mf2
in3mf3
1
0.5
0
0.005
0.01
0.015
0.02
0.025
input variable "input3"

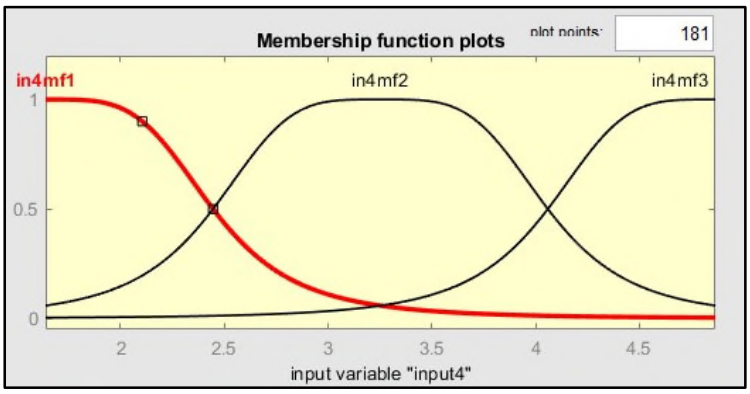
Membership function plots
plot points:
181
in4mf1
in4mf2
in4mf3
1
0.5
0
2
2.5
3
3.5
4
4.5
input variable "input4"

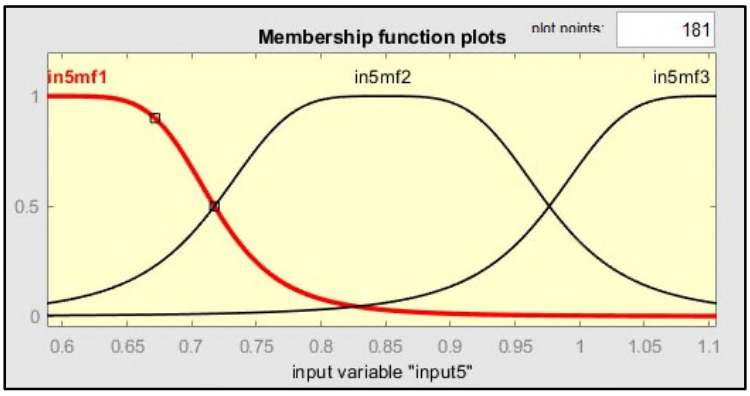
Membership function plots
plot points:
181
in5mf1
in5mf2
in5mf3
1
0.5
0
0.6
0.65
0.7
0.75
0.8
0.85
0.9
0.95
1
1.05
1.1
input variable "input5"

(c)

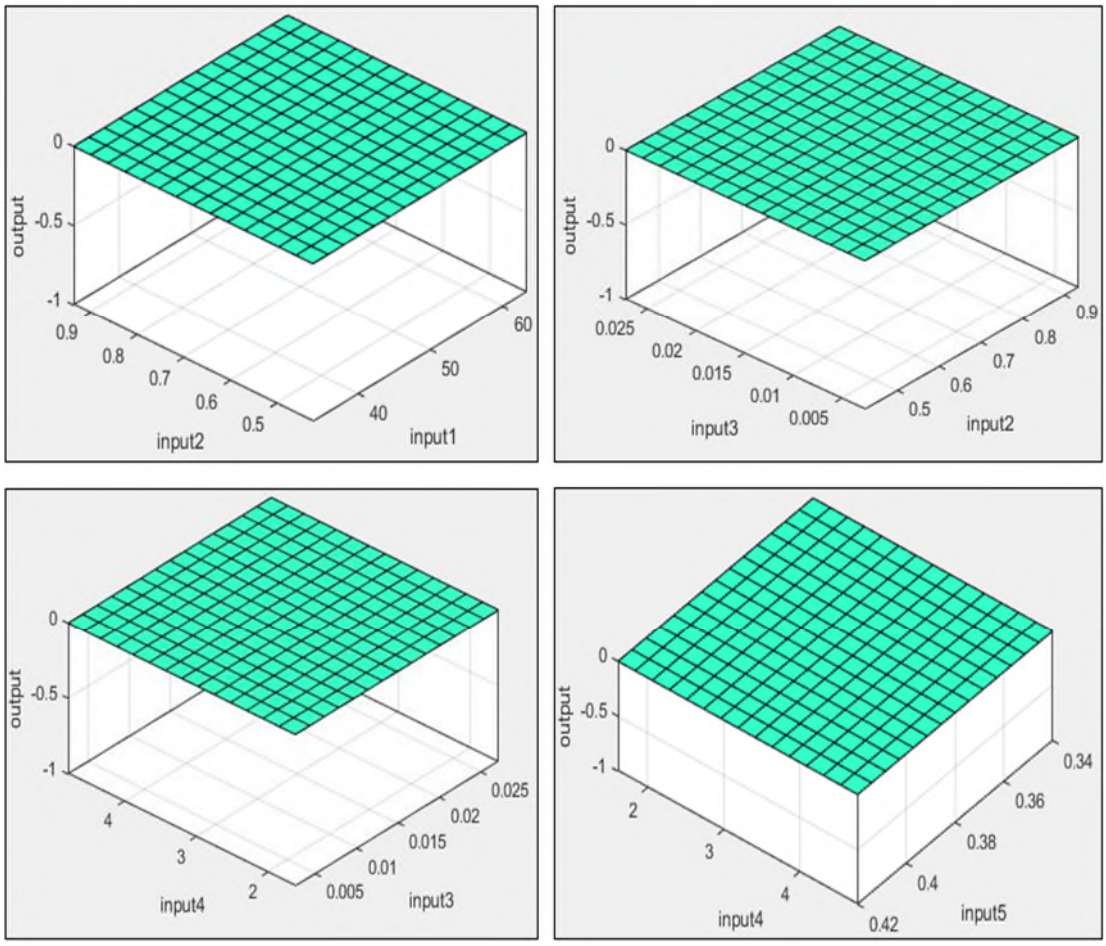

(d)

Figure 4.6 (a) Structure of proposed FIS**;** (b) Simulink architecture; (c) Membership function plot for input variables for gbellmf**;** (d) Surface plot of the input variable with the output

ANFIS output data was obtained by downloading scope data from the MATLAB workspace. The measured experimental data and ANFIS output were plotted, as shown in **Figure 4.7 (a)**. The average relative error was 1.25%. This process was repeated for other datasets. **Figure 4.7 (b)** represents the plot of relative error. The present study on gabion stepped spillways shows some key differences and improvements over the model used in past findings as shown in **Table 4.3**. **Salmasi and Özger (2014)** applied an ANFIS-based neuro-fuzzy approach to estimate energy dissipation in the skimming flow regime of stepped spillways. Their model achieved determination coefficients (R^2) of 0.974 for training and 0.966 for testing, with

relatively low error indices, demonstrating that ANFIS can successfully capture the nonlinear behavior of stepped spillway hydraulics.

Gabion stepped spillways, when modeled with ANFIS, yielded RMSE values of 0.017 (training) and 0.024 (testing), MAE values of 1.81 and 1.06, and R^2 values of 0.985 and 0.976 respectively. These results not only confirm the reliability of ANFIS modelling in predicting energy dissipation but also indicate slightly higher predictive accuracy.

Table 4.3 Comparison with past findings

Study	Method / Model	Phase	RMSE	MAE	R^2
Salmasi & Özger (2014) (Conventional Stepped Spillway)	ANFIS	Training	–	–	0.974
		Testing	–	–	0.966
Present Study (Standard Gabion Stepped Spillway)	ANFIS	Training	0.017	1.81	0.985
		Testing	0.024	1.06	0.976

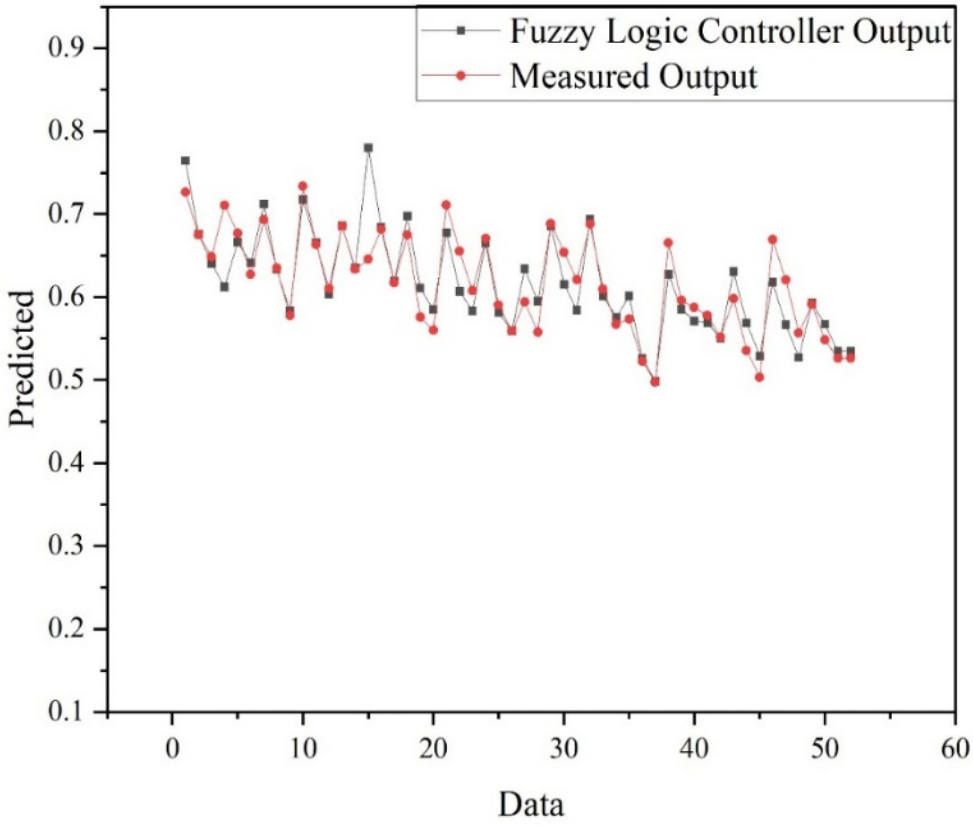
Fuzzy Logic Controller Output
Measured Output
Predicted
Data
0.1
0.2
0.3
0.4
0.5
0.6
0.7
0.8
0.9
0
10
20
30
40
50
60

(a)

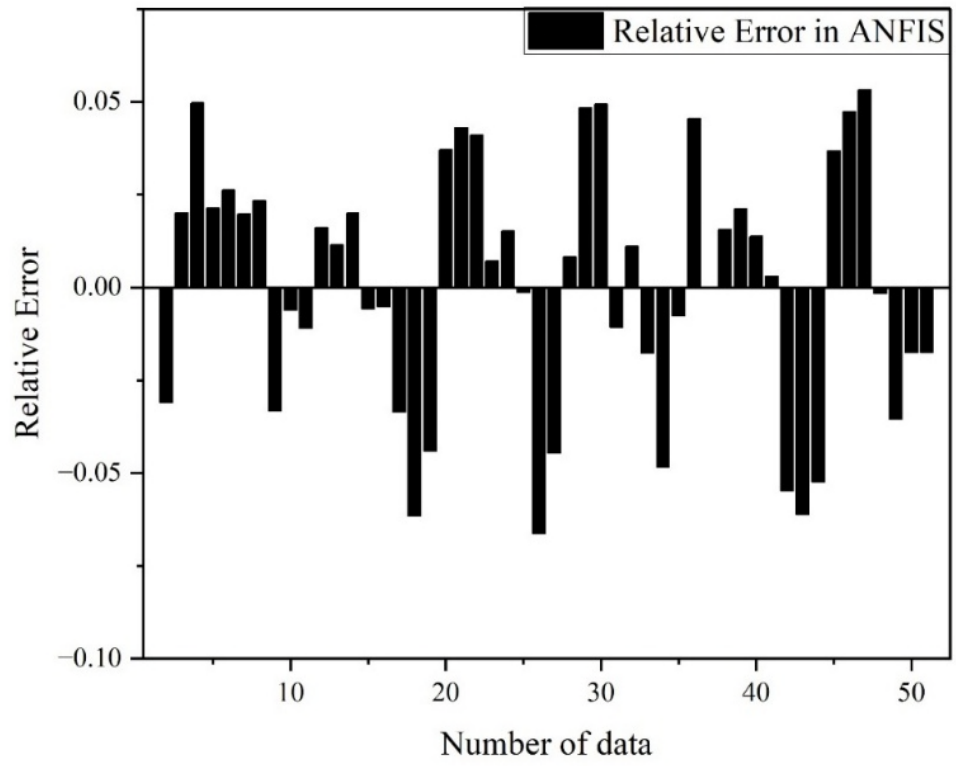
Relative Error in ANFIS
Relative Error
Number of data
0.05
0.00
−0.05
−0.10
10
20
30
40
50

(b)

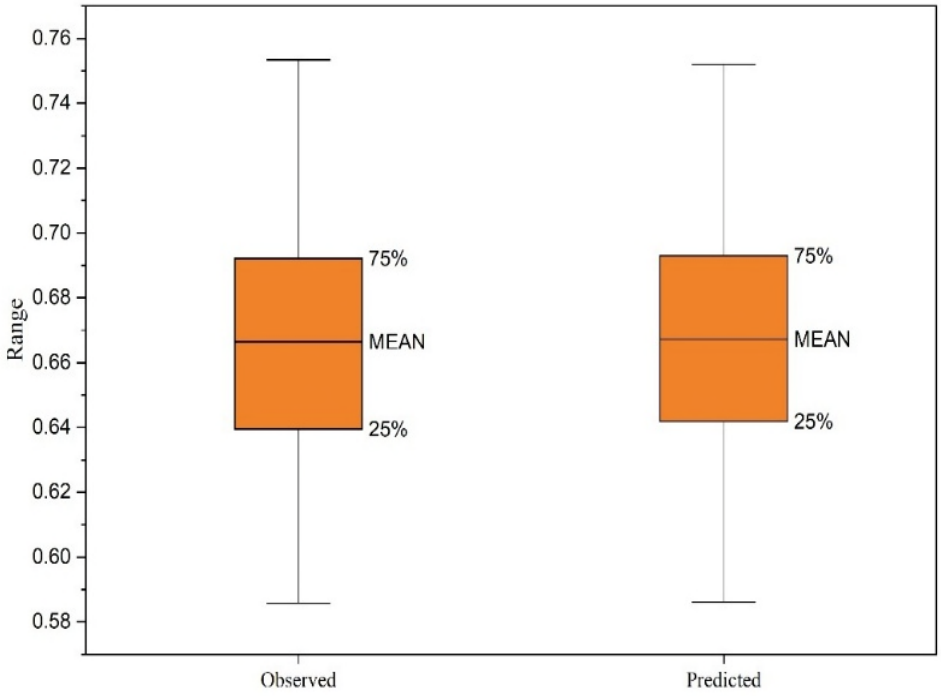

(c)

Figure 4.7 (a) The measured experimental data and ANFIS output ;**(b)** Plot of relative error; **(c)** Box and Whisker plot for observed and predicted value of energy dissipation

4.2.6.3 Box and Whisker plot for observed and predicted value of energy dissipation

The comparison between observed and predicted energy dissipation for the gabion stepped spillway is illustrated in **Figure 4.7 (c)** through box and whisker plots to validate the results. Both datasets exhibit a close statistical agreement within the range of 0.58-0.75 for energy dissipation. For the observed values, the minimum and maximum energy dissipation were 0.585 and 0.753 respectively. The mean was 0.664, while the 25th percentile (Q_1) and 75th percentile (Q_3) were 0.638 and 0.688 respectively, giving an interquartile range (IQR) of 0.050. For the predicted values, the minimum and maximum were 0.586 and 0.754 respectively, with a mean of 0.665. The 25th and 75th percentiles were 0.639 and 0.688, yielding an IQR of 0.049. The extremely close mean values (difference = 0.0012, i.e., 0.18%) and nearly identical IQRs indicate that the predictive model successfully reproduces the central tendency

and variability of the observed dataset. The whiskers show similar trends and extreme minimum and maximum values are well captured by the model. Thus, the box-and-whisker analysis provides a robust uncertainty assessment, demonstrating that model variability is consistent with observed data, and systematic prediction bias is statistically negligible. These results strengthen confidence in the reliability of the ANFIS model for practical hydraulic engineering applications. Further, it is observed that the relative energy loss decreases with increasing discharge for all spillway slopes, indicating reduced dissipation under skimming flow. Milder slopes (33.69^0) exhibit higher energy loss than steeper slopes, confirming enhanced dissipation due to increased flow interaction.

4.2.7 Discussion for Objective-1

In a gabion stepped spillway, relative energy loss is greater on milder slopes compared to steeper ones. For gabion models with higher discharge, relative energy loss decreases in skimming flow regimes. Additionally, as the drop number increases, relative energy loss declines, whereas a decrease in the drop number results in higher relative energy loss. In ANFIS, the RMSE calculated for various membership functions is lowest for the gbellmf membership function, which also provides higher classification accuracy. The average relative error between observed data and ANFIS predictions is approximately 1.25%. In present study ANFIS achieved higher predictive accuracy (R^2 = 0.985 training, 0.976 testing). This confirms both the effectiveness of gabion structures in dissipating energy and the robustness of ANFIS modelling for reliable performance estimation. The statistical and graphical analyses confirm that the predictive model accurately reproduces the observed energy dissipation of the gabion stepped spillway. The close alignment of means, medians, and interquartile ranges, along with high R^2 and very low error values. The accurate predictions provided by the ANFIS model can support engineers in optimizing spillway design by estimating energy dissipation under various flow conditions without relying solely on complex physical modelling. This enables more cost-effective and safer hydraulic structure designs

4.3 To investigate the effect of vertical obstructions and its various arrangement on energy dissipation in gabion stepped spillways

The energy dissipation was analyzed for a gabion stepped spillway with three steps and height of 0.27 m, considering the use of vertical obstructions arranged in three distinct patterns: uniform, staggered-1, and staggered-2. The skimming flow over the gabion stepped spillway having vertical obstructions 9 cm height shown in **Figure 4.8.** The set of experimental runs performed for models are given in **Appendix-II.**



(a)



(b)

Figure 4.8 Skimming flow over the gabion stepped spillway having vertical obstructions (h_v = 9 cm) (a) front view; (b) side view

4.3.1 Effect of vertical obstruction's height on energy dissipation

The experiment used vertical obstructions with heights of 3, 6 and 9 cm. The results indicate that relative energy loss is higher when vertical obstructions are present compared to a stepped spillway without them. For the same discharge per unit width, the highest relative energy loss corresponds to greater obstruction heights. The maximum energy loss was observed in the staggered-1 pattern with 9 cm vertical obstructions. When obstructions are there, water flows over them reducing the generation of currents. As the velocity increases, this effect diminishes.

For uniform patterns, vertical obstructions placed on the steps generate eddies and create turbulence as water flows through. Some sections allow water to pass freely between the obstructions. In the staggered-1 pattern, obstructions are positioned so that each row alternates, with one obstruction placed at the center between two obstructions in the following row. This arrangement generates eddies near the obstructions, making it more effective at dissipating the kinetic energy of the water.

The staggered-2 pattern also enhances energy dissipation compared to the uniform pattern.

4.3.2 Effect of h/y_c and F_0 on energy dissipation

Figure 4.9 (a) illustrates the relationship between $\Delta E/E_0$ and h/y_c for various relative heights of vertical obstructions across different patterns. As the value of h/y_c increases, the relative energy loss also increases. Among the patterns analyzed, the staggered-1 pattern with $h_v = 9$ cm, shows the highest energy loss at the maximum h/y_c =1.68, surpassing the energy dissipation observed in the uniform and staggered-2 patterns. **Figure 4.9 (b)** shows the plot between relative energy loss and upstream Froude number. In the case of maximum height of vertical obstruction, the staggered-1 pattern holds good results in relative energy dissipation. The relative energy dissipation is a maximum of 78% for the 0.065 value of the upstream Froude number for the staggered-1 pattern and minimum of 58% for the 0.059 value of the upstream Froude number for without obstruction.

For $F_0 = 0.10$ and $h_v = 9$ cm, the percentage increase in relative energy dissipation is as follows: 35.42% for the uniform pattern obstruction, 45.83% for the staggered-1 pattern obstruction, and 39.58% for the staggered-2 pattern obstruction compared to the case without obstruction. On the other side with $F_0 = 0.10$ and $h_v = 6$ cm, the percentage increase in relative energy dissipation in the case of uniform pattern obstruction is 20.83 %, in the case of staggered-1 pattern obstruction it is 37.5 % and in the case of staggered-2 pattern obstruction, it is 29.17 % as compared to without obstruction.

Similarly, for $F_0 = 0.10$ and $h_v = 3$ cm, the percentage increase in relative energy dissipation in the case of uniform pattern obstruction is 14.58 %, in the case of staggered-1 pattern obstruction it is 29.17 % and in the case of staggered-2 pattern obstruction, it is 16.67 % as compared to without obstruction.

This further leads to the observation that the obstructions cause localized turbulence and additional eddies, which dissipate a portion of the flow's kinetic energy. This effect is more pronounced when the obstruction patterns are strategically designed, such as in uniform or staggered configurations. The obstruction increases air entrainment into

the flow, leading to more significant mixing between air and water. This aeration further dissipates energy by reducing the velocity and flow intensity. Relative energy loss corresponding to the $F_0 = 0.10$ and $h_v = 9$, 6 and 3 cm are shown in **Table 4.4**.

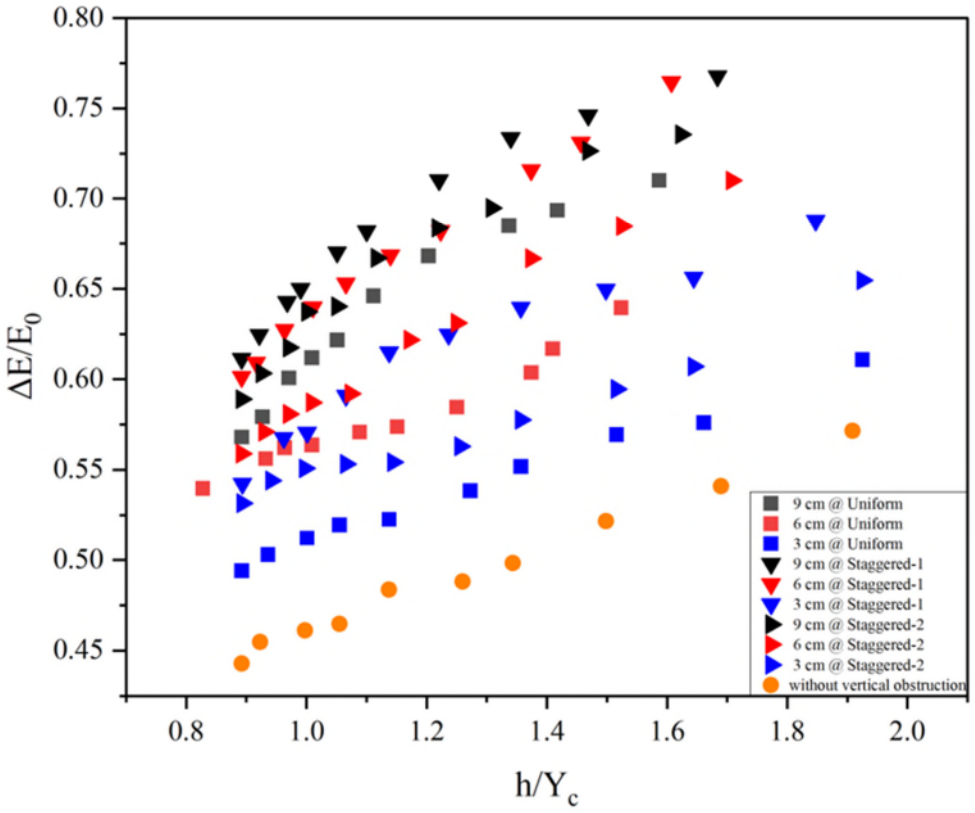

(a)

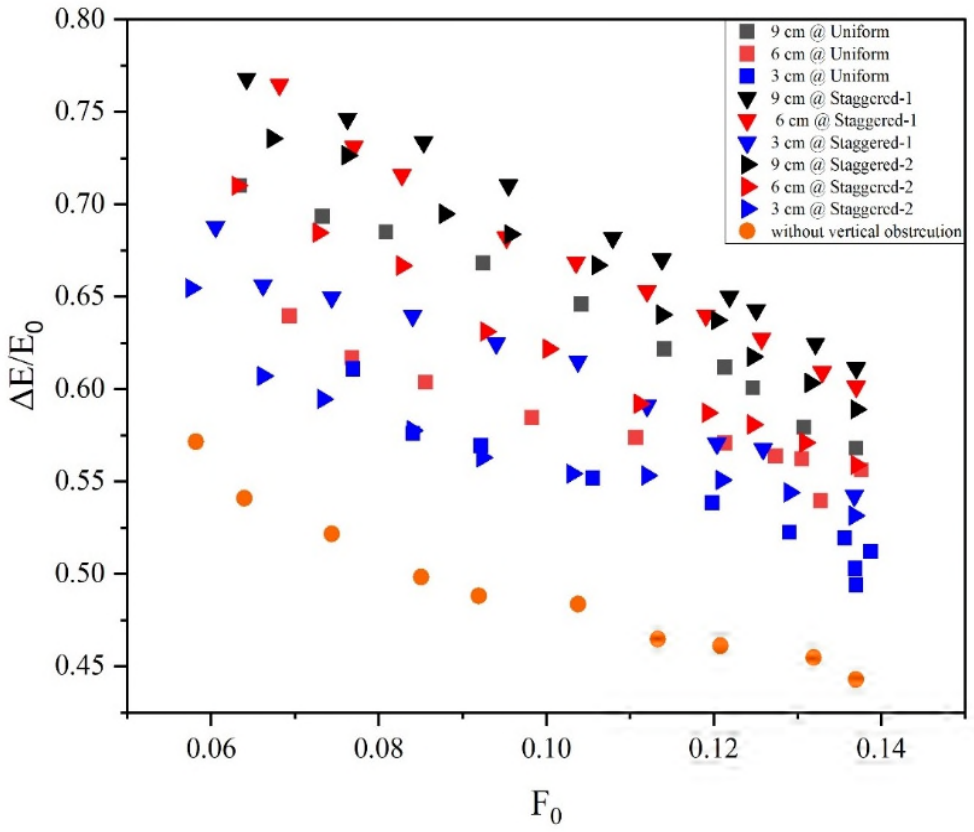

(b)

Figure 4.9 Plot between; (a) $\Delta E/E_0$ vs h/Y_c; (b) $\Delta E/E_0$ vs F_0; for different relative heights of vertical obstruction for various patterns

Table 4.4 Relative energy loss corresponding to the $F_0 = 0.10$ and $h_v = 9$, 6 and 3 cm

h (cm)	*hv* (cm)	*hv/h*	Condition	Uniform pattern	Staggered-1 Pattern	Staggered-2 pattern	Without obstruction
9	9	1	$\Delta E/E_0$ (h_v=9cm)	0.65	0.70	0.67	0.48
	6	0.67	$\Delta E/E_0$ (h_v=6cm)	0.58	0.66	0.62	
	3	0.33	$\Delta E/E_0$ (h_v=3cm)	0.55	0.62	0.56	

4.3.3 Validation of Experimental Findings

ELM modelling is done for experimental setup of 180 runs for each model corresponding to the three downstream slopes. ELM modelling is done by developing a generalized program in the MATLAB (Version: R2023a) workspace for the dataset. 180 runs of data set were divided into two parts in which 70% are the training data (126 data points) and 30% testing part (54 data points). The testing data is selected randomly, and it is independent of training data. ELM produces the best output by taking five neurons in the hidden layer and relative energy loss as output. These soft computing models have an adequate level of accuracy based on the result of fitting the observed and predicted value, and the fitted line equation $y = c_1x + c_2$ predicted the model performance. In training stage, c_1 and c_2 were 0.9811 and 0.0102 and for the testing stage 0.9617 and 0.020 respectively. The value of R^2 for the training and testing stage is 0.9812 and 0.9618 respectively shown in **Figure 4.10 (a-c)**. The average relative error calculated between observed data and ELM output is 0.75% as per **Figure 4.10 (d).**

As the values of RMSE, MAE, and NSE are close to zero, the model showed better results which are calculated from statistical formulas in equation (18),(19) and (20). The ELM model demonstrated lower MAE and RMSE values of 1.34 and 0.0026 (training) respectively, while achieving a higher $R^2 = 0.9812$. For the ELM model, the reduction in RMSE during the training and testing stages are 0.0140 and 0.0270 respectively. Additionally, the MAE for the ELM model is calculated at 0.45 and 0.083, which corresponds to 24.86% and 7.83% of the MAE values in the ELM model for both stages. NSE values are also found to be approximately 1.24% and 1.1% for both stages.

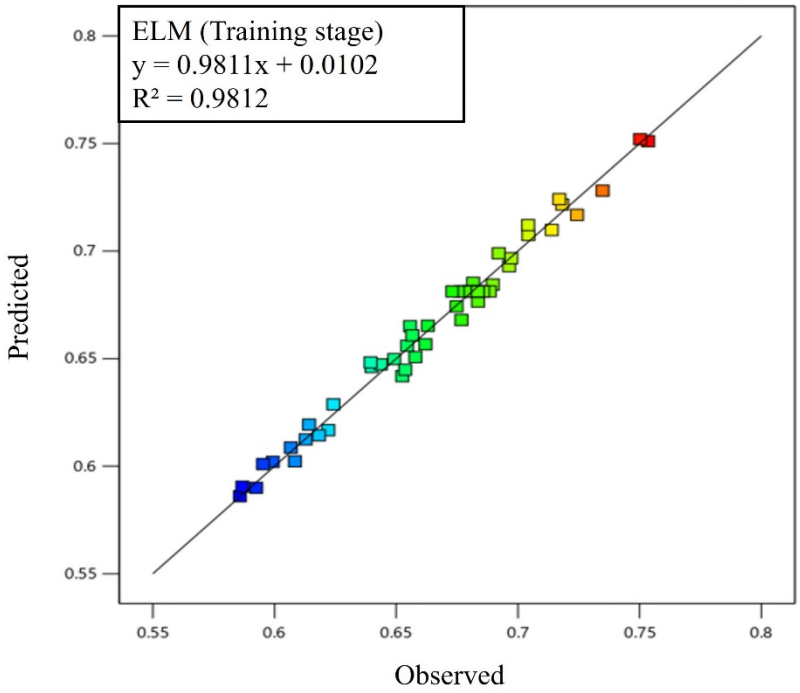
ELM (Training stage)
y = 0.9811x + 0.0102
R² = 0.9812
Predicted
Observed
0.8
0.75
0.7
0.65
0.6
0.55
0.55
0.6
0.65
0.7
0.75
0.8

(a)

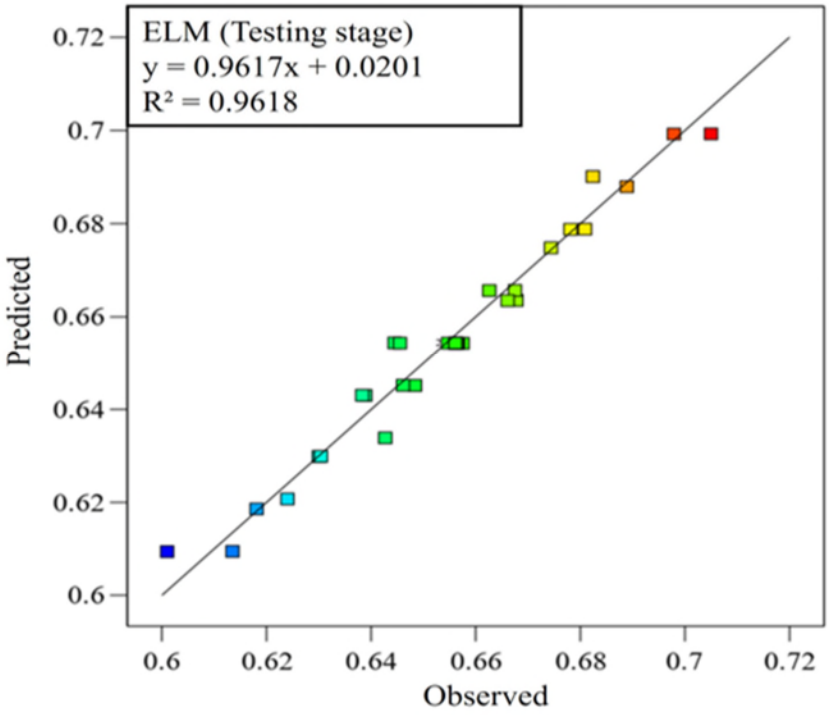
ELM (Testing stage)
y = 0.9617x + 0.0201
R² = 0.9618
Predicted
Observed
0.72
0.7
0.68
0.66
0.64
0.62
0.6
0.6
0.62
0.64
0.66
0.68
0.7
0.72

(b)

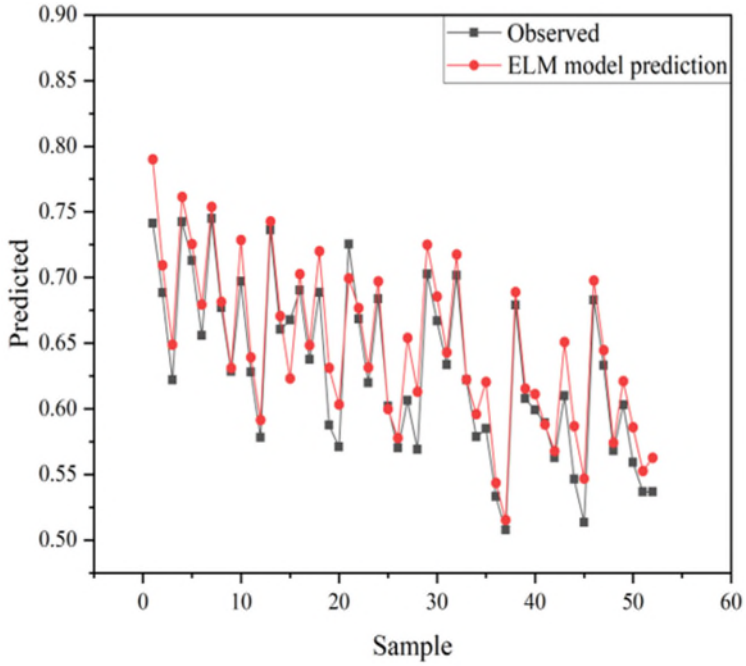

(c)

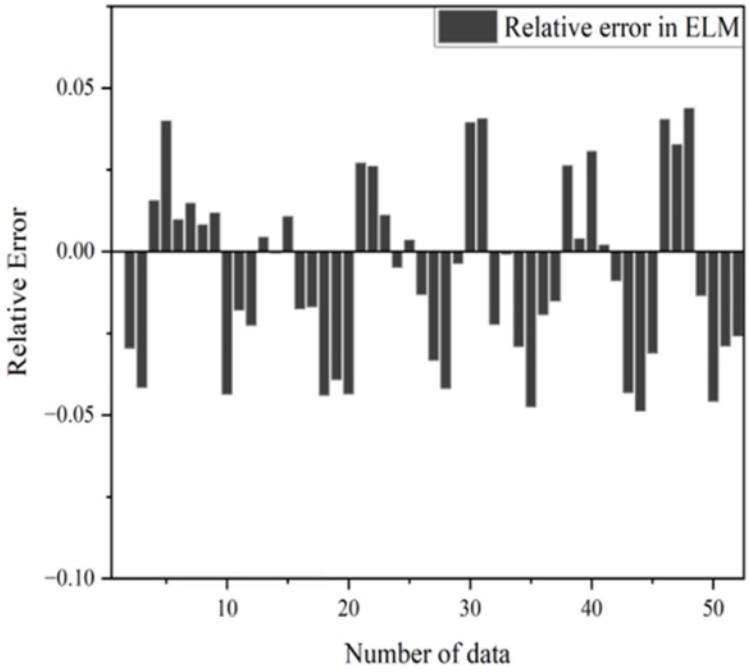

(d)

Figure 4.10 Observed and predicted value for (a) training; (b) testing stage for ELM; (c) Comparisons of the observed data with the predicted data of ELM; (d) Relative error

4.3.3 Discussion for Objective-2

Introducing vertical obstructions significantly enhances relative energy dissipation, with the staggered-1 configuration achieving the highest relative energy loss, showing a maximum increase of 45.83%, followed by the staggered-2 and uniform patterns compared to the case without obstructions. Different obstruction heights were tested, and their influence on energy dissipation was observed, showcasing that obstruction height plays a critical role in hydraulic performance.

4.4 To investigate the influence of a triangular gabion sill placed on the steps of a gabion spillway on energy dissipation across different downstream slopes and discharge conditions

Triangular Gabion Sill was placed on step-1, step-2 and step-3 separately of the gabion stepped spillway. For models GT-4, GT-5 and GT-6 the average value of energy loss is between range of 55 % to 81 % for sill placed on step-2 which is higher than sill placed on step-1 and step-3 concerning the various range of flow rates. The form-drag effects of the step forms and the recirculating vortices between the gap of steps and sill are responsible for energy loss. The rough surface due to meshes and stones also makes the higher flow resistance. The model shows higher relative energy loss with slope 33.69^0 than slopes 45^0 and 63.43^0 which was also evaluated by **(Salmasi et al., 2012) (Chinnarasri et al., 2008)**. Therefore, the model having a lower value of slope dissipated more energy than a higher slope. Thus, from all sets of experimental combinations, GT-4 having a slope of 33.69^0 is more efficient in improving hydraulic behavior. Physical model set up in the laboratory flume with triangular gabion sill on step-1 shown in **Figure 4.11**. The set of experimental runs performed for models are given in **Appendix-III.**

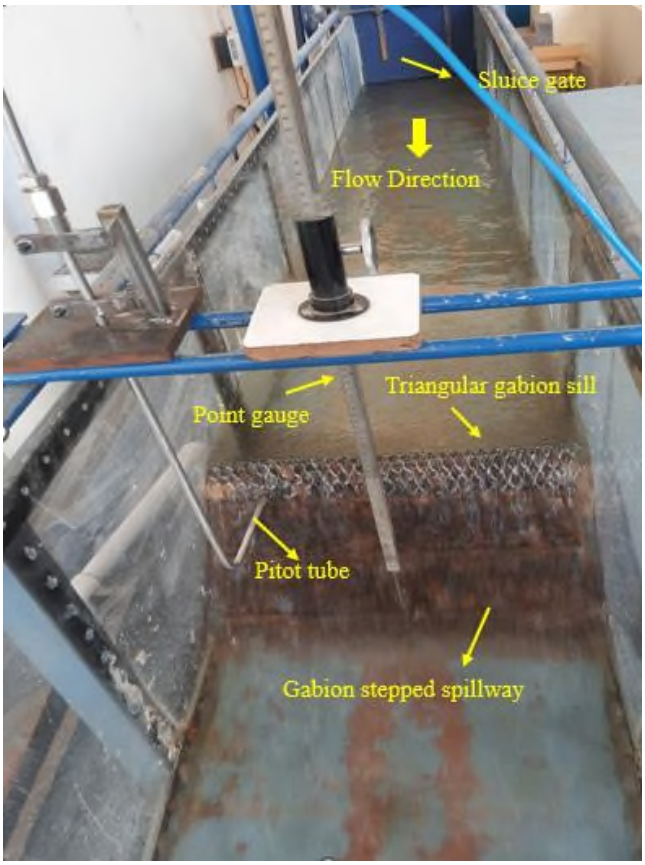

Figure 4.11 Physical model set up in the laboratory flume with triangular gabion sill on step-1

4.4.1 Comparison of results based on Y_c/h

Figure 4.12 shows the plot between Y_c/h and E_L for GT-4, GT-5 and GT-6 (Gabion stepped spillway with triangular gabion sill placed on step-2). It is noticed that as values of Y_c/h increase, relative energy loss decreases. The values of Y_c/h are in scattered nature in all test runs with the similar finding of **(Salmasi and Özger, 2014)**. The average relative error in the values of energy loss between the GT-4 and GT-5 models is 0.1% and GT-5 and GT-6 models are 0.5% respectively.

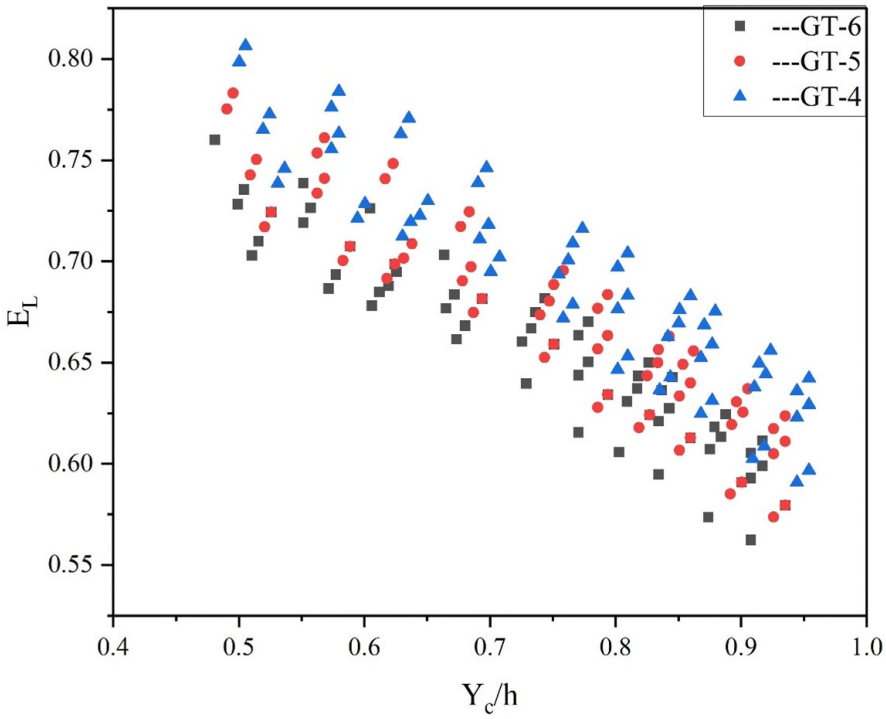

Figure 4.12 Y_c/h vs E_L plot for GT-4, GT-5 and GT-6 models for sill on step-2

4.4.2 Comparison of results based on D_N

Relative Energy loss is a function of drop number which is a dimensionless parameter as shown in equation (6). **Figure 4.13** represents the plot between D_N and E_L . If the slope of the spillway is introduced, then the modified drop number will be $q^2 tan(\theta)^2 / g{H_s}^3$. The value of the drop number ranges from 0.004 to 0.030. Models GT-4, GT-5 and GT-6 yield the energy loss for sill on step-2 which is higher than sill on step-1 and step-3 concerning the drop number. So it is clear from the present finding that by increasing the drop number relative energy loss in each GT model decreases and the same was observed in the previous finding **(Salmasi et al., 2012)**. The average relative error for energy loss in the GT-4 and GT-5 model is 0.2 % and GT-5 and GT-6 model is 0.6%.

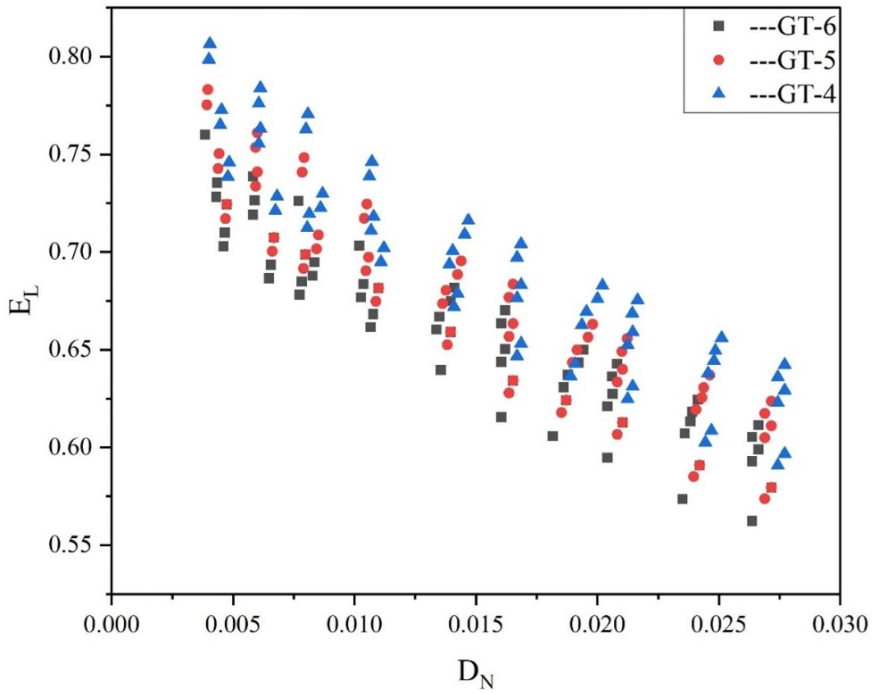

Figure 4.13 D_N vs E_L plot for GT-4, GT-5 and GT-6 models for sill on step-2

4.4.3 Comparison of results based on F_1

The F_1 vs E_L plot is shown in **Figure 4.14**. The values reflect the discrepancies while plotting and Froude number shows the proportional relations with the relative energy loss.

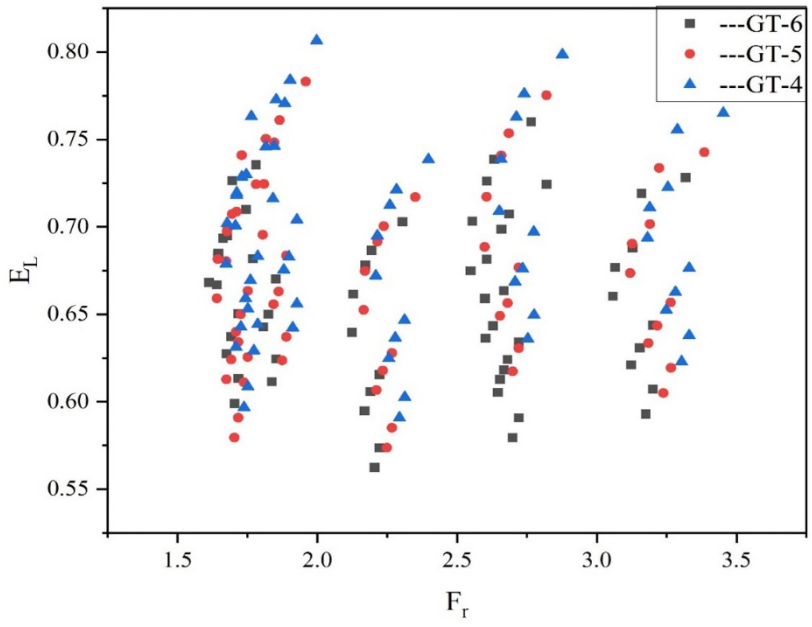

Figure 4.14 F_1 vs E_L plot for GT-4, GT-5 and GT-6 models for sill on step-2

4.4.4 Effect of t/l on energy loss

Figure 4.15 represents the plot between the discharge versus relative energy loss for different t/l values for the GT-4 model. The t/l values for triangular gabion sill heights 15cm, 11cm and 7 cm are 0.802, 0.588 and 0.374 respectively. This shows that the higher t/l value for the sill creates significant energy loss. The average relative error between the t/l = 0.802 and t/l = 0.588 for energy loss is 0.21% and for the t/l= 0.588 and t/l = 0.374 is 1%.

Figure 4.16 shows another plot for t/l = 0.802 for 33.69^0 spillway slope models GT-1, GT-4 and GT-7 between discharge and relative energy loss and observed that the scattered point shows a significant energy loss with higher t/l value for GT-4 model. Thus, it shows that with a higher value of t/l the relative energy loss increases for milder slope up to a certain extent.

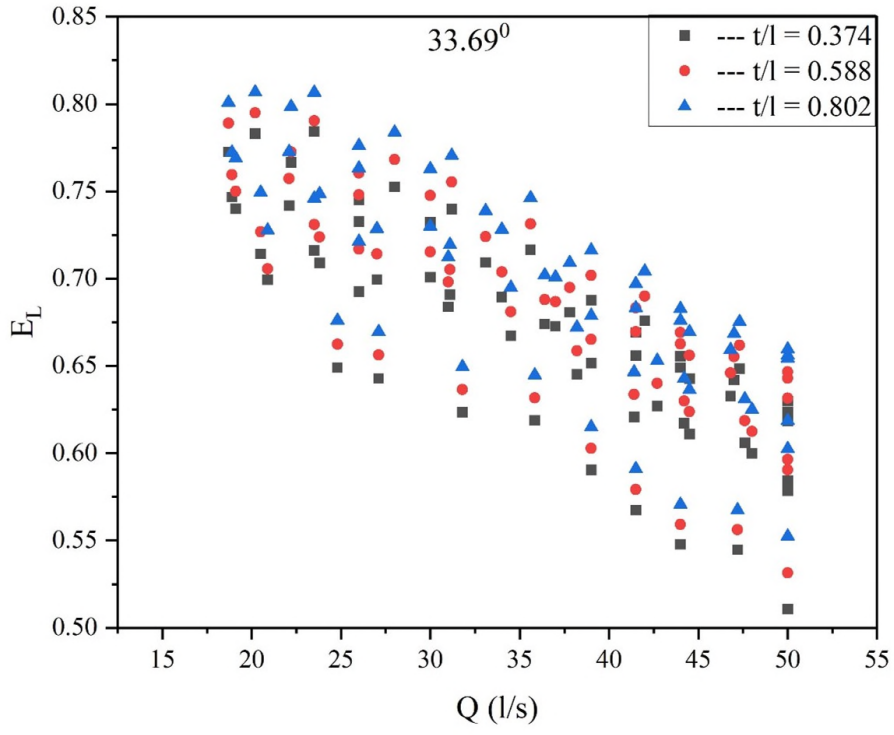

Figure 4.15 Q vs E_L plot for different t/l values for sill on step-2

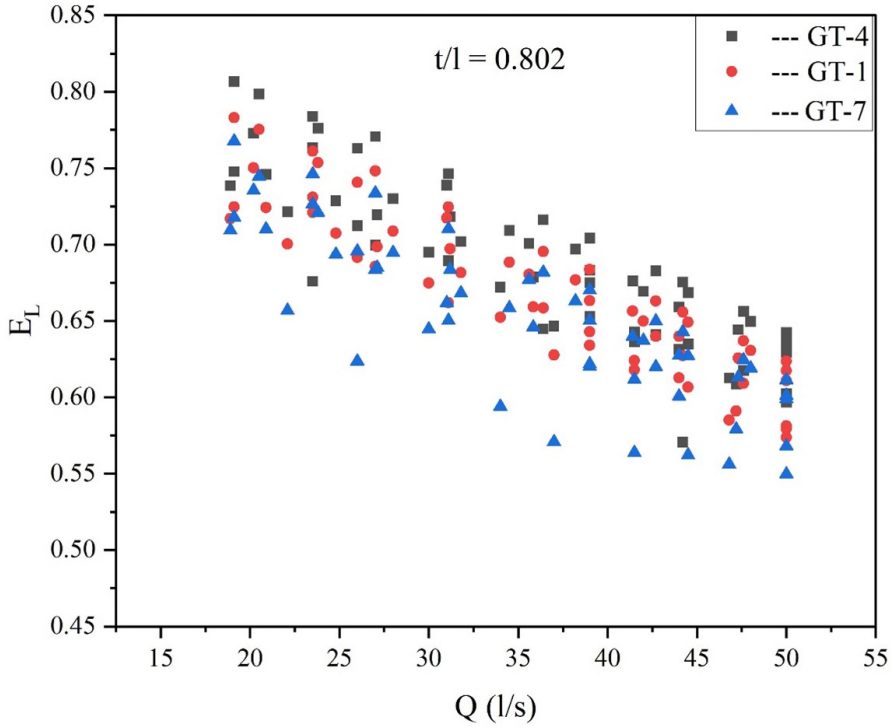

Figure 4.16 Q vs E_L plot for t/l = 0.802 for 33.69^0 spillway models

4.4.5 Soft computing result

A dataset consists of five input variables, and a single output is taken in modelling using ANN, ANFIS and ELM. In ANFIS, FIS input parameters were spillway slope (S), critical depth to step height ratio (Y_c/h), drop number (D_N), Froude number (Fr), relative sill ratio (t/l) and one output is relative energy dissipation ($\Delta E/E_0$) as shown in **Figure 4.17**, considered after sensitivity analysis. The selection of the five input variables spillway slope (S), critical depth to step height ratio (Y_c/h), drop number (D_N), Froude number (Fr) and relative sill ratio (t/l) is based on their direct physical relevance to flow regime, energy dissipation mechanisms and structural geometry of stepped and gabion spillways as established in earlier experimental and analytical studies. These parameters collectively represent flow intensity (D_N, Fr), geometric control (S, Yc/h) and sill-induced disturbance (t/l) which are known to govern turbulence generation, nappe breakup and cavity recirculation.

4.4.5.1 ANN modelling result

ANN modelling is done for the datasets collected from experimental run. The same set of inputs is used for model to ensure a fair comparison and build on critical network. Total five neurons are selected in a single hidden layer, and output is computed after modelling. In training and testing stage, the value R^2 is 0.9270 and 0.8851 as shown in **Figure 4.22**.

4.4.5.2 ANFIS modelling result

All programs were coded in MATLAB. Three data sets were used to predict energy loss through the gabion-stepped spillway, which had a triangular gabion sill over the steps in Neuro-fuzzy Designer. Different membership functions were selected for 100 training epochs and the training error tolerance limit was set to $\pm$0.01. Datasets were imported to the MATLAB workbench which had five input variables and one output variable (refer **Figure 4.17)**. Then training data was further entered into neuro fuzzy designer from the workbench and FIS was generated. Membership functions were listed in the fuzzy designer tab. Three adaptive layers were selected for each input variable. FIS is generated using a grid partition and for training Hybrid method is adopted. After the FIS is trained, the model is validated using the testing data that is independent of the data used to train the FIS. Different membership functions with RMSE value and classification accuracy (%) for datasets are shown in **Table 4.5**. ANFIS structure for gbellmf membership function having higher average classification accuracy as shown in **Table 4.6**. In dataset-2, minimal training RMSE is 0.017 for gbellmf membership function is observed. 54 Testing data and FIS output with output (energy dissipation) are plotted in neuro-fuzzy designer represented in **Figure 4.18**.

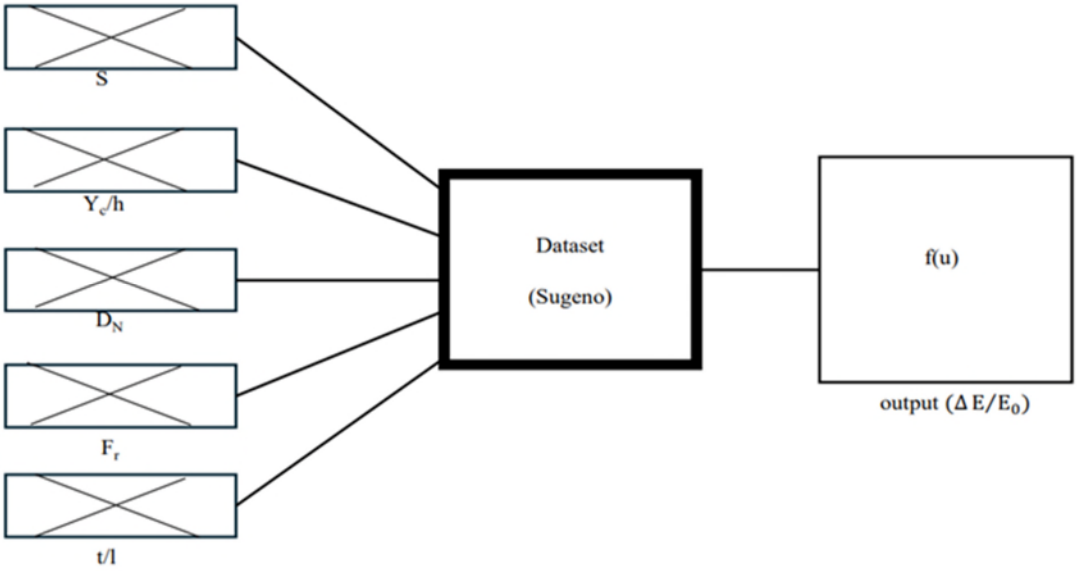

Figure 4.17 Structure of proposed FIS with five input and one output

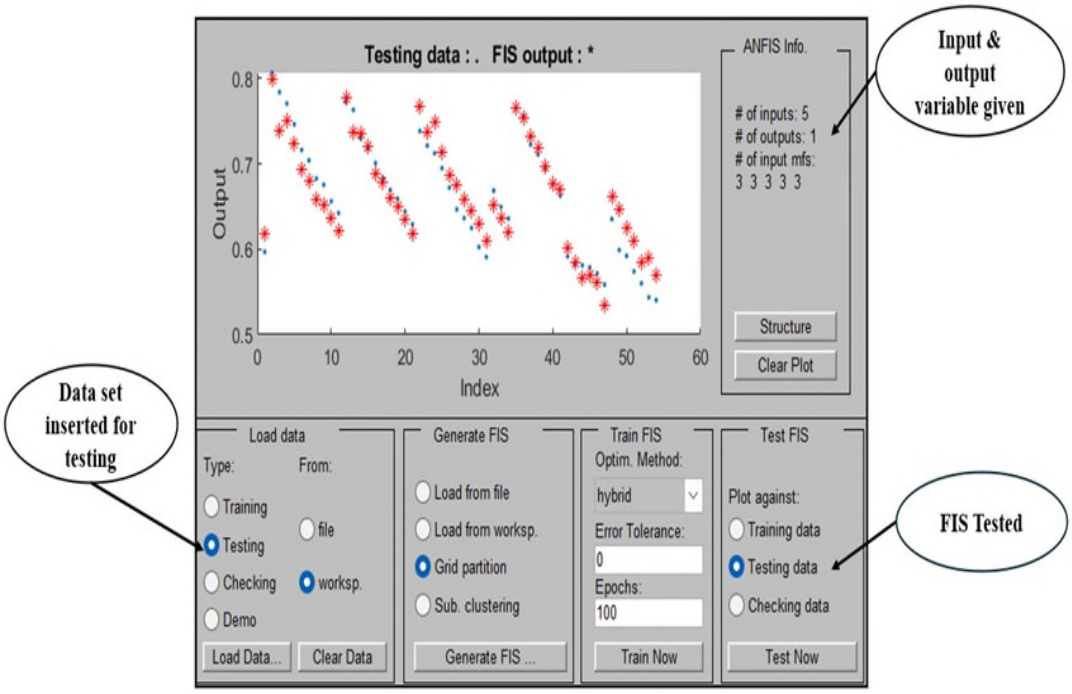

Figure 4.18 Testing data and FIS output versus output (rate of energy dissipation)

Table 4.5 Test performance of different membership functions

Membership function	Minimal training RMSE Data Set-1	Classification Accuracy (%)	Minimal training RMSE Data Set-2	Classification Accuracy (%)	Minimal training RMSE Data Set-3	Classification Accuracy (%)	Average Classification Accuracy (%)
trimf	0.792	99.208	0.225	99.775	0.730	99.270	99.418
trampmf	0.325	99.675	0.156	99.844	0.420	99.580	99.700
gbellmf	0.192	99.808	0.017	99.983	0.130	99.870	99.887
gaussmf	0.88	99.12	0.512	99.488	0.930	99.070	99.226
gauss2mf	0.945	99.055	1.226	98.774	1.330	98.670	98.833
pimf	0.965	99.035	0.721	99.279	0.839	99.161	99.158
dsigmf	1.045	98.955	1.327	98.673	1.191	98.809	98.812
psigmf	1.026	98.974	1.120	98.880	1.930	98.070	98.641

Table 4.6 ANFIS structure for membership function (gbellmf)

Number of nodes	524
Number of linear parameters	243
Number of non-linear parameters	45
Total number of parameters	288
Number of training data pairs	180
Number of checking data pairs	95
Number of fuzzy rules	243

4.4.5.3 Membership functions plot

The membership function can be plotted for input variables in **Figure 4.19 (a-c)**. MF1, MF2 and MF3 are plotted for different inputs. for selected membership functions the values of input variables are plotted with respect to the output. Prediction of input values can also be done with the help of these plots.

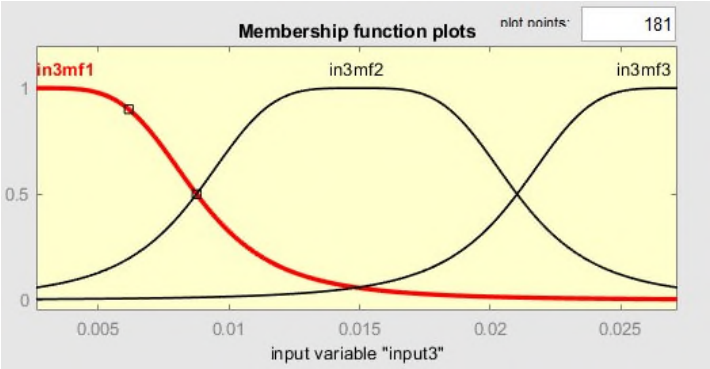

(a)

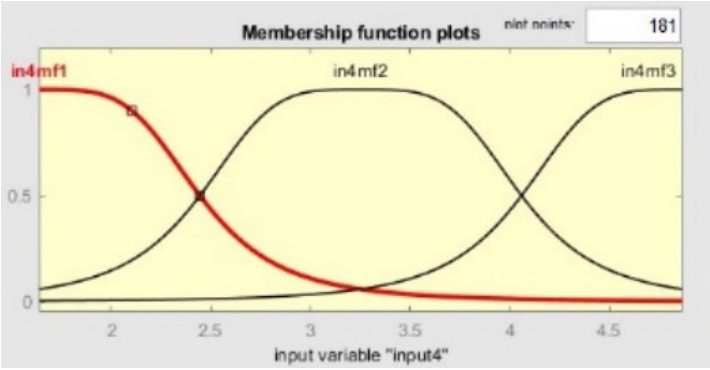

(b)

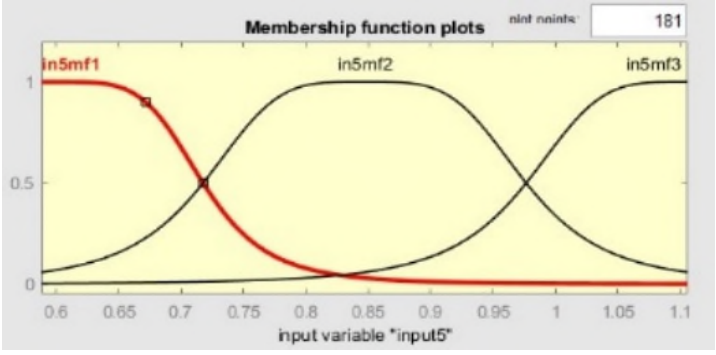

(c)

Figure 4.19 (a-c) Membership function plot for input variables for gabellmf type MF

4.4.5.4 Surface plots

These plots can be seen in the surface viewer of the neuro-fuzzy designer. Input variables are plotted with respect to the output shown in **Figure 4.20 (a-d)**. The variation of the range of two input variable values is represented with the range of output function.

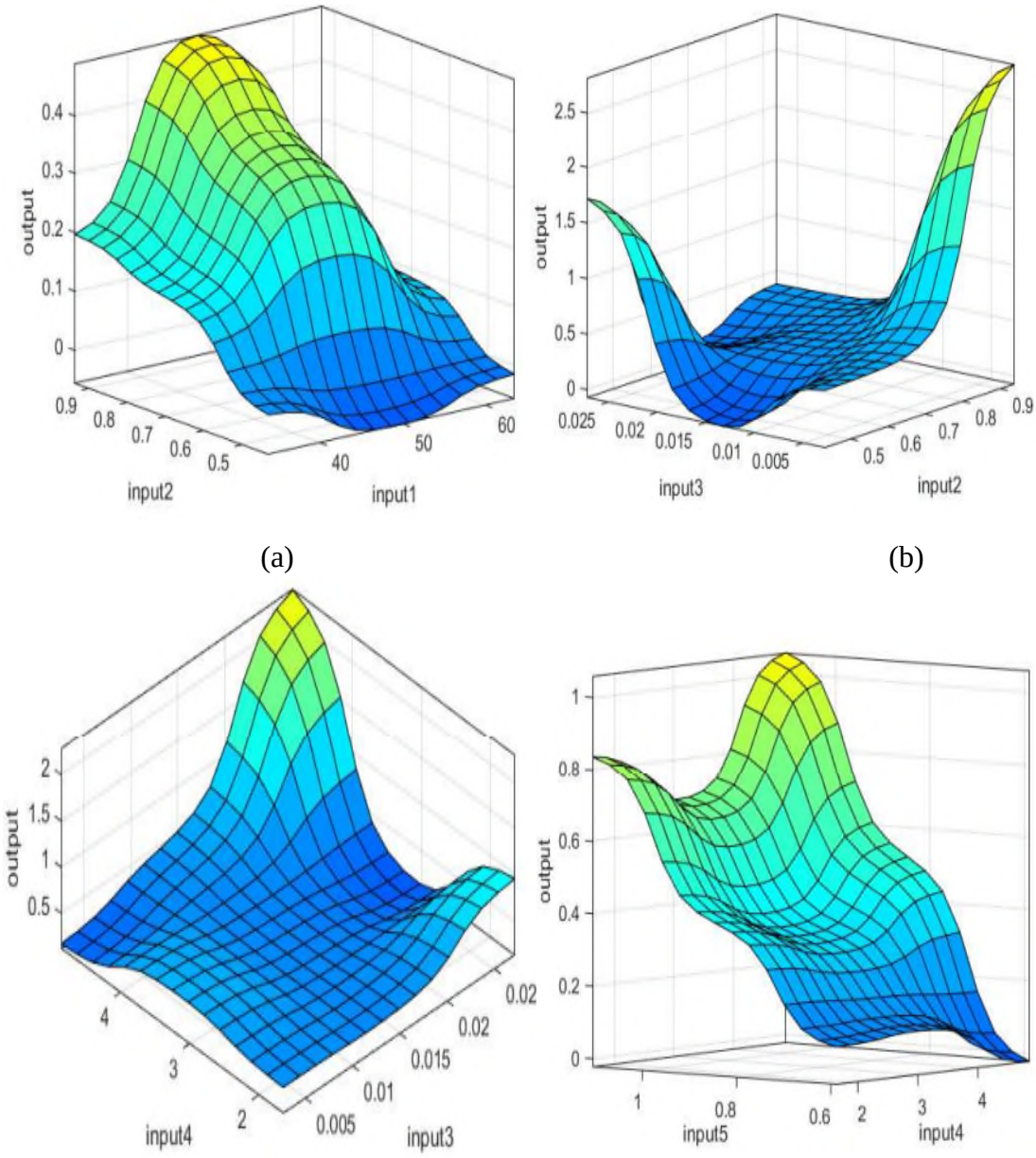

Figure 4.20 (a-d) Surface plot of the input variable with the output

To get the ANFIS output, scope data is downloaded from the workspace of MATLAB. Observed data in the experimental study and ANFIS predicted data are plotted as shown in **Figure 4.21**. The average relative error between observed data and ANFIS output data calculated is 1.25% which is found minimum compared to all other datasets.

The following relation in equation (21) may be used to represent the relationship between the modified drop number and the relative energy loss in the gabion-stepped weirs by **(Chinnarasri et al. 2008)**:

$$\frac{\Delta E}{E_o} = 0.53\ {D_N}^{-0.05} \tag{21}$$

As per the present study, a similar relationship is evaluated for GT models on sill-2 for slope 33.69^0 in equation (22):

$$\frac{\Delta E}{E_o} = 0.409\ {D_N}^{-0.12} \tag{22}$$

The result of the present study for Model GT4, GT5 and GT6 (sill placed on step-2) is compared with the previous studies as shown in **Figure 4.21**. With the higher value of the drop number, the value of relative energy loss decreases for $D_N <$ 0.06. Skimming flow and transition flow regime occur in the channel with larger discharge which leads to relative energy loss. Based on the observation, the model flow rate per unit width was 2.8 $m^3/s/m$ which gives slightly more relative energy loss corresponding to the drop number obtained in the findings of **(Peyras et al. 1992)**. Model GT4 has a higher value of E_L concerning the value of D_N for a 33.69^0 model slope which shows similar trends to the past studies. This also comprises the same trend for the model GT5 and GT6. Models consisting of the triangular gabion sill with the larger value of discharge hold significant results for skimming and transition flow.

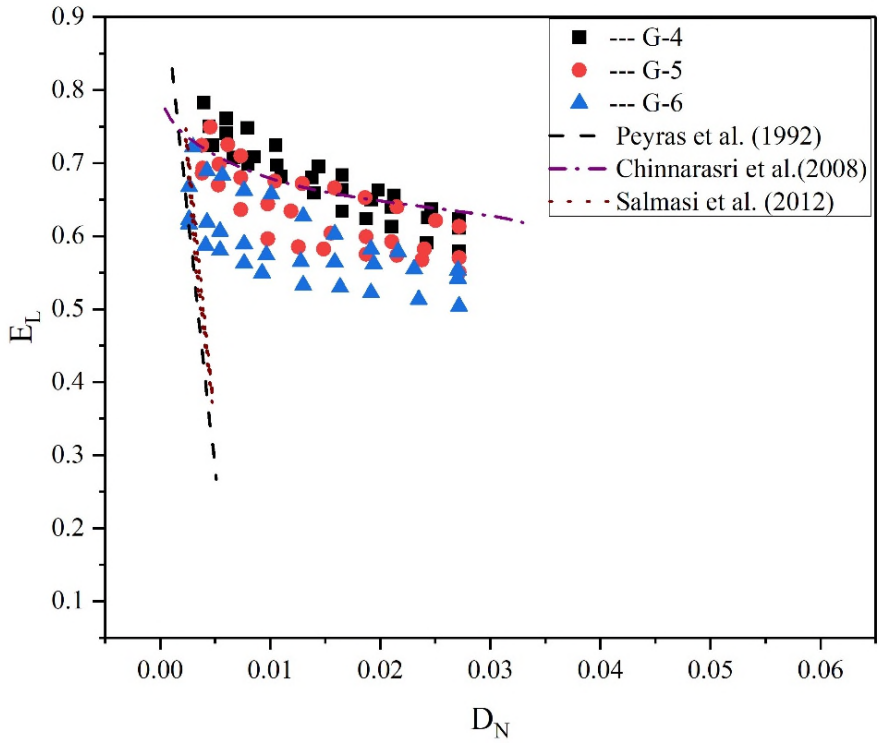

Figure 4.21 Comparison of the results with the previous study

Linear equations are developed for observed and predicted relative energy loss data, which is plotted using Response surface methodology (RSM) in the Design Expert (version-13) tool. The values of the R^2 for training and testing are 0.9721 and 0.9526, which were found similar to the findings of **Salmasi and Ozger (2014)** having a value of $R^2 = 0.9670$, as shown in **Figure 4.23**.

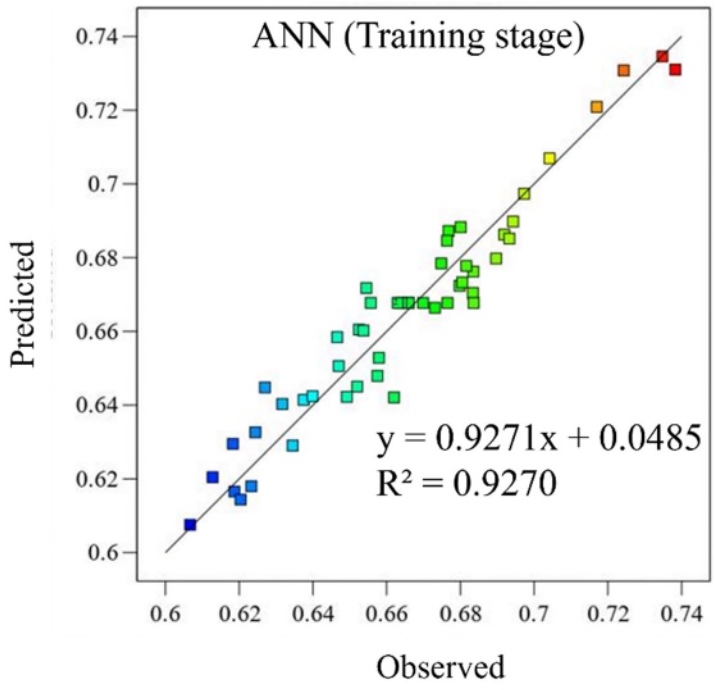

(a)

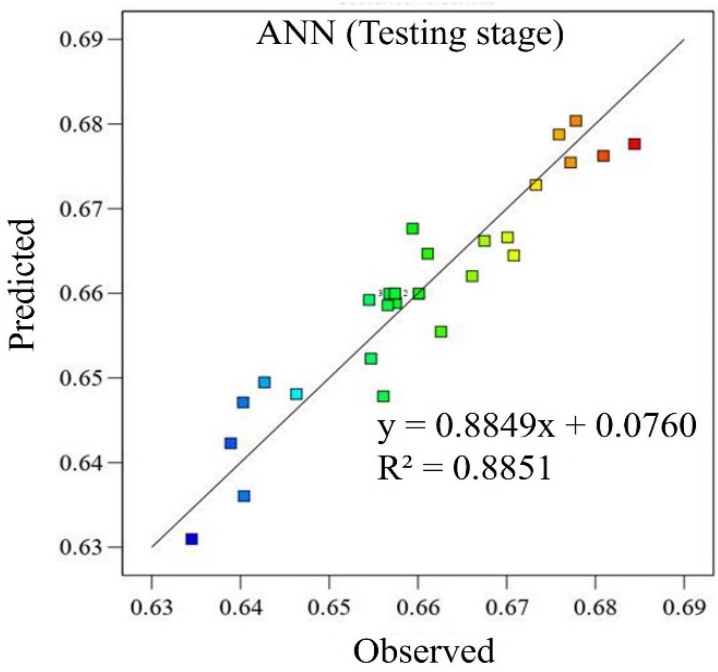

(b)

Figure 4.22 (a-b) Training and Testing dataset for observed and predicted data of ANN

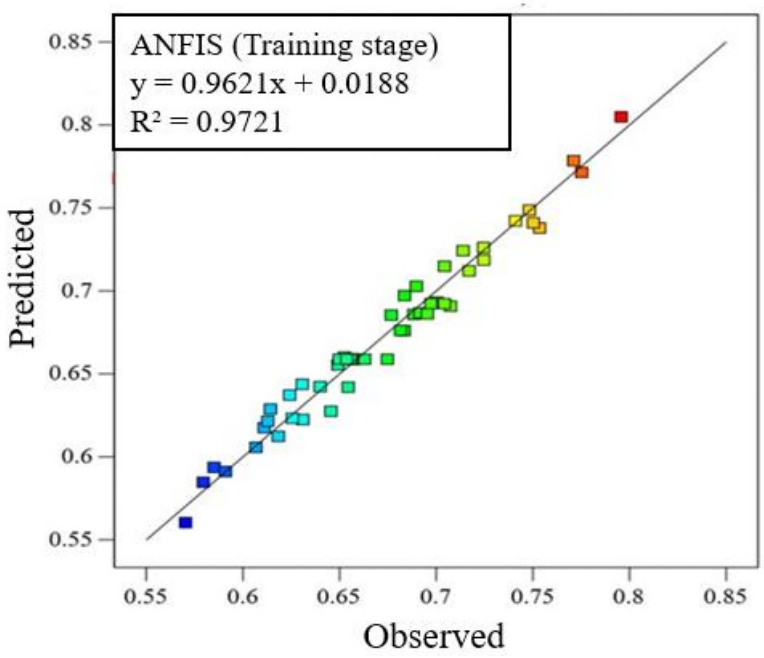

(a)

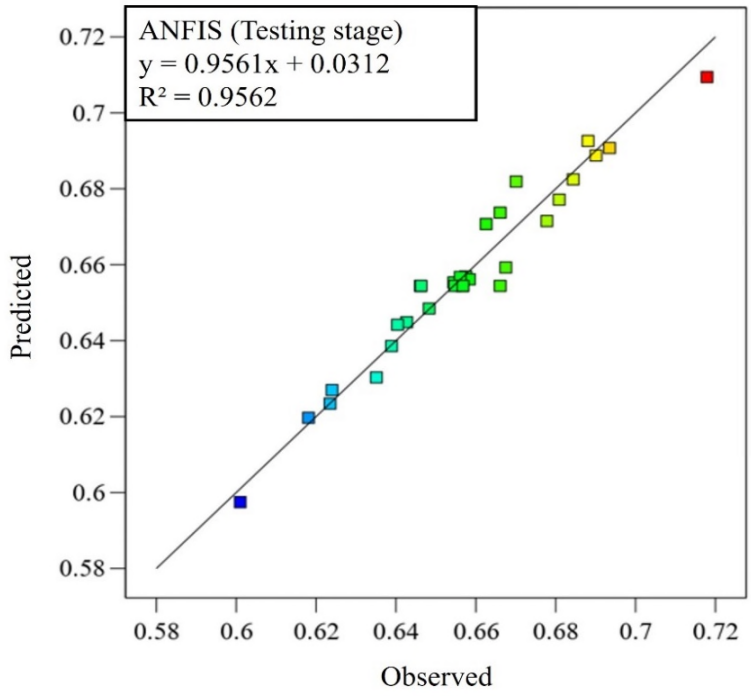

(b)

Figure 4.23 (a-b) Observed and predicted value for the training and testing stage for ANFIS

4.4.5.5 ELM modelling result

ELM modelling is also done by developing a generalized program in the MATLAB workspace for the dataset. ELM produces the best output by taking five neurons in the hidden layer and relative energy loss as output. Like ANFIS modelling, training and testing data are selected randomly. These soft computing models have an adequate level of accuracy based on the result of fitting the observed and predicted value, and the fitted line equation $y = c_1x + c_2$ predicted the model performance.

The ELM model performs with greater accuracy when the values of c_1 and c_2 approached 1 and 0, respectively. In this case, c_1 and c_2 were 0.9843 and 0.0104 for the The ELM model showed higher accuracy, with values of c_1 and c_2 being closer to 1 and 0, respectively. In the training stage, c_1 is 0.9843 and c_2 is 0.0104 while in the testing stage c_1 is 0.9677 and c_2 is 0.0211. The ANFIS model results show better accuracy than the ANN model in terms of c_1 and c_2 coefficient as in the training stage, c_1 is 0.9621 and c_2 is 0.0188 while in the testing stage c_1 is 0.9561 and c_2 is 0.0312.

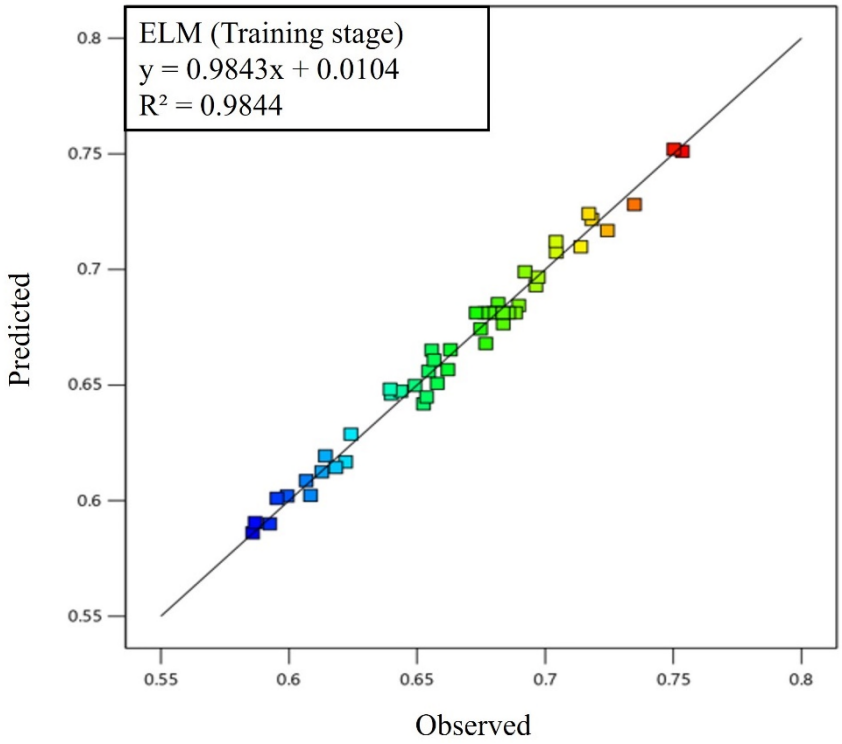

(a)

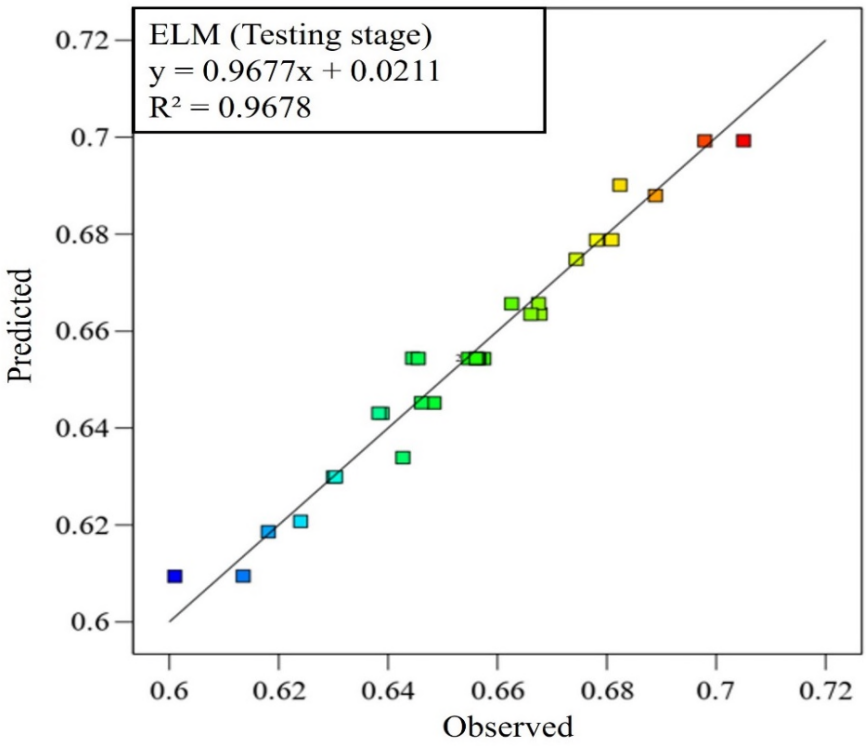

(b)

Figure 4.24 (a-b) Observed and predicted value for training and testing stage for ELM

4.4.5.6 Comparison of modelling result

In **Figure 4.25**, the combined predicted output graph for the observed data, along with the results from the ANN, ANFIS, and ELM models, is presented. Based on the observations, the GT-4 model demonstrates superior efficiency in energy dissipation. Among the soft computing models, the ELM outperforms both the ANN and ANFIS models, providing more accurate predictions. **Figure 4.26** (a-c) illustrates the relative errors for each model compared to the observed data. The ELM model exhibits the smallest relative error, indicating its higher accuracy relative to the other models.

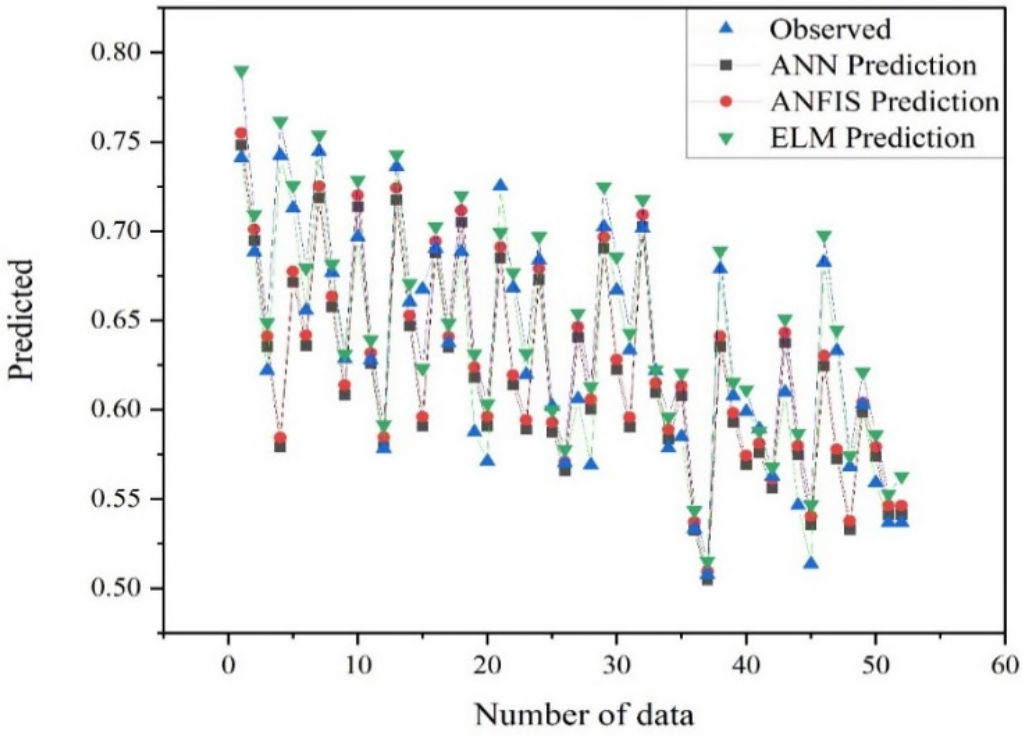

Figure 4.25 Comparisons of the observed data with the predicted data of ANN, ANFIS and ELM model

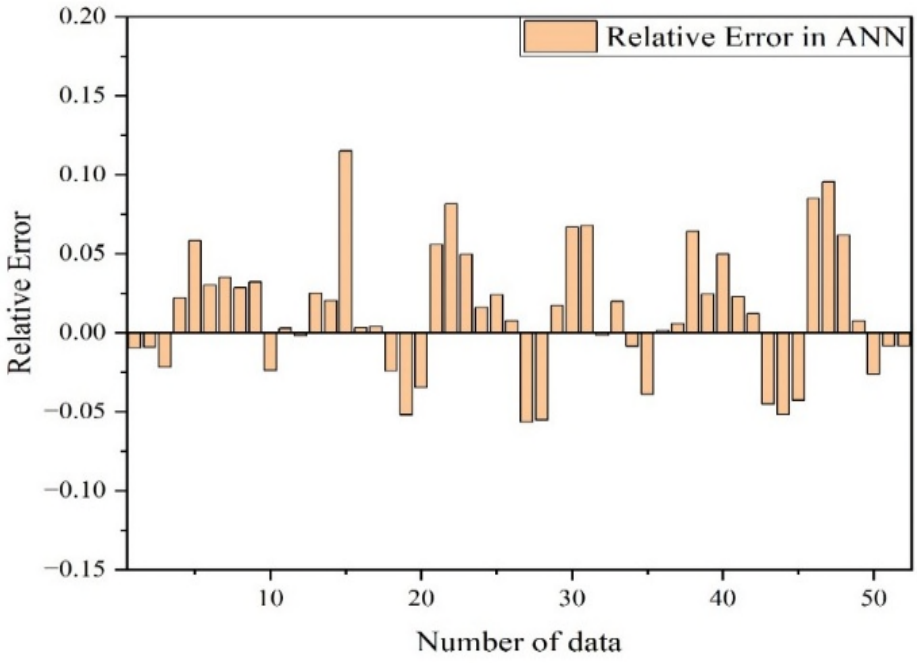

(a)

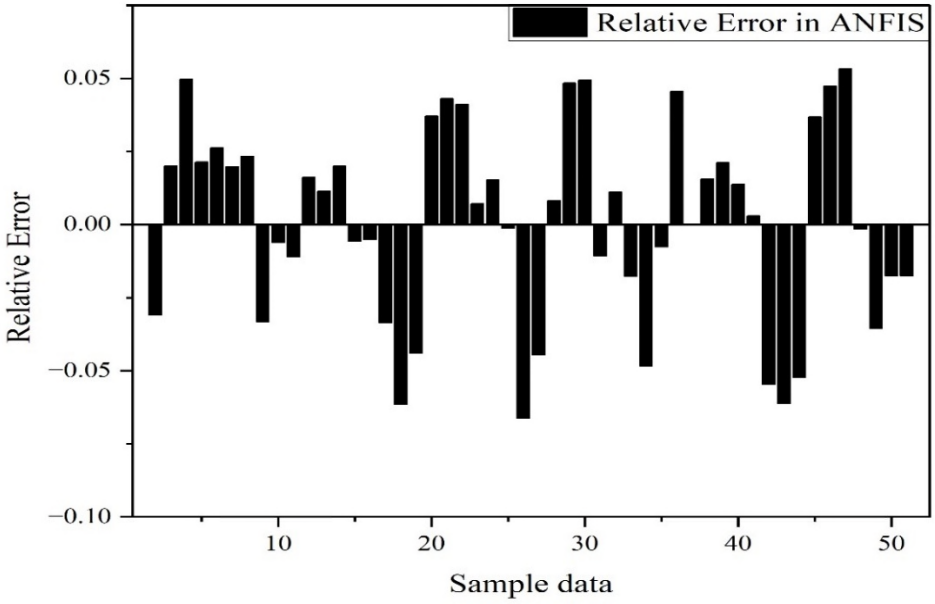

(b)

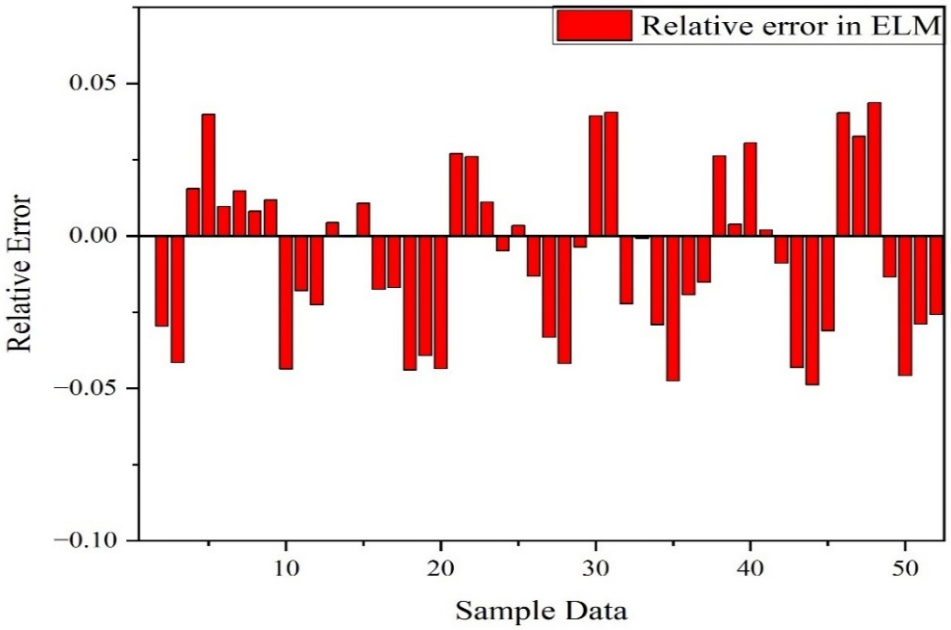

(c)

Figure 4.26 (a-c) Error between observed data with the predicted data of ANN, ANFIS and ELM model

Table 4.7 shows the performance parameters of the model testing and training phases. For dataset-2, the calculated RMSE, MAE and NSE are found to be minimum calculated using the equations (18), (19) and (20) and the value of the correlation coefficient (R^2) from the training and testing phase is evaluated from equation (17).

The Artificial Neural Network (ANN) and Adaptive Neuro-Fuzzy Inference System (ANFIS) models were compared to the Extreme Learning Machine (ELM) model based on a number of parameters. In comparison to the ANN and ANFIS models, the ELM model's Root Mean Square Error (RMSE) values throughout the training and testing stages were 0.0028 and 0.0035 respectively. This suggests that the ELM model outperformed the others in both phases in terms of predicted accuracy. Furthermore, the ELM model's Coefficient of Determination (R^2), which was 0.9844 for the training phase and 0.9678 for the testing phase, was greater than that of the ANN and ANFIS models. These results suggest that the ELM model explains a greater proportion of the variance in the data, indicating a better fit compared to the other models. Furthermore, the Mean Absolute Error (MAE) values for the ELM model were found to be the smallest, demonstrating that it consistently outperforms both the ANN and ANFIS models in terms of minimizing prediction error.

Table 4.7 Performance parameters of models

Model	Phase	RMSE	MAE	NSE	R^2
ANN	Training	0.058	2.01	0.9271	0.9270
	Testing	0.066	1.46	0.8849	0.8851F
ANFIS	Training	0.017	1.81	0.9721	0.9721
	Testing	0.031	1.06	0.9561	0.9562
ELM	Training	0.0028	1.36	0.9844	0.9844
	Testing	0.0035	0.977	0.9677	0.9678

The following fitness equation for GT models is calculated using regression analysis and the value of R^2 found for 1/(1-*K*) and D_N in **Table 4.8** which shows relatively better agreement with the previous findings of Salmasi et al. (2012), Rajaei et al. (2020):

Table 4.8 Fitness equation for GT model with a value of R^2

Model	Slope *(V:H)*	Fitness Equation	R^2
GT-1	1:1.5	$1/(1-K) = -0.083ln\ (D_N) + 0.2768$	0.9656
GT-4	1:1.5	$1/(1-K) = -0.082ln\ (D_N) + 0.3247$	0.9763
GT-7	1:1.5	$1/(1-K) = -0.094ln\ (D_N) + 0.2389$	0.9805
GT-2	1:1	$1/(1-K) = -0.068ln\ (D_N) + 0.290$	0.9404
GT-5	1:1	$1/(1-K) = -0.075ln\ (D_N) + 0.3347$	0.9842
GT-8	1:1	$1/(1-K) = -0.078ln\ (D_N) + 0.277$	0.9917
GT-3	1:0.5	$1/(1-K) = -0.047ln\ (D_N) + 0.3224$	0.9855
GT-6	1:0.5	$1/(1-K) = -0.073ln\ (D_N) + 0.2876$	0.9687
GT-9	1:0.5	$1/(1-K) = -0.046ln\ (D_N) + 0.361$	0.9252

4.4.5.7 Discussion for Objective-3

The study investigated the hydraulic performance of a gabion stepped spillway incorporating triangular gabion sills placed at different step locations and downstream slopes. The experimental results verified that the relative energy loss is strongly influenced by flow rate, sill position, downstream slope and flow regime. Under skimming flow conditions, relative energy loss decreases with increasing discharge and higher drop numbers, while milder downstream slopes exhibit greater energy dissipation compared to steeper slopes. The incorporation of triangular gabion sills significantly enhances the energy dissipation capacity of gabion stepped spillways, yielding up to a 10% improvement in relative energy loss compared to conventional gabion stepped spillways. Among the sill configurations tested, placement on the second step was found to be the most effective, dissipating up to 4% more energy than placement on the third step. Although the sill positioned on the first step showed slightly lower energy dissipation than the third step, it still contributed significantly to

overall energy reduction. Additionally, a marginal increase in relative energy loss was observed with decreasing relative sill ratio.

Further, soft computing techniques were successfully used to predict relative energy loss. Comparative analysis revealed that the Extreme Learning Machine (ELM) model outperformed the Artificial Neural Network (ANN) and Adaptive Neuro-Fuzzy Inference System (ANFIS) models, achieving greater predictive accuracy with lower RMSE values and higher coefficients of determination during both training and testing phases. These findings confirm the effectiveness of triangular gabion sills in improving spillway performance and highlight the robustness of ELM as a reliable modelling tool for hydraulic energy dissipation studies.

4.5 To evaluate and compare the hydraulic performance and energy dissipation efficiency of various gabion stepped spillway configurations with rigid stepped spillways under different slope conditions.

(a) Comparison of standard gabion stepped spillway versus rigid stepped spillway

(b) Gabion stepped spillway having triangular gabion sill with rigid stepped spillway

(c) Gabion stepped spillway having vertical obstruction with rigid stepped spillway

The comparison between the best model outputs from the objectives are compared with the rigid stepped spillway having identical spillway height of 0.33 m for downstream slope of 33.69°, 45°and 63.43. As GT-4 model and model with staggered-1 with 11 cm height vertical obstructions were compared with standard gabion model and rigid spillways.

Figure 4.27 presents the variation of relative energy loss (E_L) with discharge (Q) for the rigid stepped spillway (R1), standard gabion model (GS-1), GT-4 model, and the model with staggered-1 vertical obstructions (11 cm height), all having an identical spillway height of 0.33 m and tested under downstream slopes of 33.69°, 45° and 63.43°.

A consistent trend is observed across all configurations, where the relative energy loss (E_L) decreases with an increase in discharge. This behavior indicates that at higher flow rates, the capacity of the structures to dissipate energy reduces due to increased flow momentum and reduced relative turbulence effects.

Among all the tested models, the model with staggered-1 vertical obstructions exhibits the highest energy dissipation throughout the entire range of discharges. The E_L values for this model range approximately from 0.78 at lower discharges 20 L/s to about 0.65 at higher discharges 50 L/s. The improved performance can be attributed to the staggered arrangement of vertical obstructions, which enhances flow disruption, induces turbulence, and increases energy loss.

The GT-4 model demonstrates the second-highest energy dissipation efficiency. Its E_L values vary approximately between 0.76 and 0.61 over the tested discharge range. Although slightly lower than the staggered obstruction model, GT-4

still provides substantial energy dissipation due to improved flow interference compared to conventional configurations.

The standard gabion model (GS-1) shows moderate performance, with E_{Ll} values ranging from approximately 0.69 to 0.55. While it performs better than the rigid stepped spillway, its relatively uniform structure results in less turbulence compared to the modified models.

The rigid stepped spillway (R1) exhibits the lowest energy dissipation among all configurations. The E_l values decrease from about 0.61 at low discharge to nearly 0.51 at high discharge. This indicates that the rigid structure offers limited resistance to flow and generates comparatively lower turbulence, resulting in reduced energy loss. These results clearly demonstrate that the introduction of vertical obstructions, particularly in a staggered configuration, significantly enhances energy dissipation performance. This improvement is evident across all tested discharges and downstream slopes, making the staggered-1 model the most effective among the studied configurations.

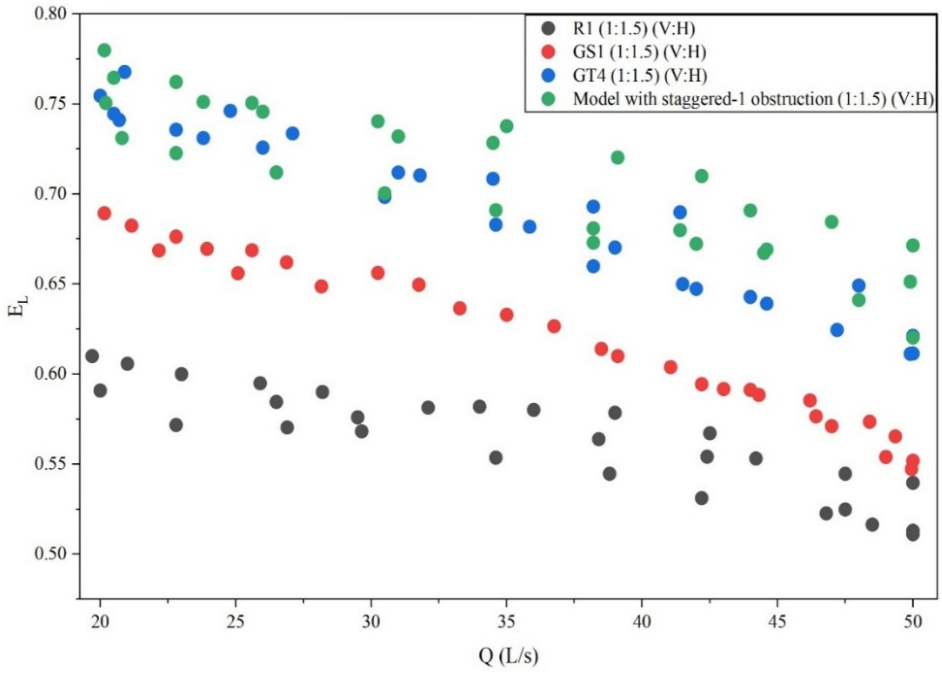

Figure 4.27 Variation of relative energy loss (E_L) with discharge (Q) for the rigid stepped spillway (R1), standard gabion model (GS-1), GT-4 model, and the model with staggered-1 vertical obstructions

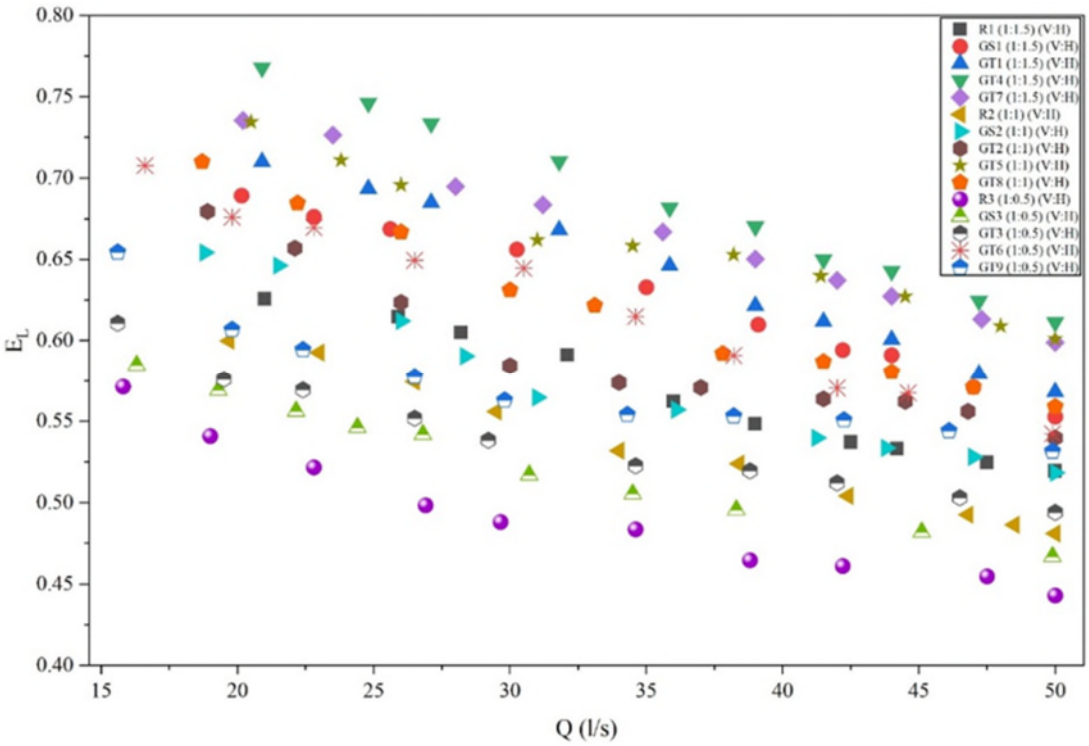

Figure 4.29 Combined plot for Relative Energy loss versus discharge

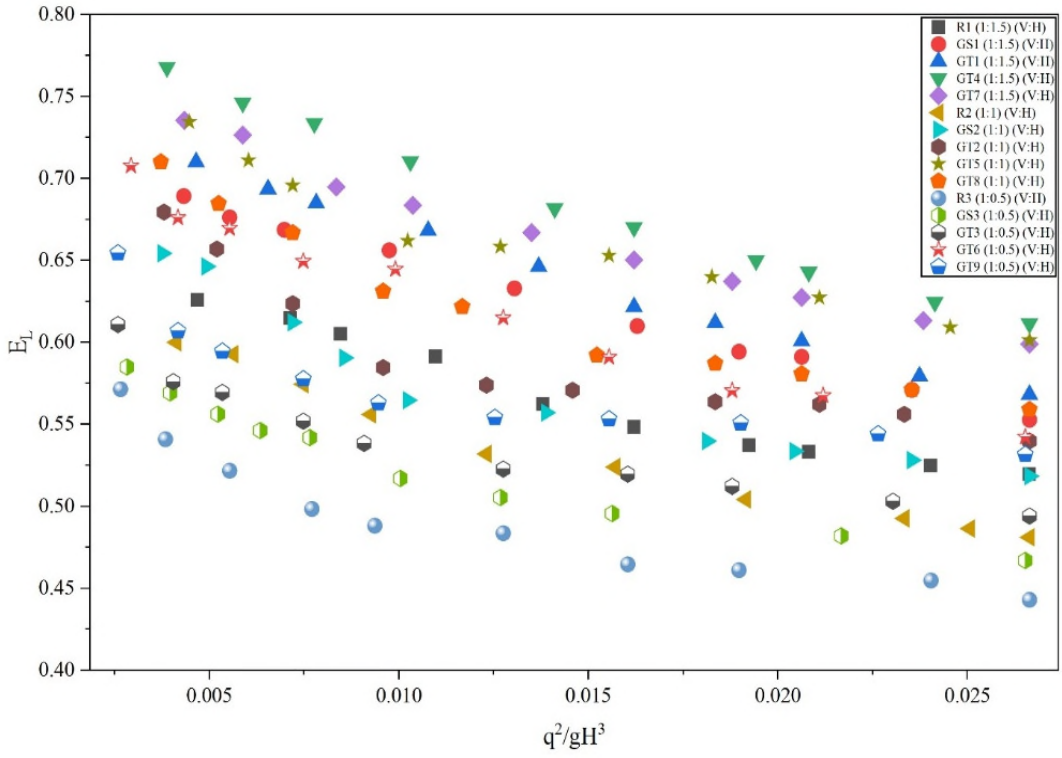

Figure 4.28 Relative Energy loss versus drop number plot

Chapter 5: CONCLUSION, FUTURE SCOPE AND SOCIAL IMPACT

5.1 General

This chapter includes the final findings from the study performed and conclusive statements based on their validation. It also consists of the future work and social impact.

5.2 Conclusion

The conclusion is as follows from the experimental and soft computing findings:

- Milder downstream slopes consistently produce greater relative energy loss than steeper slopes, confirming their suitability for improved energy dissipation in gabion spillway systems.
- The experimental results show that for porosity 34% and flow discharge, the standard gabion stepped spillway with a milder slope (33.69°) exhibits notably higher relative energy loss compared to steeper slopes (45° and 63.43°), confirming that reducing the slope angle, increases flow resistance and turbulence within the porous matrix.
- Relative energy loss decreases with increasing discharge under skimming flow conditions, while higher drop numbers reduce energy dissipation efficiency.
- The gbellmf membership function in ANFIS produced superior prediction performance compared to other membership functions, indicating its suitability for spillway energy dissipation analysis. The model achieved excellent performance metrics (Training $R^2 = 0.985$, Testing $R^2 = 0.976$; Training RMSE $= 0.017$, Testing RMSE $= 0.024$) with a mean relative error of only 1.25%, as a cost-effective soft-computing tool for optimizing the hydraulic design of standard gabion stepped spillways.
- Introducing vertical obstructions significantly enhances relative energy dissipation, with the staggered-1 configuration achieving the highest relative

energy loss, showing a maximum increase of 45.83%, followed by the staggered-2 and uniform patterns compared to the case without obstructions.

- ELM validation of the experimental data yielded excellent performance metrics; Training $R^2 = 0.9812$, Testing $R^2 = 0.9618$, Training RMSE $= 0.0026$ and a mean relative error of only 0.75%. The ELM model's fast training and strong generalization confirm its suitability as a cost-effective soft-computing tool for optimizing the design of gabion stepped spillways with obstructions under varying hydraulic conditions.
- Among the tested triangular gabion sill, placement on the second step provides the most effective energy dissipation performance. The experimental results demonstrate that gabion stepped spillways fitted with triangular gabion sills (GT models) achieve up to 10% higher relative energy loss compared to conventional gabion stepped (GS) and rigid stepped (R) spillways. Among all sill positions tested, placement on the second step (GT-4, GT-5, GT-6) consistently yields the highest energy dissipation (62-72%), outperforming sills on the first or third steps by up to 4%. This improvement is attributed to enhanced jet deflection, turbulence generation, and cavity recirculation at an optimal hydraulic location.
- Soft computing techniques such as ANN, ANFIS and ELM successfully predicted the relative energy loss with high accuracy, validating their applicability for hydraulic modelling. ELM outperforms both ANN and ANFIS, achieving the lowest RMSE values (0.0028 for Training, 0.0035 for Testing) and the highest R^2 values (0.9844 for Training, 0.9678 for Testing).
- Statistical and graphical evaluations confirmed strong agreement between experimental observations and model predictions, establishing reliability of the adopted methodologies.
- Overall, the study confirms that gabion stepped spillways integrated with optimized sill and obstruction configurations, together with advanced soft computing models, provide an efficient and economical approach for improving hydraulic energy dissipation and spillway safety.

5.3 Social Impact

This research has the following social impacts and aligned with the United National Sustainable development goal (SDGs):

- Gabion stepped spillways provide an economical and environmentally sustainable solution due to the use of locally available and permeable construction materials to support safe water management. This aligned with SDG-6 goal for Clean Water and Sanitation.
- Improved energy dissipation in spillways enhances the safety and stability of dams and hydraulic structures, thereby reducing the risk of downstream flooding and structural failure.
- Environmentally friendly gabion structures help in minimizing erosion, flood management and improving ecological compatibility in river and spillway environments that relates to the SDG-13 goal of Climate Action.
- It involves innovative hydraulic engineering design, resilient infrastructure and spillway development that correlated the Industry, Innovation and Infrastructure goals of SDG-9.

5.4 Limitations and scope of future work

The present study has the following limitations:

- Experiments were conducted under steady, clear-water flow conditions only, unsteady flows, sediment transport and debris effects were not considered.
- The experimental readings were taken for the specific range of discharge and neglecting any kind of losses.
- Long-term performance aspects such as clogging, material degradation and maintenance of gabion structures were not evaluated.
- Machine learning models were trained on experimental data within a specific parameter range and their predictive accuracy may decrease when extrapolated beyond this range.

The scope of future research as follows:

- Future studies can investigate different shapes, sizes and materials of gabion sills and obstructions to further improve energy dissipation efficiency in stepped spillways.
- Hydraulic Jump analysis can also be done at the downstream section resulting from the turbulence created due to flow over the gabion stepped spillway.
- The performance of gabion stepped spillways can be analyzed under a wider range of hydraulic conditions, including extreme flood events and sediment transport scenarios.
- Advanced computational techniques such as CFD modelling can be integrated for more accurate prediction and optimization of spillway performance.
- Optimization studies considering cost, sustainability, and hydraulic efficiency can be carried out for the development of eco-friendly spillway systems.